Robust mechanical joining of cast aluminium components (RobuCAP)

Public report

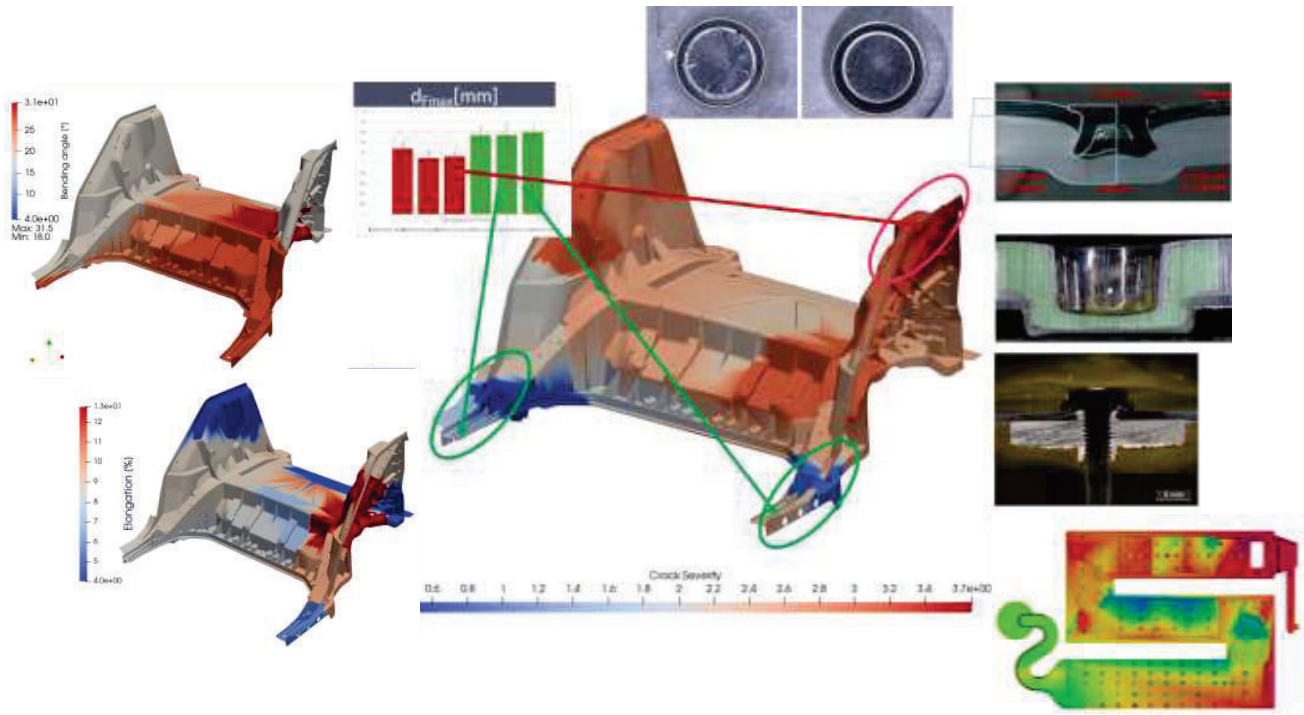

Project within FFI Circularity
Authors Andreas Reeb, Oscar Andersson, Peter Ottosson, Priyanka Ravishankar
Date 2025-04-30

FFI Fordonsstrategisk Forskning och Innovation

Content

FFI in short

FFI, Strategic Vehicle Research and Innovation, is a joint program between the state and the automotive industry running since 2009. FFI promotes and finances research and innovation to sustainable road transport.

For more information: www.ffisweden.se

1 Summary

Mechanical joining plays a key role in Body-in-White (BIW) assembly of cast aluminium alloys. However, their often-limited ductility poses challenges such as cracking during joining. The RobuCAP project, titled *Robust mechanical joining of cast aluminium components*, aimed to enhance the robustness of joining of cast aluminium alloys in automotive applications. This initiative was part of the FFI Circularity program and involved collaboration among several partners; Volvo Cars, Atlas Copco, BTM Scandinavia, Tucker, and RISE, which led the research efforts as project coordinator.

The automotive industry is increasingly using cast aluminium alloys, including recycled material, due to their potential for circularity and weight reduction. However, these materials often have limited ductility, which poses significant challenges for mechanical joining processes such as self-piercing riveting (SPR), clinching, and flow drill fastening (FDF). The RobuCAP project sought to address these challenges by investigating the joinability of large structural castings, known as megacastings, and improving the robustness of mechanical joining methods.

The project had several key objectives:

1. To identify the factors influencing joinability by analysing microstructural variations and defects in cast materials.
2. To develop and evaluate testing methods that characterize material properties relevant to mechanical joining.
3. To optimize mechanical joining processes through experimental investigations and numerical simulations.
4. To assess the feasibility of disassembly and re-manufacturing to support circularity in automotive manufacturing.
5. Assess innovative methods to improve joinability of cast aluminium components.

The project was divided into several work packages (WPs), each focusing on different aspects of the research:

WP1: Materials and Test Objects Extensive material characterization was performed using various methods, including tensile testing, hardness measurements, microstructural analysis, and the developed Pierce-Cupping Test (PCT). The investigations showed significant local property variation in megacastings, making conventional testing (e.g. tensile testing) insufficient for joinability prediction. The PCT, however, proved particularly effective in evaluating local ductility and crack susceptibility, providing reliable assessments for joinability. PCT enabled reliable assessments in areas as small as 20 mm^2, corresponding to typical joint sizes.

WP2: Experimental Studies SPR, clinching, and FDF processes were experimentally evaluated. SPR joinability was assessed using various material combinations, with efforts

focused on reducing cracking through process optimization. Clinching trials revealed significant local property variations that impacted joint quality. SPR joining trials and statistical analyses were performed using a small reference tool ("snake tool") and a large demonstrator ("soft tool") to study crack severity in relation to joining location and to improve joinability through rivet-die optimization. A secondary goal was to cluster rivet-die combinations to reduce line complexity and minimize tool changes. Cracking analysis revealed a correlation between crack occurrence and casting flow length, highlighting the influence of microstructural features. Pore size and density were also identified as critical defects, causing local stress concentration and initiating cracks. FDF joinability was tested with different fasteners, showing promising results.

WP3: Numerical Studies Numerical simulations were conducted to predict joinability and optimize joining processes. These simulations showed good agreement with physical experiments but highlighted the need for further refinement in material models and process parameters. The use of GISSMO for fracture modelling in SPR and PCT simulations was explored but faced challenges in implementation.

WP4: Alternative Processes Hybrid joining methods, which combine mechanical joints with adhesive bonding, were investigated for their impact on fatigue life. It was seen that adhesive bonding, i.e. hybrid joints, significantly improved the fatigue strength compared to dry SPR joints without adhesive. Tucker Plasma Joining (TPJ) was evaluated as an innovative method for joining dissimilar materials, demonstrating generally good joinability of challenging material combinations.

The project concluded that material properties, particularly ductility and defect density, are critical for joinability. The PCT emerged as a valuable tool for local material characterization. Numerical simulations can predict joinability but require further development. Hybrid joining methods and TPJ offer promising alternatives for improving joint robustness.

Future research should focus on optimizing process windows, developing plasma or heat-assisted SPR, improving quality control, and understanding recycling practices for secondary aluminium. Moreover, future research should focus on developing simulation models and computational aids for mechanical joining.

Overall, the RobuCAP project has increased the understanding of mechanical joining processes for cast aluminium component and provided tools for more robust and predictable automotive manufacturing practices.

2 Sammanfattning på svenska

Projektet RobuCAP, "Robust mekanisk fogning av gjutna aluminiumkomponenter", syftade till att förbättra fogningen av gjutna aluminiumlegeringar i fordonsapplikationer. Detta initiativ var en del av forskningsprogrammet FFI Cirkularitet och involverade

samarbete mellan flera partners, inklusive Volvo Cars, Atlas Copco, BTM Scandinavia, Tucker och RISE. RISE var projektledare och projektkoordinator.

Användningen av stora gjutna aluminiumlegeringar, bland annat med återvunnet material, ökar inom fordonsindustrin på grund av deras potential för cirkularitet och viktminskning. Dessa material har dock ofta begränsad duktilitet, vilket utgör betydande utmaningar för mekaniska fogningsprocesser som självstansande nitning (SPR), stuknitning eller clinchning och flytborrskruvning eller flow drill fastening (FDF). RobuCAP-projektet syftade till att hantera dessa utmaningar genom att undersöka fogningen av stora strukturella gjutningar, kända som megacastings, och förbättra robustheten hos mekaniska fogningsmetoder.

Projektet hade flera nyckelmål:

1. Identifiera faktorer som påverkar fogningen genom att analysera mikrostrukturella variationer och defekter i gjutna material.
2. Utveckla och utvärdera testmetoder för att karakterisera materialegenskaper som är relevanta för mekanisk fogning.
3. Optimera mekaniska fogningsprocesser genom experimentella undersökningar och numeriska simuleringar.
4. Bedöma möjligheten till demontering och återtillverkning för att stödja cirkularitet inom fordonsindustrin.
5. Utvärdera innovativa metoder för att förbättra fogningen av gjutna aluminiumkomponenter.

Projektet var uppdelat i flera arbetspaket (WP), var och en fokuserade på olika aspekter av forskningen:

WP1: Materials and Test Objects Omfattande materialkarakterisering utfördes med olika metoder, inklusive dragprovning, hårdhetsmätningar, mikrostrukturanalys och den nyutvecklade Pierce-Cupping Test (PCT). Undersökningarna visade betydande lokala egenskapsvariationer i stora gjutkomponenter, vilket gjorde konventionella testmetoder (t.ex. dragprovning) otillräckliga för att förutsäga fogning. PCT visade sig vara särskilt effektiv för att utvärdera lokal duktilitet och sprickbenägenhet, vilket gav mer tillförlitliga bedömningar för fogning. PCT möjliggjorde tillförlitliga bedömningar i områden så små som 20 mm², motsvarande typiska fogstorlekar.

WP2: Experimental Studies SPR, clinchning och FDF-processer utvärderades experimentellt. SPR-fogning bedömdes med olika materialkombinationer, med fokus på att minska sprickbildning genom processoptimering. Clinchförsök visade lokala egenskapsvariationer som påverkade fogkvaliteten. SPR-fogningstester och statistiska analyser utfördes med hjälp av en mindre referenskomponent ("snake tool") och en större demonstrator ("soft tool") för att studera spricksvårighetsgrad i relation till fogens placering och förbättra fogningen genom optimering av nit-dyna-kombinationer. Ett annat

mål var att klustra nit-dyna-kombinationer för att minska produktionskomplexiteten och minimera verktygsbyten. Sprickanalys avslöjade en korrelation mellan sprickförekomst och gjutlängd, vilket betonade mikrostrukturella egenskapers påverkan. Porstorlek och densitet identifierades som kritiska defekter, vilket orsakade lokal stresskoncentration och initierade sprickor. FDF-fogning testades med olika fästelement och visade goda resultat.

WP3: Numerical Studies Numeriska simuleringar genomfördes för att förutsäga fogning och optimera fogningsprocesser. Dessa simuleringar visade god överensstämmelse med fysiska experiment men betonade behovet av ytterligare förfining av materialmodeller och processparametrar. Användningen av GISSMO för sprickmodellering i SPR och PCT-simuleringar utforskades men visade utmaningar vid implementering.

WP4: Alternative Processes Hybrid fogningsmetoder, som kombinerar mekaniska fogar med limning, undersöktes för deras påverkan på utmattningslivslängd. De visade att limning, dvs. hybridfogar, avsevärt förbättrade utmattningsstyrkan jämfört med torra SPR-fogar utan lim. Tucker Plasma Joining (TPJ) utvärderades som en innovativ metod för att sammanfoga olika material och visade generellt god fogning av utmanande materialkombinationer.

Projektet drog slutsatsen att materialegenskaper, särskilt duktilitet och defekttäthet, är avgörande för fogning. PCT framstod som ett värdefullt verktyg för lokal materialkarakterisering. Numeriska simuleringar kan förutsäga fogning men kräver ytterligare utveckling. Hybrid fogningsmetoder och TPJ erbjuder lovande alternativ för att förbättra fogens robusthet.

Framtida forskning bör fokusera på att optimera processfönster, utveckla plasma- eller värmeassisterad SPR, förbättra kvalitetskontroll och förstå återvinningspraxis för sekundärt aluminium.

Sammanfattningsvis har RobuCAP-projektet avsevärt ökat förståelsen för mekaniska fogningsprocesser för gjutna aluminiumkomponenter och bidragit till mer robusta och hållbara tillverkningsmetoder inom fordonsindustrin.

3 Background

Aluminium offers significant potential for circular manufacturing through material recycling. However, cast aluminium alloys, particularly recycled variants, present challenges for manufacturing processes such as joining due to their material properties. To achieve lower weight, fewer parts, and reduced manufacturing complexity compared to conventional steel sheet parts, the use of aluminium cast parts has increased in recent years. As a result, Volvo Cars is developing its own cast parts, with future car bodies expected to incorporate large structural aluminium components, known as mega castings. Tesla pioneered this approach in the automotive industry, and several other manufacturers are actively investigating the concept.

Although cast aluminium parts have been used for decades, they were traditionally limited to smaller components in car body designs. In Sweden, car body structures have historically been steel-intensive, relying mostly on sheet materials. Steel sheet designs can be joined using well-established processes like resistance spot welding (RSW). However, cast materials exhibit different mechanical properties, requiring new approaches in manufacturing and design when introducing mega castings.

The as-cast properties of aluminium are strongly influenced by the microstructure formed during solidification. Without heat treatment, cast aluminium parts often exhibit low ductility, which poses challenges for mechanical joining processes. Heat treatment can improve ductility but is energy-intensive and costly, making it undesirable for large-scale automotive production. Consequently, manufacturers are developing primary aluminium alloys that achieve sufficient strength and ductility without heat treatment. However, these alloys exhibit significant property variations within a single casting due to differences in solidification rates between thin and thick sections. This variation, along with defects such as porosity or intermetallic phases in recycled aluminium, affects the performance of joining processes.

Mega castings reduce the number of joints in a vehicle, simplifying assembly, but the remaining joints become more critical in terms of structural integrity and crashworthiness. Selecting suitable joining technologies is crucial for integrating cast aluminium parts into vehicle structures while ensuring mechanical performance, process reliability, and compatibility with circularity goals. Mechanical joining methods are particularly promising for these applications, especially when cast parts need to be joined to high-strength steel or other dissimilar materials.

4 Purpose, research questions and method

4.1 Purpose:

The purpose of this project was to enhance the understanding of mechanical joining processes for cast aluminium components in automotive applications, with a specific focus on joinability, process robustness, and circularity.

The project aimed to:

- Identify key factors influencing joinability by analysing how microstructural variations and defects in cast materials affect the performance of Self-Piercing Riveting (SPR), Clinching, and Friction Drill Fastening (FDF).
- Develop and evaluate testing methods to characterize material properties relevant for mechanical joining, considering local variations inherent to casting processes.
- Optimize mechanical joining processes by defining process windows, analysing failure mechanisms, and improving joint quality based on experimental investigations and numerical simulations.

- Assess the feasibility of disassembly and re-manufacturing to support circularity in automotive manufacturing, exploring strategies for end-of-life separation and repair of joined cast components.

4.2 Research questions:

- What are the mechanisms for SPR, Clinching and FDF leading to faulty joints and how are they correlated with microstructural properties of the cast material?
- Which material properties can be used to evaluate joinability and how can these material properties be determined in cast materials where material variations are dependent on many other factors?
- Can numerical simulations be used to efficiently predict joinability, process robustness and optimise joining processes with consideration of material variations and statistical distribution of defects?
- How can joined cast parts be disassembled and re-manufactured and what determines the durability of re-manufactured joints?

4.3 Method:

The project was structured into five work packages (WP), each addressing different aspects of the investigation into the joinability of cast aluminium components. A combination of experimental methods, numerical simulations, and validation approaches was used to evaluate joinability, material properties, and process robustness.

Material Characterization and Test Specimen Preparation (WP1)
The project started with the selection and characterization of relevant cast aluminium materials. The "snake tool", a specially designed casting geometry, was used to produce specimens with controlled variations in mechanical properties. These specimens allowed for systematic assessment of material variability and its impact on joinability. As a demonstrator a real megacasting part, further referred to as soft tool floor, based on experimental castings from Volvo Cars was used in the project to investigate joinability on real production parts.

To characterize the materials, the following methods were applied:

- **Tensile testing** – to determine mechanical properties relevant for joinability.
- **Hardness measurements** – to assess local material variations.
- **Microstructural analysis (cross-sections and microscopy)** – to identify defects and microstructural features influencing joinability.
- **V-Bend testing** – to analyse porosity and internal defects.
- **Charpy testing –** to determine toughness.
- **Drop tower testing –** to determine impact response.

- **Pierce-Cupping-Test (PCT)** – A newly developed method to determine ductility of the material very locally

The materials were tested in cooperation with suppliers and Volvo Cars (VCC), which also provided production demonstrators (e.g., a spring tower) to validate the results.

Experimental Joining Investigations (WP2)
Mechanical joining processes—Self-Piercing Riveting (SPR), Clinching, and Flow Drill Fastening (FDF)—were experimentally evaluated to determine their suitability for cast aluminium components. Each process was studied in dedicated sub-work packages. The work included joining tests, process optimization and evaluation of the joinability according to requirements from Volvo Cars. The joining tests were conducted on snake tools as well as on soft tool floors.

Numerical Simulations for Joinability Prediction (WP3)
Key aspects of the numerical approach included:

- **Failure model adaptation** – incorporating material failure criteria to enhance prediction accuracy.
- **Elimination of remeshing issues** – improving numerical stability and reducing computational errors.
- **Statistical analysis** – studying material property variations and their effect on process robustness.
- **Component-level simulation** – considering fixture effects and global stiffness variations.

These simulations were validated using the experimental data generated in WP2.

Alternative and Innovative Process Investigations (WP4)
To address cases where mechanical joining processes exhibited limitations, WP4 explored alternative methods, such as:

- **Local heat treatments**
- **Tucker Plasma Joining –** A new process with integrated heat treatment
- **Investigations of fatigue properties of cracked joints –** These investigations were added to the project scope to give insight into the role of cracks in the joint button during fatigue loading. A master thesis study on this subject was conducted within the project.

Project Management and Dissemination (WP5)
WP5 covered project coordination, tracking of milestones, and dissemination of results.

This structured approach ensured that the project systematically investigated **joinability, material characterization, numerical prediction, and process optimization** for cast aluminium components in automotive applications.

5 Objective

This project focused on evaluating the suitability of three mechanical joining methods—Self-Pierce Riveting (SPR), Flow Drill Fastening (FDF), and clinching—for joining cast aluminium components. The primary aim was to assess how variations in cast material properties affected the robustness and performance of these joining processes.

The project investigated three key challenges:

1. Joinability of Mega Castings
The project investigated how local variations in the casting structure—such as microstructural inhomogeneities, porosity, and residual stresses—affected the mechanical joining process. The goal was to optimize joining parameters to improve process robustness and joint integrity for cast aluminium components.

2. Assessment of Material Properties
A key challenge was identifying reliable testing methods for characterizing the ductility of cast aluminium in a way that correlates with its behaviour during mechanical joining. The project evaluated different testing, and characterization approaches to determine their relevance for predicting joint performance.

3. Disassembly and Circularity
To support repairability and sustainable end-of-life strategies, the project explored whether the investigated joints allowed for non-destructive separation or efficient joint replacement methods. This included evaluating how the joining techniques influenced material recovery and recyclability.

6 Results and deliverables

6.1 WP1 Materials and test objects

In WP1 two components have been used as test objects, see Figure 1; a smaller test tool, henceforth referred to as snake tool and a demonstrator tool, a prototype car body component, henceforth referred to as soft tool floor. During the project, both objects in various alloys and thicknesses were used for various analyses and evaluation. Due to confidentiality, the exact alloying content is not published.

6.1.1 Test materials

Snake tool			
Version	Nominal thickness	Alloy	Variants
1.0	2.50 mm	Alloy 4	Casted using different MRA; 20B, 31A, 31B

1.2	3.00 mm	Alloy 4	
Soft tool floor			
Batch	Nominal thickness on investigated flanges	Alloy	Variants
9	3-4 mm	Alloy 4 (Hi Si)	Minor difference in alloy composition between batches Different injection velocities for batches
10	3-4 mm	Alloy 4 (Hi Si)	
11	3-4 mm	Alloy 4 (Hi Si)	
12	3-4 mm	Alloy 4 (Hi Si)	
13	3-4 mm	Alloy 4 (Hi Si)	
14	3-4 mm	Alloy 4 (Hi Si)	
15	3-4 mm	Alloy 4 (Hi Si)	
16	3-4 mm	Alloy 4 (Hi Si)	

Figure 1 CAD representation of snake tool (left) and soft tool floor (right). Not to scale.

6.1.2 Snake tool

6.1.2.1 Brinell hardness measurements

Brinell hardness measurements were taken from different specimens and different batches. There was no significant difference in Brinell hardness detected even between Start, Middle and End sections of the snake tool. This leads to the conclusion that Brinell Hardness measurement is not a meaningful test method to discern local material property variations in cast materials, where internal defects can affect ductility and material behaviour to a large extend.

6.1.2.2 Microstructural analysis

Microstructural analysis was conducted on the snake tools start, end and middle section. While middle section and start section showed similar microstructure, the end section

showed a significant higher number of shrinkage pores, especially in the edge regions. On the other hand, the microstructure and distribution of dendrites and silicon phases was much finer, see Figure 2 bottom, 500x magnification. Some round shaped intermetallic phases could be observed in all samples.

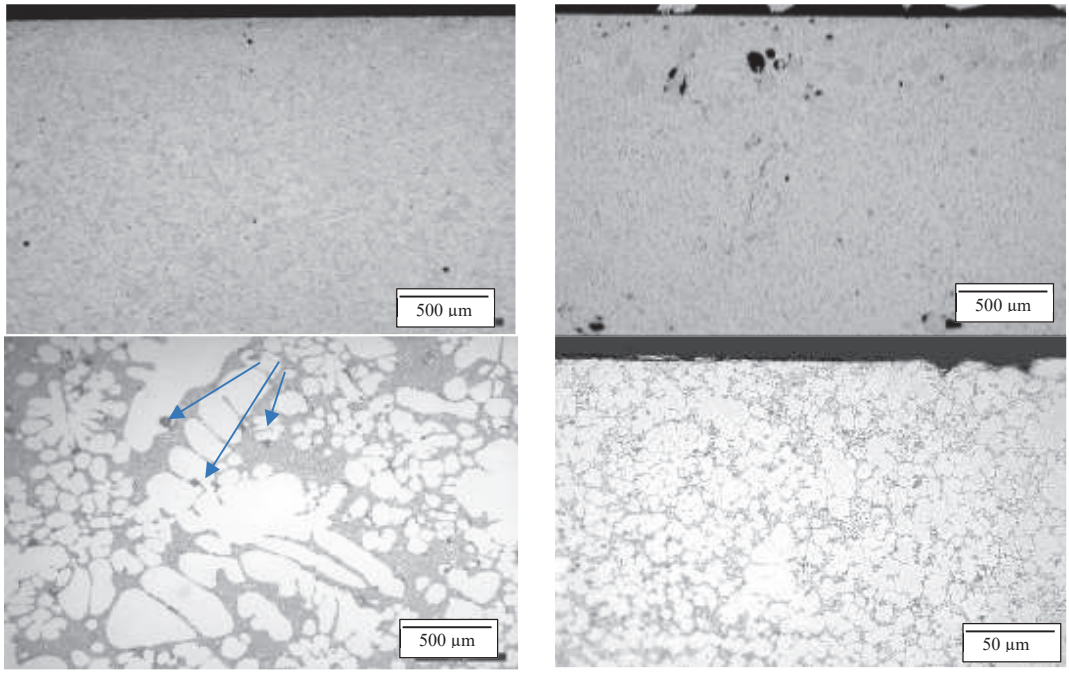

Figure 2 Micrographs from snake tool start (left) in 50x and 500x magnification and end section (right) in 50x and 500x magnification

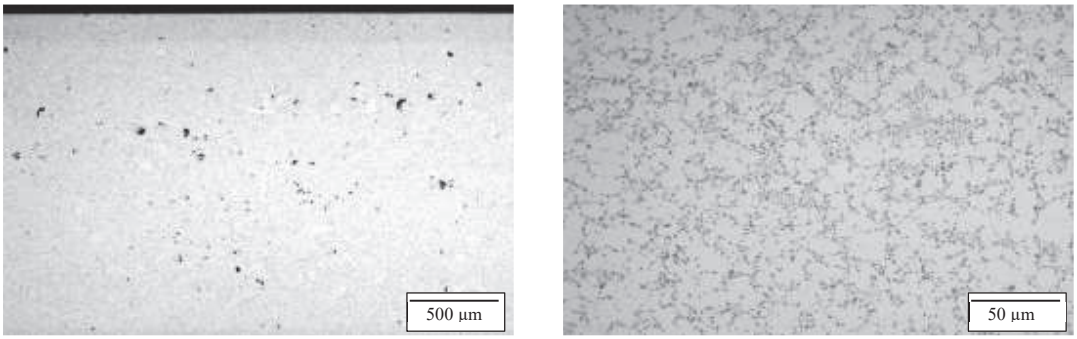

Figure 3 End section of the snake tool after heat treatment at 500C for 1h in 50x and 500x magnification

For investigation of the microstructure in the soft tool locations were chosen based on joinability in terms of crack severity in the joint button. The three locations with most cracking and three locations with lowest amount of cracking in the button were chosen and compared. When comparing those two groups it becomes clear that the major difference again can be seen in pore density. Locations that showed no or only a minor amount of cracking where almost pore free while locations where button cracking was observed show a higher pore density and larger pore sizes, with major shrinkage pores up to 800 µm in size.

Figure 4 Overview of 6 locations with lowest amount of cracking (left, green) and highest amount of cracking in joining tests (right, red) in 1,25x magnification

Dendrite size, distribution of silicon phases and intermetallic phases showed only minor differences (see Figure 5). A quantitative analysis was not conducted. The intermetallic phases show a rother round shape, analogous to the observations from the snake tool analysis.

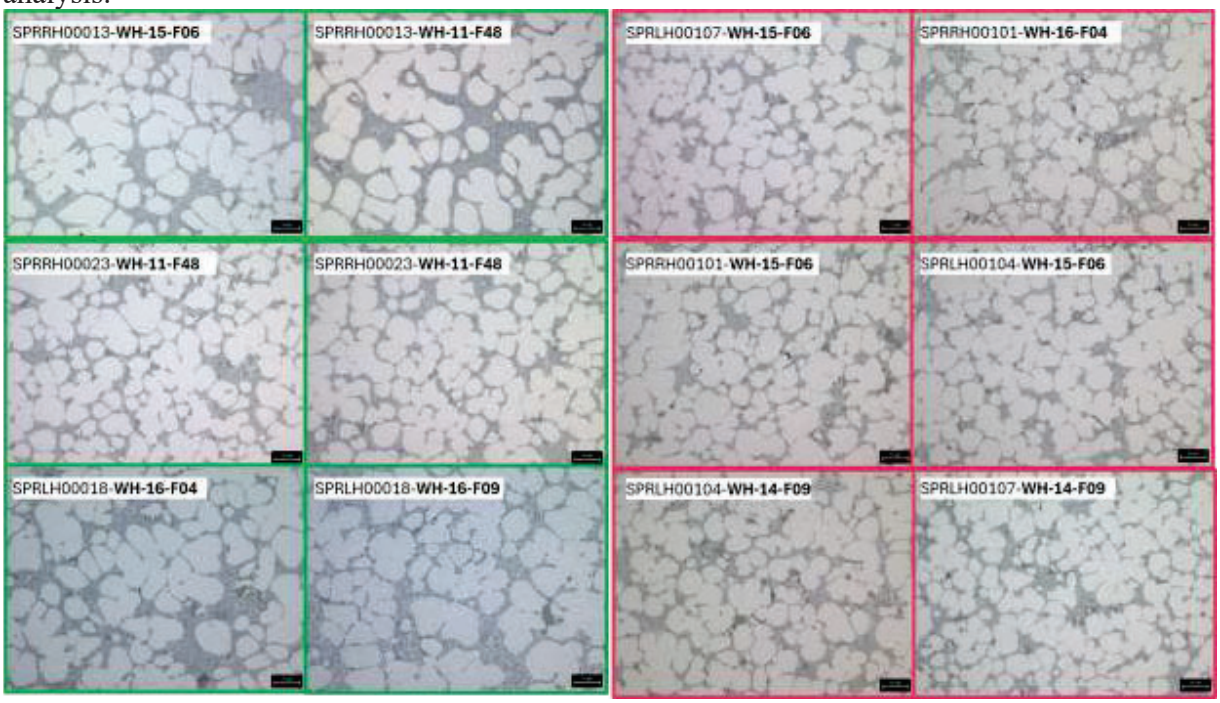

Figure 5 Microstructure of 6 locations with lowest amount of cracking (left, green) and highest amount of cracking (right, red) in 50x magnification

Microstructural investigations of both the snake tool and the soft tool floor reveal significant differences in material properties that can impact mechanical performance. The snake tool exhibits variations in dendrite formation and silicon distribution, with coarser structures at the Start and finer ones toward the End. The main distinction is the pore density, which influences the formation of cracks, particularly in the End sections. Minor intermetallic inclusions with a favourable round shape were observed, which likely have a lesser impact on mechanical properties. Heat treatment was found to refine the silicon structure, softening the material and reducing the risk of cracking during joining. Crack severity in joint buttons appears to correlate with the local pore distribution. It is assumed that these pores will lead to stress concentrations during the forming step of the SPR process. More ductile base material, e.g. resulting from postproduction heat treatment (softening treatment) are probably able to reduce stress concentrations around pores by local plastic deformation and therefore a beneficial effect of the heat treatment on reducing cracks in the joint button is observed.

The soft tool floor, in contrast, demonstrated a more homogeneous microstructure, with uniform dendrite and silicon morphology. However, a high pore density was observed in the flange areas, where severe joint button cracking was observed. Additionally, pores along the edges indicate a high risk for crack initiation, which can compromise joinability. Despite minor intermetallic inclusions with favourable shapes, the presence of pores remains the dominant factor affecting failure mechanisms.

6.1.2.3 Chemical analysis

Spectral analysis of the chemical composition of snake tools manufactured with different MRAs (mould release agents) were conducted. No significant differences between those samples could be observed. Due to confidentiality, the exact chemical composition of the material and specifications of the MRAs are not published in this report.

6.1.2.4 Tensile testing:

The mechanical testing was conducted on tensile specimens machined from two different material batches, 20B and 31B, which had been treated with distinct release agents to assess their influence on material properties and joinability.

Sample Preparation

The test specimens were extracted from a snake tool casting, which allowed for systematic sampling across different regions of the cast part to capture property variations. From each casting (snake tool), a total of nine specimens were prepared, with three taken from each of the following segments:

- First segment (start) – S1, S2, S3
- Second segment (middle) – M1, M2, M3
- Third segment (end) – E1, E2, E3

This segmentation ensured that the local material variations within the casting could be studied systematically. The specimens were extracted transversal to melt flow direction according to Figure 7.

Mechanical Testing

The tensile tests were conducted using a Sintech 20/D servo-electric test machine equipped with a 100 kN load cell (see Figure 6). The tests were performed under controlled displacement conditions with:

- A displacement rate of 1 mm/min
- A grip pressure of approximately 5 bar

Digital Image Correlation (DIC) Analysis

To capture strain evolution and local deformations during loading, a GOM ARAMIS 12M Digital Image Correlation (DIC) system was utilized. The ARAMIS 12M system, equipped with a 12-megapixel camera, acquired images at a frequency of 0.5 Hz throughout the test.

This setup allowed for precise strain field measurements and the detection of inhomogeneous deformation behaviour, particularly in relation to microstructural variations and defect distributions in the cast material.

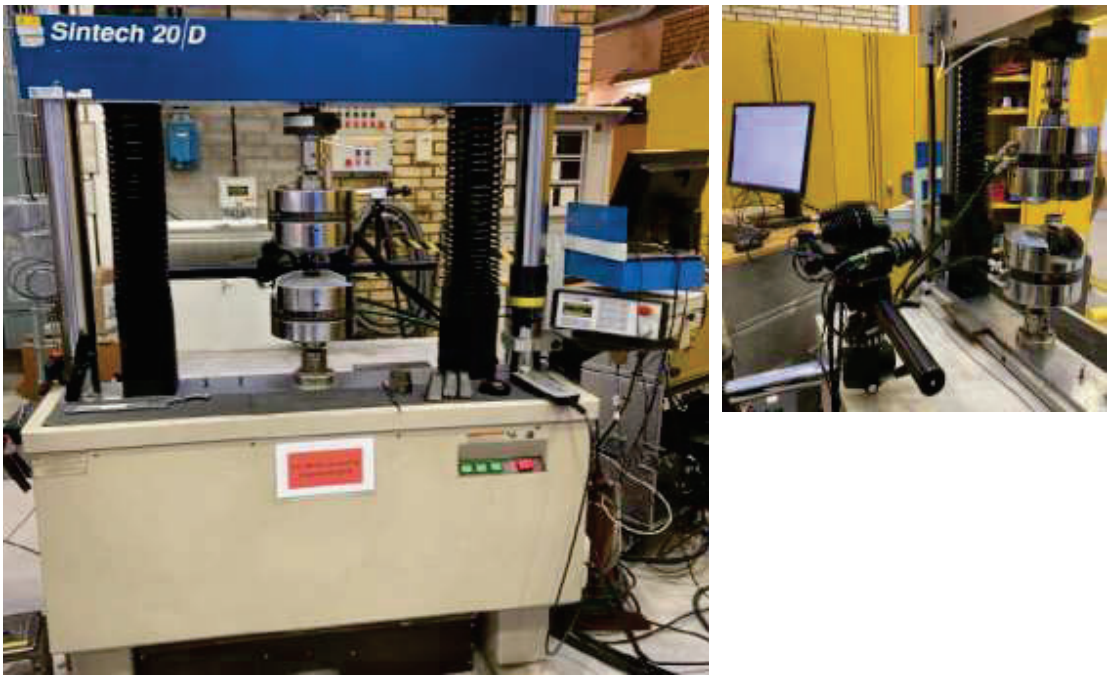

Figure 6 Test-setup for tensile testing with DIC

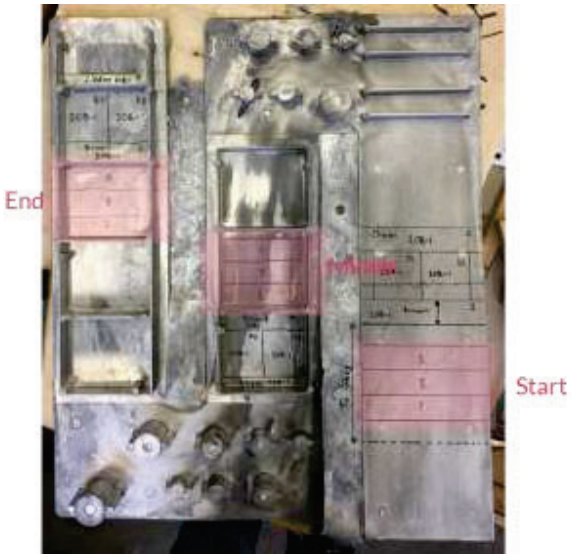

Figure 7 Specimen extraction plan for snake tool 20B-1 and 31B-1

Results and analysis:

Figure 8 shows the stress-strain diagrams measured by DIC. The test curves showed some various in tensile strength and elongation to failure as expected for cast materials. The specimens taken from the end section of the snake tool showed the values in elongation to failure and highest elongation to failure in the start section in both snake tools. However, only in snake tool 31B-1 the tensile strength was significantly reduced for the end section

specimens. Also, the standard deviation for elongation to failure was much smaller in 31-B-1 for the end section.

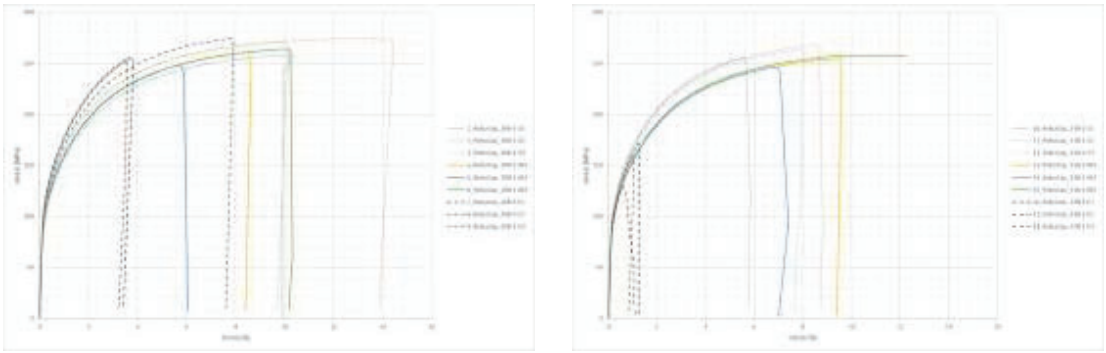

Figure 8 Stress-strain diagramms: Specimens from snake tool 20B-1 (left) and 31B-1 (right)

Figure 9 shows the average elongation to failure and tensile strength for the tested specimens. No consistent difference between the elongation to failure for the Start and Middle section of the snake tool was observed. However, the elongation to failure in the Start section of snake tool 31B-1 was significantly lower than the one for snake tool 20B-1. Only snake tool 31B-1 showed a significant lower elongation to failure in the End section with an correlating reduction in ultimate tensile strength.

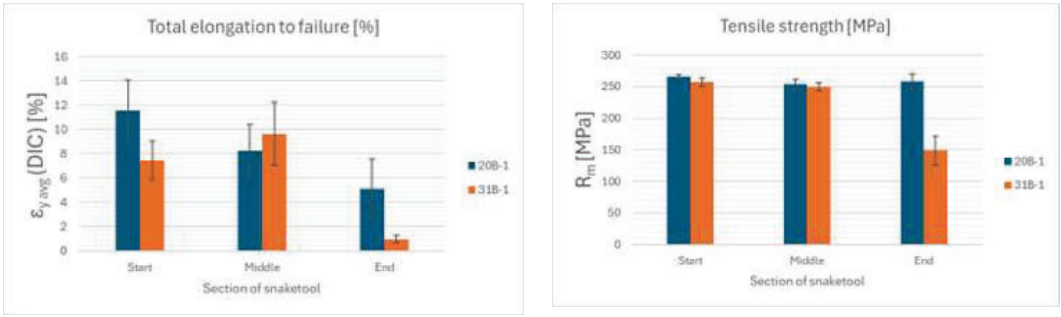

Figure 9 Total elongation to failure ($\varepsilon_{Y\,avg}$) and tensile strength of the tested specimens

Figure 10 shows the average elongation to failure for each specimen.

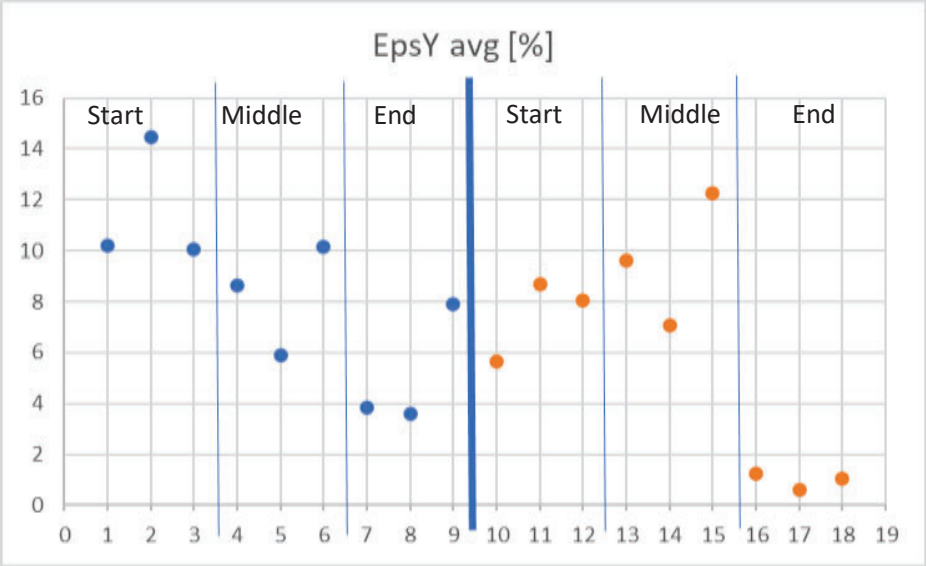

Figure 10 Total strain to failure (EpsY avg [%]) of each specimen tested. Snake tool 20B-1 (left, blue points) and 31-B1 (right, orange points)

Figure 11 shows DIC measurements visualizing strain localizations in loading direction (ε_y), where red represents higher elongation values and blue lower elongation values. The strain localisations in specimens from Start and Middle section, showed in general a slightly more homogeneous distribution of the strain over the measurement section, however also the End section of snake tool 20B-1 showed similar strain distributions to the Start section. In 30B-1 the strain localisations are much more localized and distributed over the specimen, leading to the conclusion that the defects in this specimen group were much higher and explaining the comparatively low elongations to failure and tensile strength.

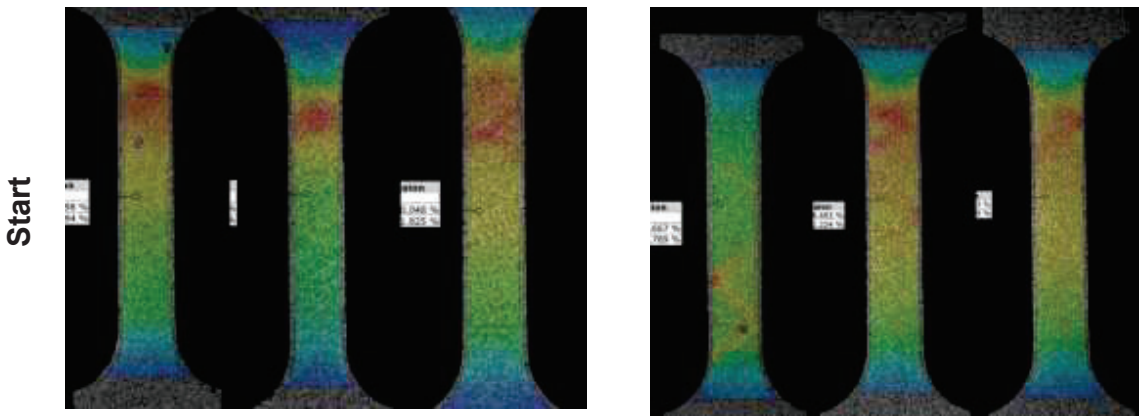

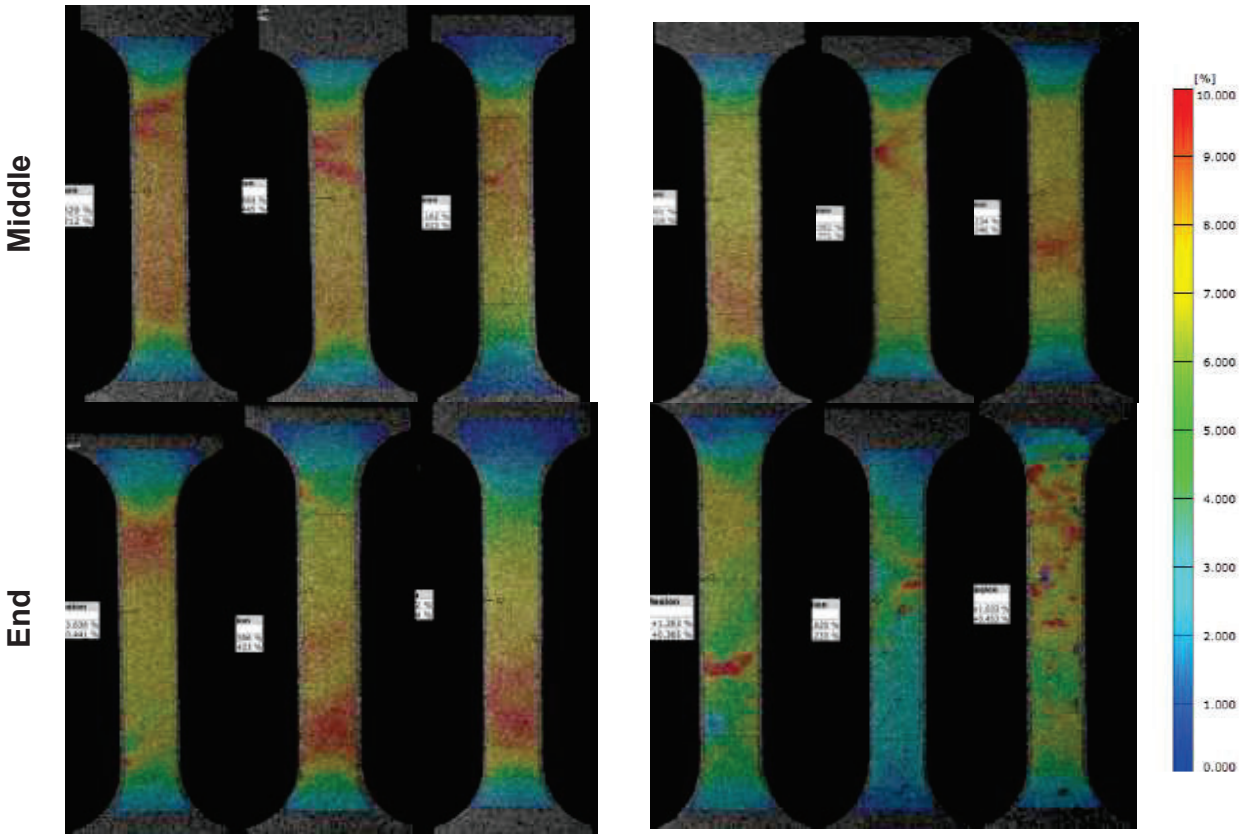

Figure 11 DIC strain distribution eps_y in specimens from snake tool 20B-1(left) and 31B-1(right)

The fractographic analysis (Figure 12 and Figure 13), revealed pores as crack intuition sites the samples.

Figure 12 Fractographic analysis of samples from start area in 20B-1

Figure 13 Fractographic analysis of samples from start area in 31B-1

Tensile tests on soft tool floor

Tensile tests have been conducted by Volvo Cars accompanying their casting trials. In total 13 positions of the snake tool have been investigated, and test series were conducted on different batches of castings. Elongation to failure varied widely between 1.9% to 15.7%. This highlights the challenges with cast aluminium parts in general where large variations stemming from internal defects and microstructural differences can occur.

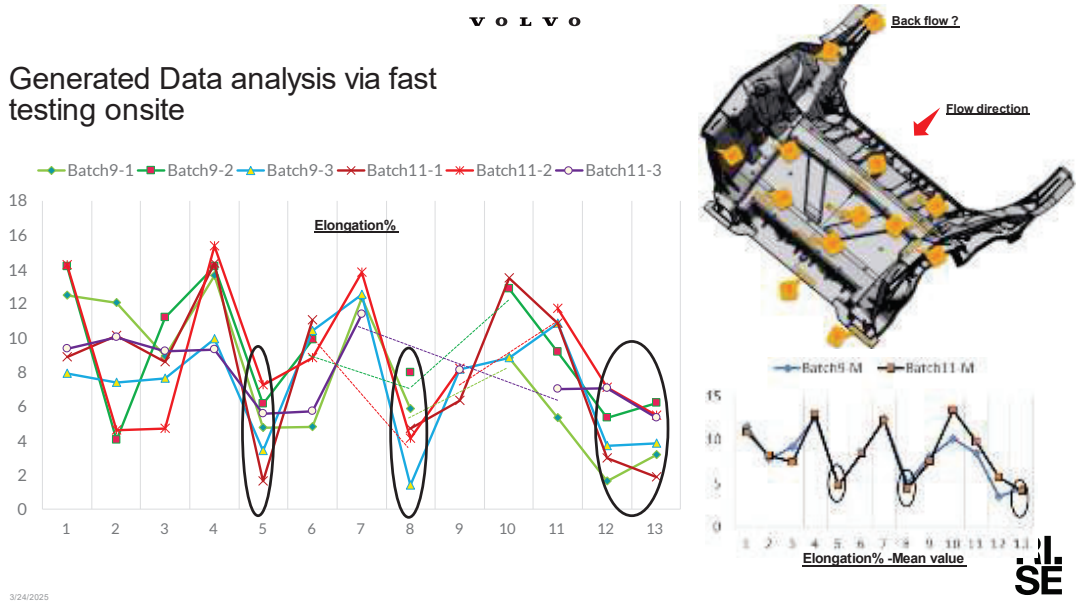

Figure 14 Elongation at failure values at different locations and different batches of the soft tool floor

6.1.2.5 Drop tower tests

Drop tower testing (without further instrumentation) is a simple method to qualitatively check for differences in the impact response of different materials. In this project it was used to see if this method can be sensitive to local differences in cast aluminium and give conclusions about the materials ductility with a rather high deformation velocity, reflecting the forming velocity in SPR or clinching processes.

For these investigations a steel ball with a weight of 1.3 kg and radius of 10 mm was dropped from a height of 0.75 m resulting in a impact energy of 9.56 J. Rectangular samples were prepared from the start of the snake tool (Position 1), start of the end section (Position 4) and end of the end section (Position 7). The experiments were conducted on a snake tool version 1.0 with 2.5 mm thickness. Material deformation and cracking were investigated on the bottom side of the samples.

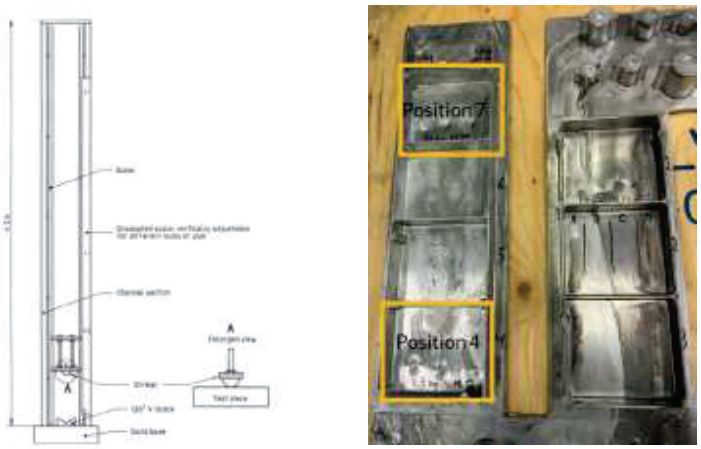

Figure 15 Schematic test setup and tested regions of the snake tool (Position 1 was located at the very start of the snake tool)

Three tests were performed transversal to flow direction. The resulting deformation and cracking is shown in Figure 16. A significant difference between the impact damage was observed between start and end of the snaketool. Slighter more pronounced cracking in the center of position 4 and position 7 was noted and increased with distance to the ingate of the casting. Position 1 showed only minor deformation but no visible cracking of the casting.

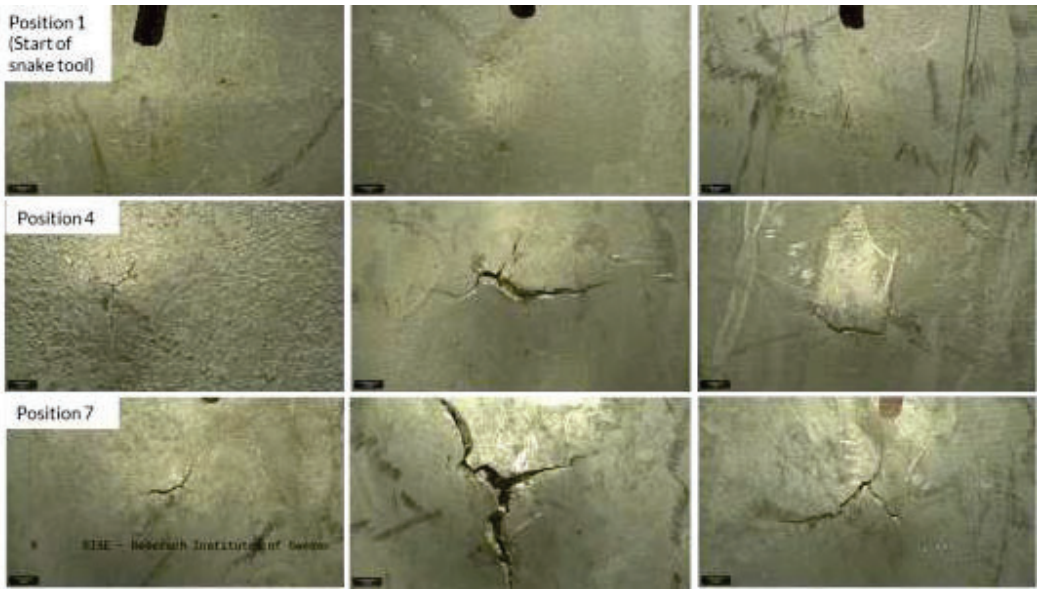

Figure 16 Cracking pattern on snake tool after PCT trials

6.1.2.6 V-bend test

Bending tests play a critical role in evaluating ductility and cracking behaviour. In a three-point bend test, a load is applied at the midpoint of a supported sample until it either reaches a predetermined angle or fractures. The criteria for failure are typically based on the presence, size, and frequency of cracks on the outer surface, as specified by the relevant material standards or end-user requirements. Various factors influence the outcome of this test, including the distance between supports, the radius of the indenter (often referred to as the punch), the final loading angle, and the crack size and frequency that indicate failure.

All tests were performed on a Shimadzu Universal Testing Machine equipped with a 50 kN load cell, using a three-point (V-bend) configuration that featured a 0.40 mm punch radius to concentrate bending stress at the specimen's midpoint. The machine's software (Trapezium) continuously recorded load and displacement data, enabling precise calculation of bending angles and monitoring of crack initiation and propagation. The samples from the start, middle, and end sections of each snake tool batch were placed on fixtures (rollers) and subjected to a pressing speed of 5 mm/min until visible cracking occurred. For each batch, 3-4 samples were tested per location to ensure consistency.

Figure 17: V-bend setup

In automotive applications, the VDA238-100 test specification has gained prominence due to its stringent guidelines on sample dimensions, punch tip radius, roller spacing, and roller radius. These parameters help reduce variability and ensure consistent, reliable test results. Adjustable support rollers, arranged according to VDA 238-100 standards, ensured proper spacing and alignment for consistent bending conditions. This study focuses on V-bend tests performed on three batches of a "snake tool" (Batch numbers: 71A 4072 2784, 71A 4086 2797, and 71A 4053 2767) to assess material ductility at the Start, Middle, and End positions of each tool. The main objective was to investigate the cracking behaviour of the material under bending stress in accordance with the VDA 238-100 standard. Bending angles were calculated in line with ISO 7438 to ensure standardized measurements.

Figure 18 Start (S), Middle (M) and End (E) section of snake tool

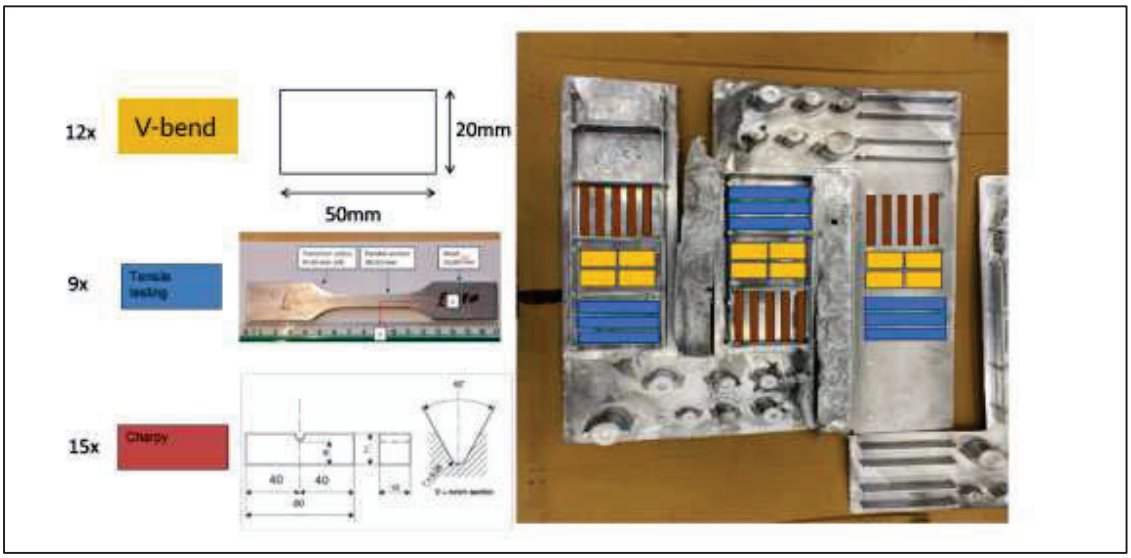

Figure 19 Samples for the V-bend test were collected from this specific location on the snake tool.

Results and Analysis:

Batch 71A 4072 2784:

- Start section cracked at 1835.23 N to 1983 N. The displacement ranges from 4.93 mm to 5.36 mm.
- Middle section cracked at 2184 N to 2522 N, indicating superior strength. The displacement ranges from 3.40 mm to 5.28 mm.
- The end section cracked at 1911 N to 1979 N. The displacement ranges from 3.50 mm to 5.11 mm.

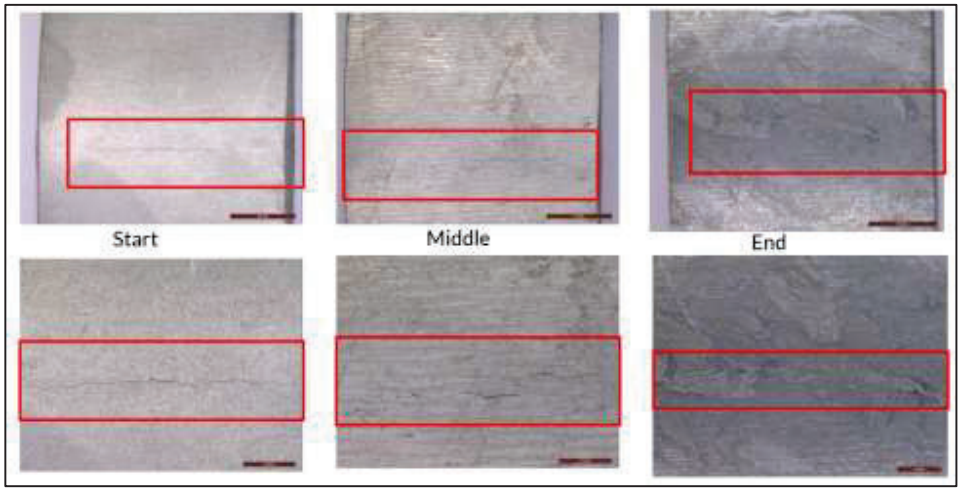

Figure 19 Crack formation in Start, Middle, and End sections of 71A 4072 2784 snake tool batch after V-Bend test

Batch 71A 4086 2797:

- Start section cracked at 1743 N to 1929 N. The displacement ranges from 4.89 mm to 5.36 mm.
- The middle section cracked at 1945 N to 2259 N, again showing the best ductility. The displacement ranges from 3.40 mm to 5.00 mm.
- The end section cracked at 1754 N to 1996 N. The displacement ranges from 4.00 mm to 5.37 mm.

Figure 20 Crack formation in Start, Middle, and End sections of 71A 4086 2797 snake tool batch after V-Bend test

Batch 71A 4053 2767:

- Start section cracked at 1729 N to 1926 N. The displacement ranges from 5.61 to 5.97 mm.
- The middle section cracked at 1707 N to 2245 N. The displacement ranges from 3.00 to 5.40 mm.
- End section cracked at 1839 N to 1918 N. The displacement ranges from 4.10 mm to 5.10 mm.

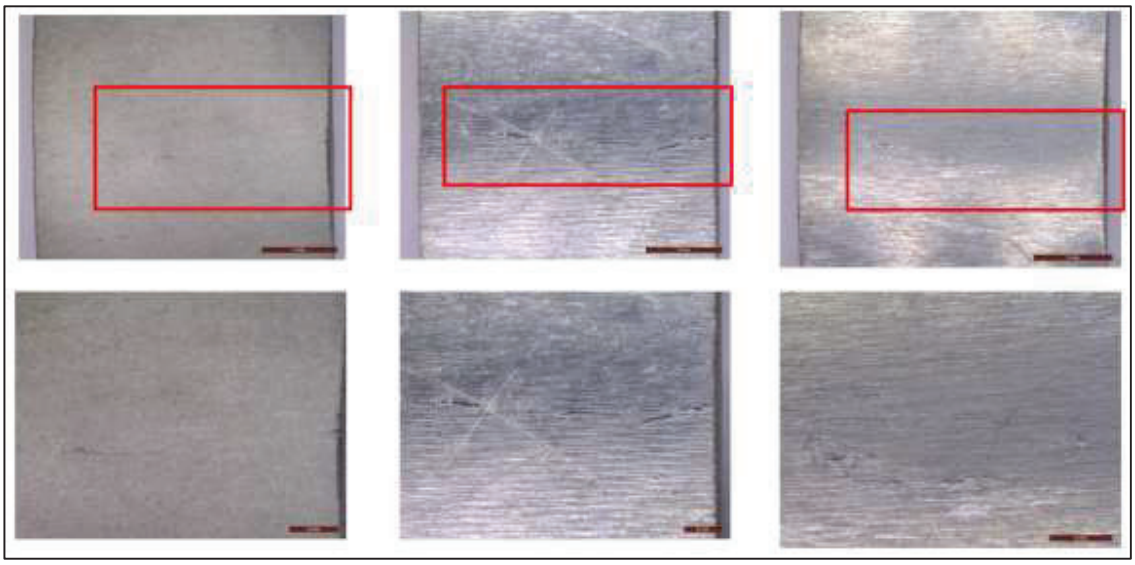

Figure 21 Crack formation in Start, Middle, and End sections of 71A 4053 2767 snake tool batch after V-Bend test

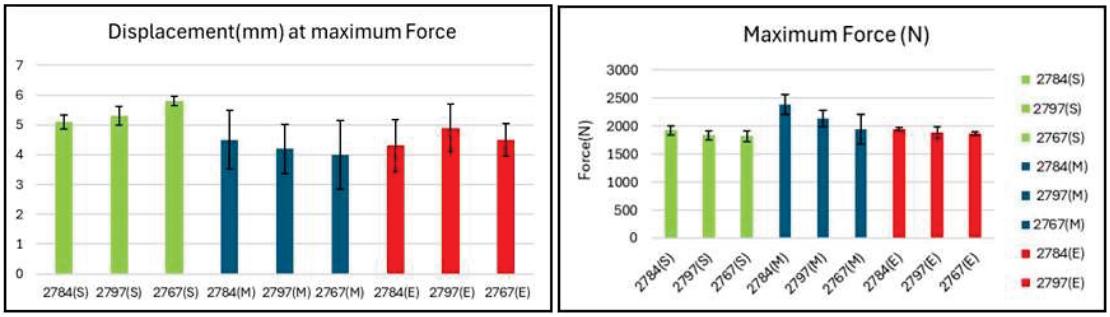

Figure 22 Maximum displacement (left) and force (right) by batch and section (Start, Middle, End) of the snake tool.

Bending angle calculation:

The bending angle for each sample was determined according to ISO 7438 by measuring the displacement at maximum applied force during the V-bend test. Across all three snake tool batches (71A 4072 2784, 71A 4086 2797, and 71A 4053 2767), the calculated angles were based on the actual thickness of the material. The overall differences among start, middle, and end positions were small relative to the standard deviations, suggesting generally consistent material properties along the tool's length.

Snake Tool	2784(S)	2784(M)	2784(E)
Bending angle average (degree)	32.7	29.3	27.5
std. dev	1.6	6.9	6
Snake Tool	**2797(S)**	**2797(M)**	**2797(E)**
Bending angle average (degree)	34.2	26.3	31.5
std. dev	2.2	5.7	5.4
Snake Tool	**2767(S)**	**2767(M)**	**2767(E)**
Bending angle average (degree)	37.6	25.7	29
std. dev	1.2	7.9	3.8

Table 1 Calculated Bending Angle according to ISO 7438 standard

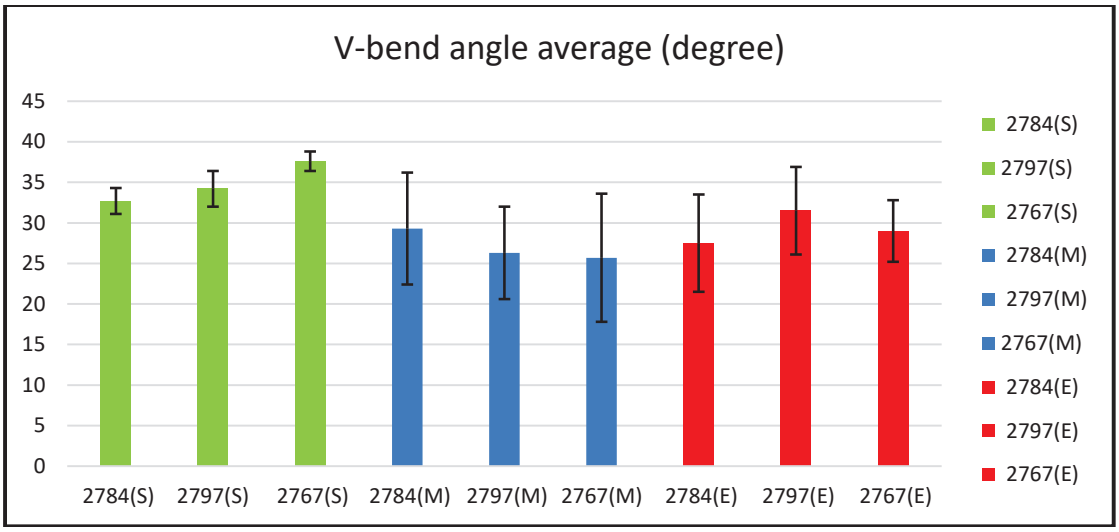

Figure 23 Calculated V-bend angle according to ISO 7438

Conclusion:

There was a slight variation in the measured material thickness between Start, Middle and End of the snake tool—despite a nominal thickness of 3 mm. The material thickness for each sample was included in the calculation of the bending angle. In all three snake tools, the Middle section exhibits the lowest bending angle, this indicate that cracking occurs earlier in these specimens, suggesting reduced ductility in that region. Although the differences in thickness between Start, Middle and End section are not significant, it is noteworthy that the start section exhibited a substantially lower standard deviation, indicating more consistent performance and better bending capability. The Middle and End sections demonstrated lower ductility.

6.1.2.7 Charpy Test

The Charpy test is performed to evaluate the toughness of a material—specifically, its ability to absorb energy during an impact. This test provides a quantitative measure of the material's resistance to sudden fracture or cracking under dynamic loading conditions. This information is particularly valuable for quality control and material selection in applications where durability and resistance to brittle failure are critical.

The Charpy test was conducted in accordance with ASTM D6110 on snake tool batches (71A 4053 2767, 71A 4086 2797, and 71A 4072 2784). The experimental setup utilized a hammer with an energy of 4 J (loss energy: 0.02 J; Hammer code: 7600.004), and specimens were prepared from the Start, Middle, and End sections of each batch. Three replicates for each specimen were tested to ensure consistency in the measurements of absorbed energy.

Figure 24 Charpy test setup

Results and Analysis:

Overall, the results (see Table 2) revealed a consistent trend across all batches: specimens from the Middle section exhibited the highest percentage of maximum energy, RE value (% shear fracture), and absorbed energy—indicating greater toughness and higher ductility. This was followed by the Start section, while the End section showed significantly lower toughness, as reflected in the lower values for all three parameters. As previously noted, the slightly increased thickness in the Middle section compared to the Start and End may have contributed to these results. Therefore, the impact strength ($J/mm^{2)}$ was calculated to allow for comparison (Figure 26). The impact strength is calculated by dividing the absorbed energy by the cross-sectional area at the notch of the specimen. ($J/mm^{2)}$.Even this comparison suggests that variations in ductility and energy absorption capacity along the snake tool are minor, but with consistently lower impact strength of the end sections and higher impact strength of the Middle section of the snake tool.

Table 2 Charpy test results

Snake tool	Absorbed energy (J)	Std dev (J)	Impact strength (J/mm^2)	Std dev (J/mm^2)
71A 4086 2797-S	2.3	0.1	0.07	0.003

71A 4086 2797-M	2.4	0.5	0.08	0.001
71A 4086 2797-E	2.1	0.19	0.07	0.006
71A 4072 2784 -S	2.4	0.03	0.08	0.001
71A 4072 2784 -M	2.56	0.18	0.08	0.006
71A 4072 2784 -E	2.1	0.19	0.06	0.005
71A 4053 2767 -S	2.29	0.11	0.07	0.003
71A 4053 2767 -M	2.53	0.29	0.08	0.009
71A 4053 2767 -E	2	0.17	0.06	0.005

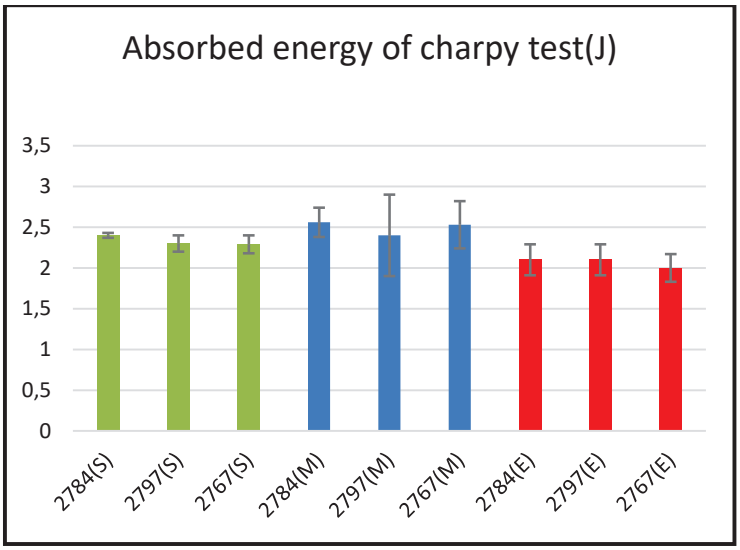

Figure 25 Charpy test results

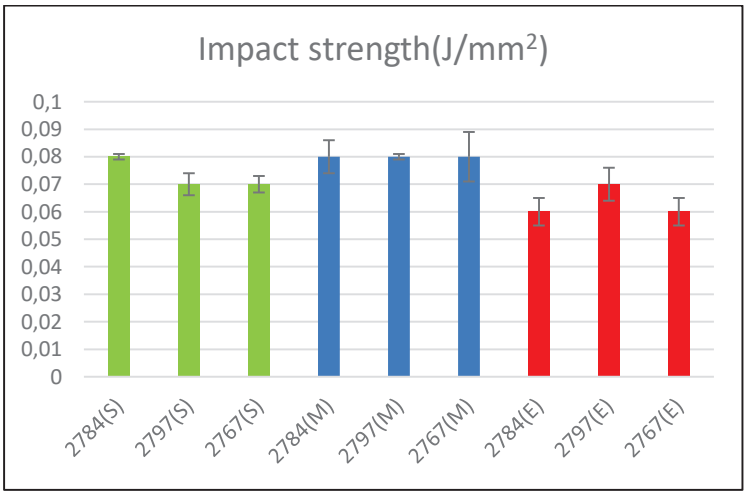

Figure 26 Charpy test results

6.1.2.8 Pierce cupping tests (PCT)

The development of the Pierce-Cupping Test (PCT) originated from the need to evaluate the local ductility of cast aluminium in a manner that reflects the actual conditions

experienced during SPR. The PCT is used to evaluate the joinability of the material by assessing its local ductility and crack susceptibility.

In contrast, traditional mechanical tests such as tensile and bending are typically destructive and rely on relatively large testing areas, which do not accurately capture the localized variations in ductility that arise from differences in alloying elements, manufacturing processes, and part geometry. Recognizing that ductility decreases with distance from the inlet and can be significantly influenced by local defects, the PCT was conceived as a method to measure ductility very locally using an indentation approach that simulates the geometrical conditions of the SPR process.

The test is designed to minimize material preparation requirements while providing reliable data on mechanical properties. The test is conducted using a tensile testing machine equipped with a 50 kN load cell. A cylindrical punch with a diameter of 5 mm is used to apply force to the material, while a die with a 10 mm diameter and a depth of 2.4 mm supports the sample. The test is performed at a crosshead velocity of 2–3 mm/min to ensure controlled deformation. During the test, a force-displacement curve is recorded, capturing the material's response until a force drop occurs at crack initiation. The key evaluation parameter is the displacement at the maximum force (d_{Fmax}), which serves as an indicator of the material's ductility and its susceptibility to cracking. A higher displacement at F_{max} suggests greater ductility, while lower values indicate a higher tendency for cracking.

The PCT method provides a fast and efficient method for evaluating local mechanical properties with minimal sample preparation. Additionally, it can be performed directly on components with minimal damage, making it a nearly non-destructive testing method. The strong correlation between PCT results and joining performance (c.f. Figure 34) makes it a valuable tool for assessing the suitability of cast materials for mechanical joining applications.

By performing indentations at multiple locations along a snake tool sample—typically at the start, middle, and end sections—the test can reveal variations in ductility within a single component and achieving an accurate, localized assessment of material ductility in cast aluminium parts.

Figure 27 PCT setup, with cylindrical punch and die with d= 10mm, t = 2,4 mm.

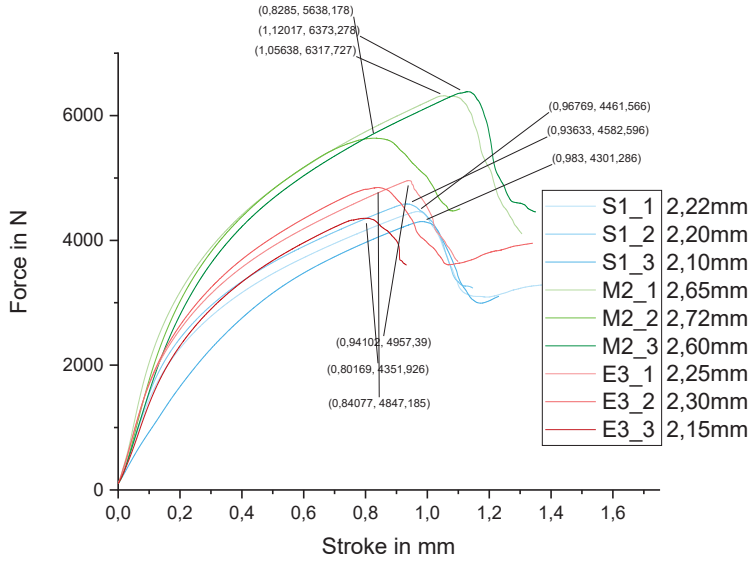

Figure 28 Example of force displacement curve and values

6.1.2.9 Crack investigations at different displacement levels

This test was carried out on a new batch of snake tool material (Batch No: 71A 4070 2782) to assess its ductility and failure characteristics across various displacements. The thickness variation among the snake tool must be mentioned. The Middle section was on average around 0.5 mm thicker than the End and Start sections. Evaluations were conducted at three

specific locations on the material: the Start, Middle, and End sections. For each of these regions, displacements ranging from 0.6 mm to 2.0 mm were applied, and the corresponding material deformation and cracking behaviours were meticulously documented.

Results and Observations

Crack Initiation at Different Locations:

- The material at the Start section exhibited cracking at 1.4 mm displacement.
- The material at the Middle section began to crack at 1.3 mm displacement.
- The material at the End section started cracking at 1.2 mm displacement.

Ductility Variation:

- The Start section demonstrated the highest ductility, sustaining more deformation before cracking.
- The Middle section followed, cracking slightly earlier than the Start.
- The End section exhibited the least ductility, failing at the lowest displacement.

Crack Formation:

- No small cracks were observed prior to failure.
- When cracks appeared, they were 360-degree cracks, leading to complete displacement of the buttons.

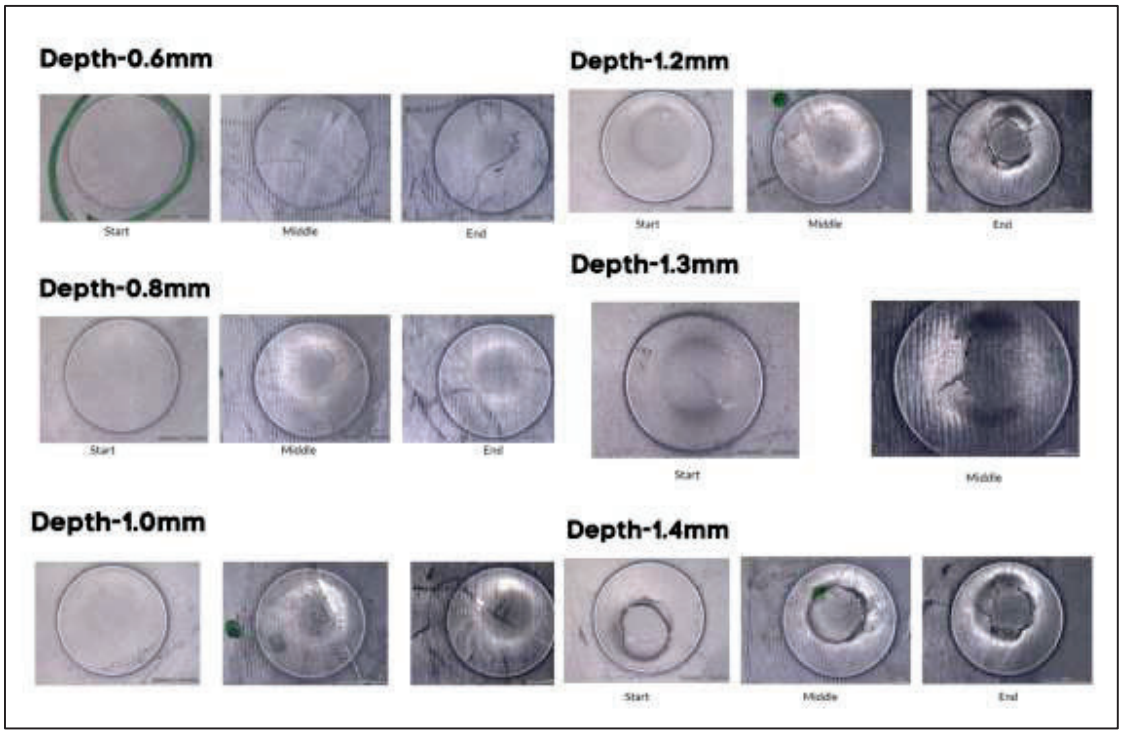

Figure 29 For the start, middle, and end points, displacements ranging from 0.6 mm to 1.4 mm were applied, and the corresponding material deformation and cracking behaviors were observed under a microscope.

Ductility mapping on snake tool by utilizing PCT

The PCT enables a high-resolution in characterization of material ductility. This has been exemplified using a snake tool (71A 4069 2781), where 120 measurement points were taken both longitudinally and transversely to the flow direction (see Figure 30).

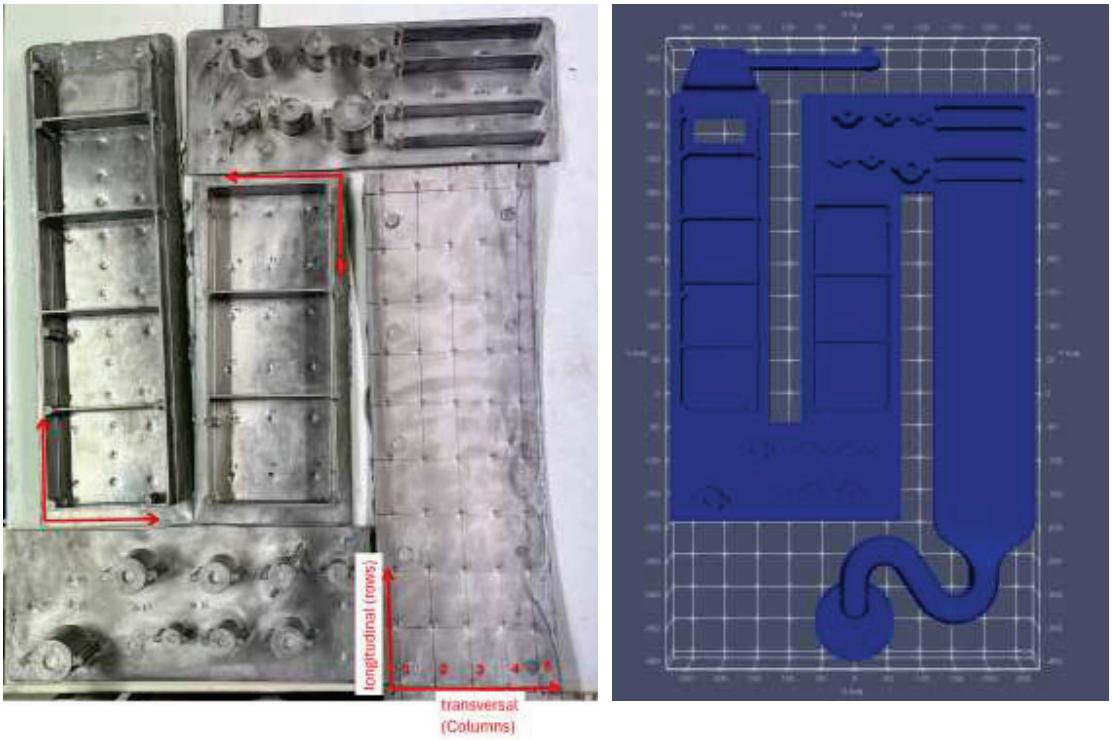

Figure 30 left: Tested snaketool (71A4069 2781) with 122 measurement points; right: Nominal geometry (CAD)

Figure 31 shows a visualization of the measurement points in a colour scale from red ($d_{PTC,Fmax}$ = 0.7 mm) to blue ($d_{PTC,Fmax}$ = 1.7 mm). The measurement points were then mapped to the complete geometry using Paraview's PointDataSetInterpolator filter with a Voronoi interpolation kernel to visualize the anticipated ductility distribution over the snake tool.

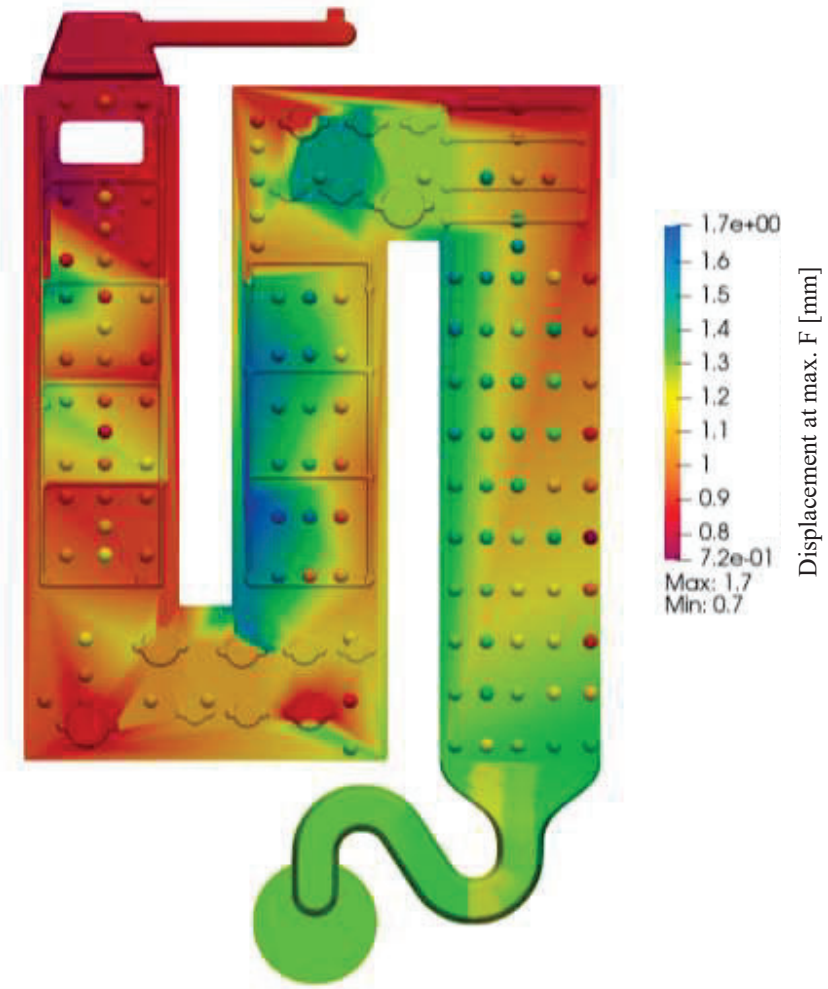

Figure 31 Visualisation of the measured displacement values in PCT with interpolation between measurement points

Figure 32 illustrates the displacement at F_{max}, measured and plotted transversally to the melt flow direction. The data is presented for Rows 1–5 in the start section and Rows 1–3 in the middle and end sections.

A consistently lower displacement value was observed in Row 5, indicating reduced ductility at one edge of the snake tool. This corresponds with visible differences in the casting surface, where Row 5 exhibited a noticeably rougher surface quality. More generally, these surface irregularities were found to correlate with lower displacement values in the middle and end sections as well.

Figure 33 shows the measured displacement values at F_{max} (dFmax) longitudinal to the melt flow direction. It can be observed that the measurement values are on average very similar in start and middle section of the snake tool and decrease in the end of the snake tool. Within the sections the values are rather stable with the exemption of the local variation's

transversal to the flow direction. The center (Column 2) of the end sections showed somewhat more variation.

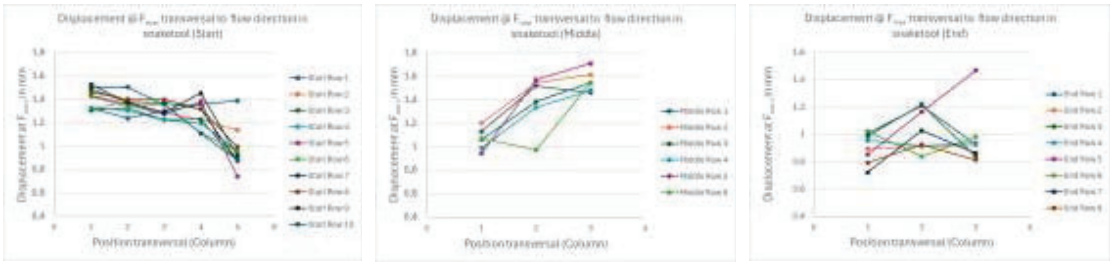

Figure 32 Displacement at F_{max} transversal to flow direction in snaketool a)Start b)Middle c)End

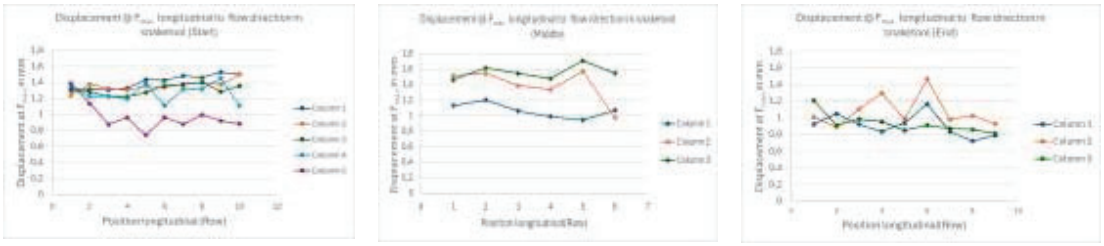

Figure 33 Displacement at F_{max} longitudinal to flow direction in snaketool a) Start b) Middle c) End

Correlation between PCT results and joint button cracking

Snake tool

To investigate the sensitivity of the ductility data measured by PCT, several positions of the same snake tool were riveted with a rivet-die combination that previously showed good sensitivity to the material changes in the snake tool, meaning that more cracks in the joint bottom are observed when ductility is anticipated to be lower (end section) and less cracks when ductility is better (start section). Fig K shows the joining locations in reference to the PCT mapping. It is clearly visible that joints placed in areas with values of dFmax > 1.3 mm show no cracking while with values < 1.1 mm cracking occurs. The threshold for cracking is of course depending on the chosen rivet-die combination which determines the actual process window.

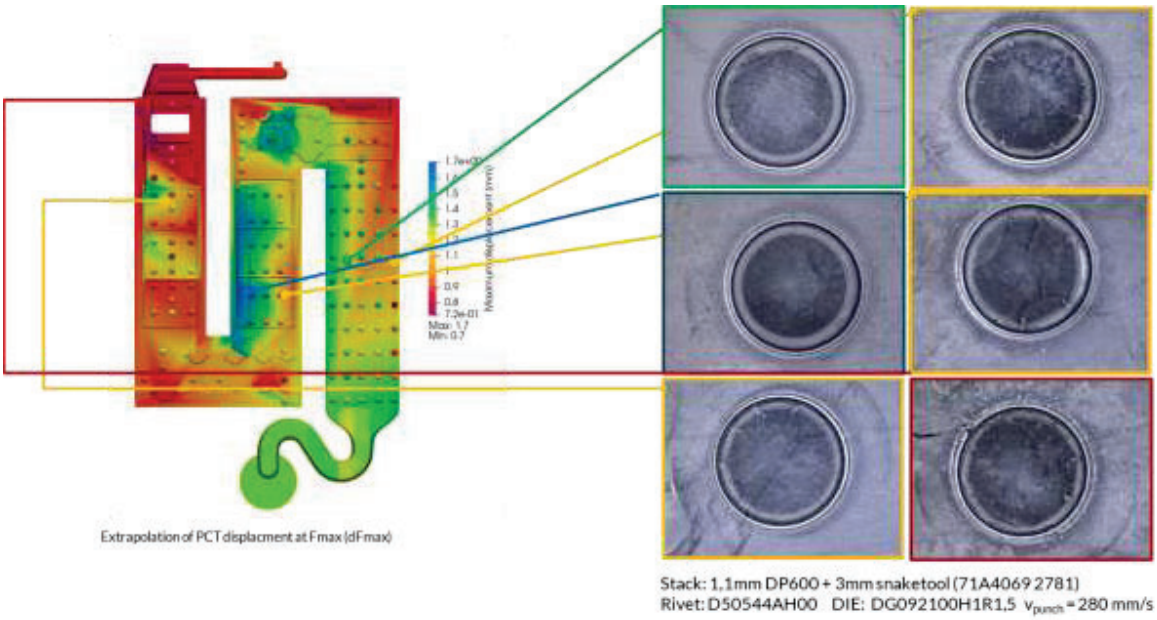

Figure 34 Mapping of PCT results on snake tool and examples of PCT cracking results

6.1.3 Soft tool floor

From the microstructural investigations, mechanical testing and joining tests it was concluded that pore density in the material has a major influence on ductility and joinability in terms of joint button cracking. The worst and best joint locations have been selected and tested with PCT to investigate the sensitivity and relevance of PCT testing values (mainly d Fmax) to joinability on the soft tool floor. Table 3 gives an overview of the investigated soft tool floors and SPR joint positions. Figure 35 shows the joining position of the most and least severe cracking areas on the soft tool floor.

Table 3 Summary of defects in cast aluminium material near selected SPR joint locations in soft tool floor

Soft tool floor batch	SPR position	Crack severity	Porosity
WH16_F04	SPRLH0104	3,67	Major shrinkage pores
WH14_F09	SPRRH0101	3,07	Large shrinkage pores
WH16_F04	SPRLH0107	3,47	Major shrinkage pores
WH11_F02	SPRRH0023	1,47	Small shrinkage pores at edge
WH09_F11	SPRLH0018	0,70	Almost no pores
WH14_F09	SPRRH0017	0,83	Almost no pores

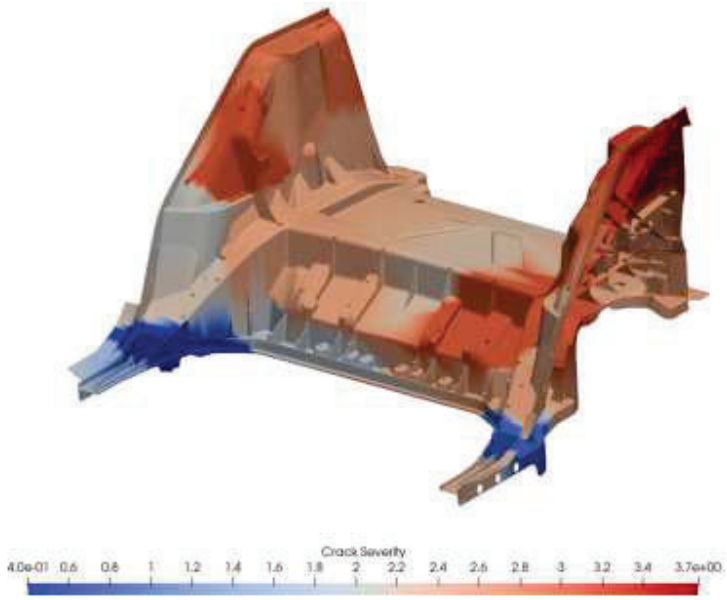

Figure 35 Crack severity approximation of soft tool floor

WH11_F02 (SPRRH0023) WH09_F11 (SPRLH0018) WH11_F02 (SPRRH0017)

Figure 36 Joint buttons with average crack severity 0.7-1.47

WH16_F04 (SPRLH0104) WH14_F09 (SPRRH0101) WH16_F04 (SPRLH0107)

Figure 37 Joint buttons with average crack severity 3.07-3.67

Figure 36 and Figure 37 show the joint button of the investigated SPR positions. No cracks were observed in Position SPRRH0023, SPRLH0018 and SPRRH0017. Different amounts of cracking were detected in SPRLH0104, SPRRH0101, SPRLH0107. The rivets were drilled out before testing to separate the casting from the top sheet.

Figure 38 presents the average results from three PCT indentations near the SPR location, approximately 5 mm from the drill hole. The PCT results showed a significant difference between the “good” and “bad” positions. However, no clear correlation was observed between the extent of cracking in the joint button and the PCT values. Notably, position SPRLH0104 exhibited slightly higher PCT values, despite being subjectively assessed as having the most severe cracking. It should be noted that crack severity remained relatively similar among positions 104, 107, and 101, and that PCT testing was performed slightly offset from the original location. Given the local variability in pore density and pore sizes, a direct correlation between PCT results and crack severity was not expected.

Due to the significant variation in wall thickness among the investigated joining positions, the PCT displacement values were normalized by dividing by the measured wall thickness. After normalization, the difference between Position 23 and Positions 104, 101, and 107 became insignificant. However, since pore density is often inhomogeneous across the wall thickness, the validity of normalizing displacement values at Fmax should be carefully considered. Additionally, a higher wall thickness typically results in higher Fmax values, leading to comparable bending stresses on the bottom side of the sample.

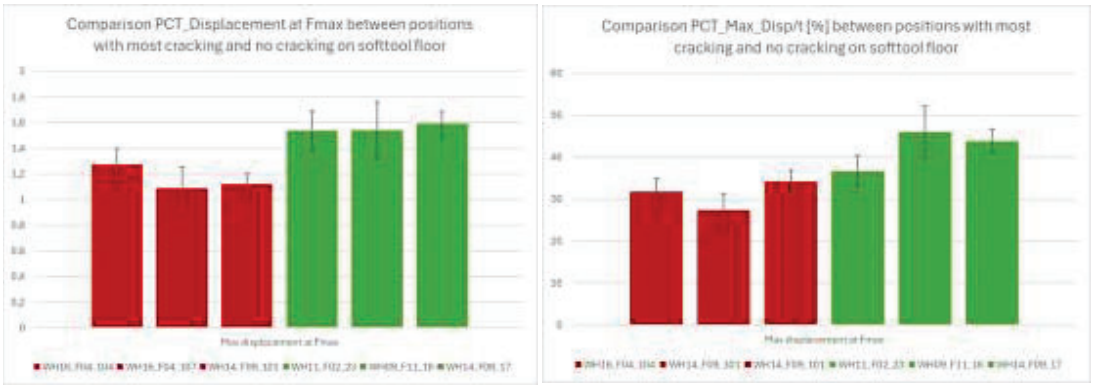

Figure 38 Displacement at Fmax during Pierce-Cupping testing

6.1.4 WP1 Conclusions

The testing of the snake tool, including microstructural and mechanical analyses, reveals several important insights into material behaviour and performance. While the overall differences between the start and middle sections of the snake tool are minimal and not significant, there is a discernible trend indicating that the material at the end section exhibits a significantly reduced ductility compared to the start and middle section. It needs to be noted that the middle section showed a slightly increased wall thickness, which can lead to misleading assumptions if not recognized. However, even after correction the results for wall thickness the difference between start and middle section was not significant.

Microstructural observations indicate that pore density and variations in dendrite and silicon distribution contribute to these differences, with coarse structures at the start

becoming finer toward the end. Pores are considered the most detrimental to ductility, as they can act as stress concentrators and initiate fracture. Heat treatment can further refine the silicon phase and potentially enhance the material's ductility. Refining the silicon phase and thereby softening the material can decrease stress concentrations by allowing for plastic deformation, which is particularly relevant for improving ductility.

By mapping of a whole snake tool, it became apparent that also surface characteristics, like inhomogeneities such as smooth and rough areas can be a first indicator of varying material properties. It should be investigated if these areas are connected to higher pore density as well or if the cracking is initiated rather on surface defects.

6.1.4.1 Discussion of material properties and mechanical testing methods:

Tensile testing with Digital Image Correlation (**DIC**) highlighted significant differences in elongation to failure between the start and end sections of the snake tool, which aligns with the joining tests in a general trend. DIC was useful to reveal strain localisations and connecting measured material properties to material defects. This could be helpful to identify areas with higher defect density or large defects, giving an indication of local variations that could affect joinability. Tests at Volvo Cars showed large material variations in the soft tool floor comparable to variations between start and end section of the snake tool. However, the larger specimen size compared to an SPR joint limits direct conclusion to material properties in joining locations on the flanges. Since the specimen size is rather large, a high probability exist that pores or other defects will be found in the specimen, therefore resulting in a low elongation to failure. Large areas of the specimen however could be unaffected by defects and therefore have a higher ductility than the tensile test is indicating. Therefore, tensile testing is deemed impractical and, in most cases, not relevant for accessing joinability on a local level. On the other hand, if the tensile test shows good ductility (>10% elongation to failure) it can be assumed that the area covered by the specimen has a good joinability). For testing on flange positions a sub-standard sized tensile test specimens could be used. The preparation efforts would however increase dramatically.

The **V-Bend test** revealed clear differences between positions, with the start position showing the best bending capability, the middle sections required the highest force for bending, and the end displaying intermediate characteristics. These variations in bending performance are primarily attributed to differences in material thickness across the sections.

The Drop-Tower and **Charpy tests** provided insights into the material's cracking behaviour and local properties, though the drop-tower test's qualitative nature and reliance on cracking as a metric were noted as limitations. The Charpy test allowed for conclusions on material ductility and the results were in alignment with tensile tests. The tested material area is small and may be suitable for detecting local deviations; however, the required sample size limits the ability to achieve high-resolution characterization of a part or flange.

Moreover, the loading condition is not comparable to that of a self-piercing riveting (SPR) operation

The PCT **(Pierce-Cupping Test)** emerged as the most effective method for revealing local variations in the casting, correlating well with joining test results. Its ability to assess local properties quickly, without the need for extensive sample preparation, and its potential for integration into handheld devices make it a valuable tool for further investigation. By addressing the limitations of conventional destructive tests, the PCT offers a promising alternative for predicting joinability in SPR processes and for ensuring that variations in material properties are properly accounted for in manufacturing and quality control. The sensitivity and relevance of this method to joinability have been demonstrated on snake tool material and soft tool floor flanges by comparing locations with severe cracking to those with minimal or no cracking. In addition, the test setup could be used on a modified handhold tool or a modified SPR C-frame making it a practical and fast method for evaluating produces parts.

In conclusion, the snake tool exhibits consistent overall properties with lowest material ductility in the End section, Start and Middle section showed no significant difference. All testing methods were sensitive for this general trend. Only with the PCT method even the local variations could be revealed. Indicating that regions exist in all sections where material ductility can be critically low and affect cracking during joining. Especially locations in the corners of the snake tool, where the melt flow likely becomes non-laminar. This observed locality of properties could be correlated to the pore density observed in microstructural investigations.

The combination of microstructural and mechanical testing has provided a comprehensive understanding of the material's behaviour, highlighting the importance of considering local differences in performance, particularly in the end sections of the tool where considerable porosity was observed. Further investigation into the dependency of results on wall thickness and other factors such like punch geometry will be crucial to optimize the PCT method and improving accuracy when comparing parts with high manufacturing tolerances.

6.2 WP2 Experimental studies

6.2.1 SPR Joinability

6.2.1.1 Joint requirements for joinability assessment

To evaluate joinability quality metrics for the forming quality and appearance quality were pre-defined by VCC standards (VCC 5531.619 and VCS 8531.29).

For the forming quality the relevant metrics were:

- 0.2 mm > Head height >-0.1 mm
- Interlock > 0.2 mm
- Remaining thickness > 0.2 mm
- No excessive rivet flaring
- No rivet compression

The appearance quality requirements according to standard were:

- Die should be completely filled
- No cracks in the sheet
- No cracks in rivet

6.2.1.2 Recycled aluminium

To assess the joinability of recycled cast aluminium, six different materials with varying recycling content and melt treatments were produced and evaluated. The evaluation focused on key criteria, including cracking behaviour, interlock quality, susceptibility to edge cracking, and process repeatability. These factors were analysed to determine the suitability of each material for joining applications.

Alloy designation		Si	Fe	Cu	Mn	Sr	Zn	RC
A1	Smelter	~6-9	0.14	0.013	~0,4-0,6	included	0.01	max.20%
A2	Recycler 1	~6-9	0.26	0.019	~0,4-0,6	included	0.02	>50%
A3	Recycler 2	~6-9	0.19	0.036	~0,4-0,6	included	0.022	95% (78% PCR)
A3F	Recycler 2 Flux treated	~6-9	0.18	0.036	~0,4-0,6	included	0.021	*95% (78% PCR)
A4	Recycler 2 + Fe 0.4; Cu&Zn 0.1	~6-9	0.40	0.11	~0,4-0,6	included	0.11	95% (78% PCR)
A4F	Recycler 2 Fe 0.4; Cu&Zn 0.1 Flux treated	~6-9	0.40	0.11	~0,4-0,6	included	0.11	95% (78% PCR)

*Wt. % of Si, Mn, Sr and Mg were kept the same through all material batches

Figure 39 Recycled aluminium specifications

All 6 material variations with up to 95% RC could be joined according to the VCC quality criteria with proposed solutions from Stanley and Atlas Copco. Since the tests have been conducted on snake tools / flat coupons, which generally showed better joinability, **the results need to be verified on real parts**.

6.2.1.3 *Statistical analysis of cracking*

A total of 33 SPR locations across 21 soft tool floors were evaluated using a 0–5 scale, where 0 indicates no cracking and 5 indicates very severe cracking, see Figure 40. The distribution of cracking is shown in the Figure below. As seen, most SPRs exhibit intermediate cracking in the range between 2 and 3 and a smaller number of SPRs exhibit very high and very low cracking severity.

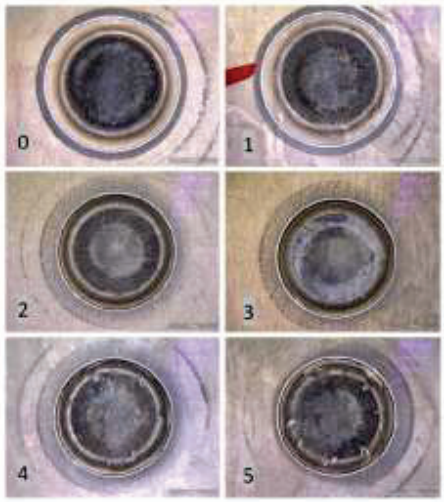

Figure 40 Cracking severity scale

Figure 41 Cracking severity distribution of SPRs in soft tool floors

While variations between different soft tool floors were relatively low, higher variations were observed between SPR locations within the soft tool floor as illustrated in Figure 42

and Figure 43, respectively. The cracking severity distribution is also illustrated graphically in Figure 35.

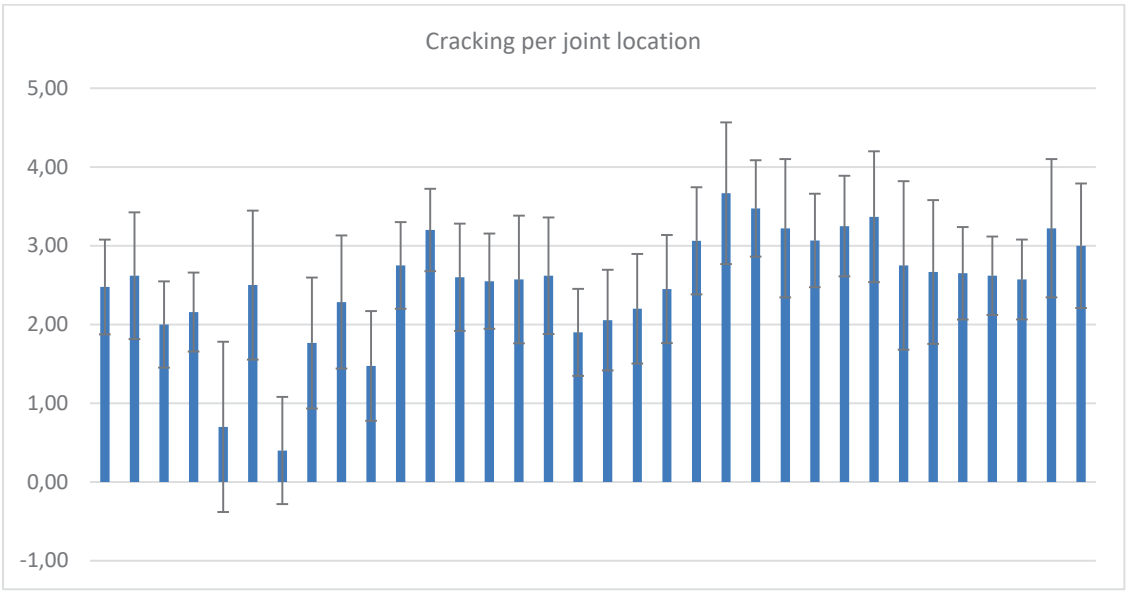

Figure 42 Cracking severity of SPRs; average per joint location

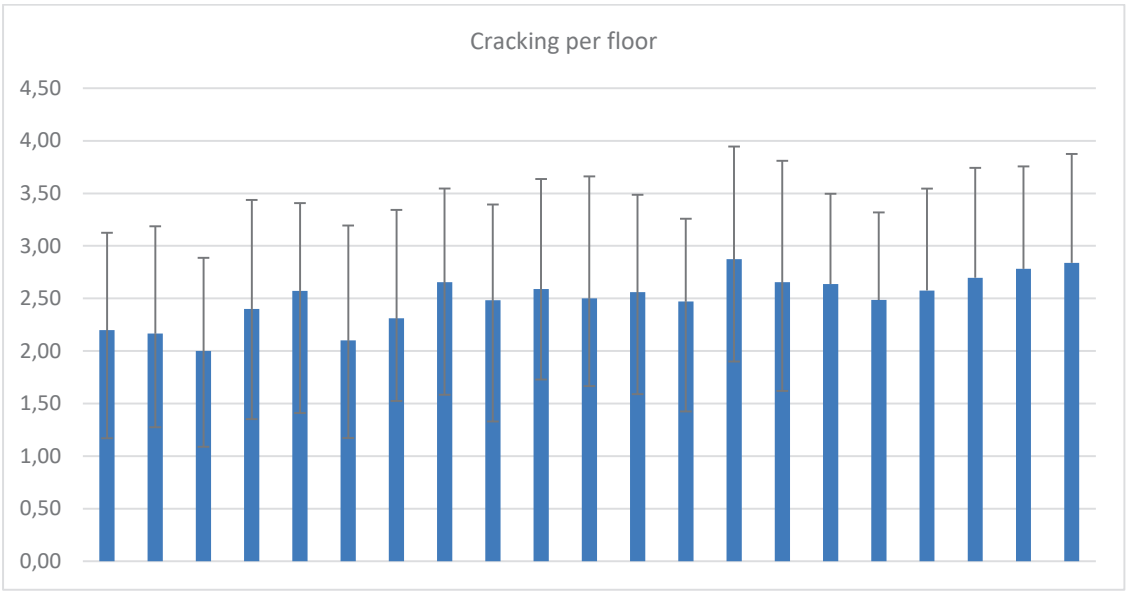

Figure 43 Cracking severity of SPRs; average per floor

All relevant available data was imported into statistics software MODDE for ANOVA analysis to find significant factors that influence cracking severity. Cracking severity was found to correlate with multiple factors, with the most significant correlations observed for the Z-coordinate, Y-coordinate, flow length, and rivet type. However, these factors are also interrelated, making it challenging to completely isolate their individual effects. Moreover, the available data was limited making it difficult to draw any definitive conclusions on the causality between different factors and cracking severity. However, the data can be used as an indication on what factors to study more closely.

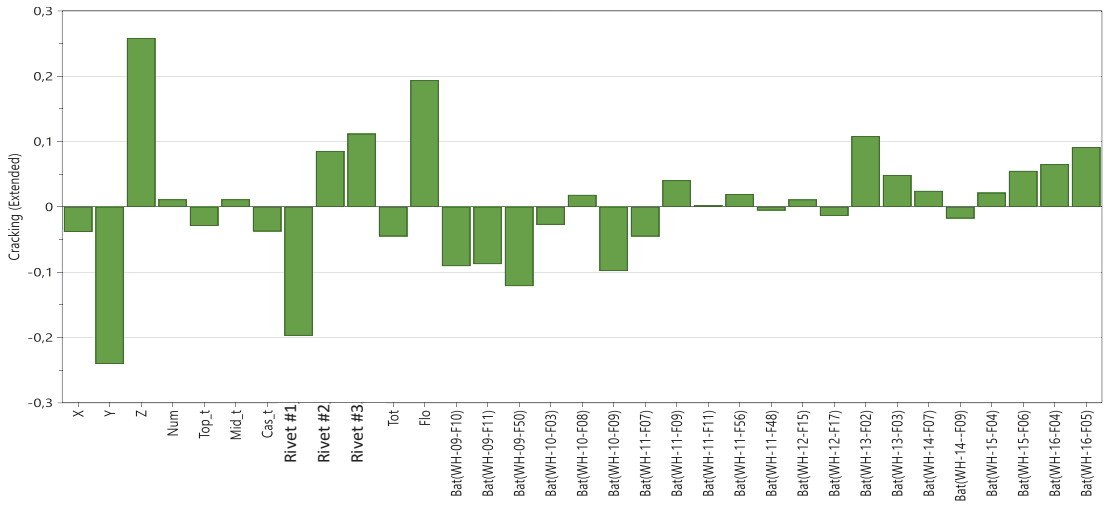

Figure 44 Scaled coefficients of factors and their influence on cracking severity

The correlation between cracking severity and mechanical properties at selected locations of the soft tool floor was also investigated. Results from elongation at break and bending angles after bending tests were mapped on the global geometry and the results were visually compared to the mapping of the cracking severity. However, due to the limited number of locations where mechanical testing had been done, it was difficult to draw any conclusions on the correlation between the mechanical properties and the cracking severity.

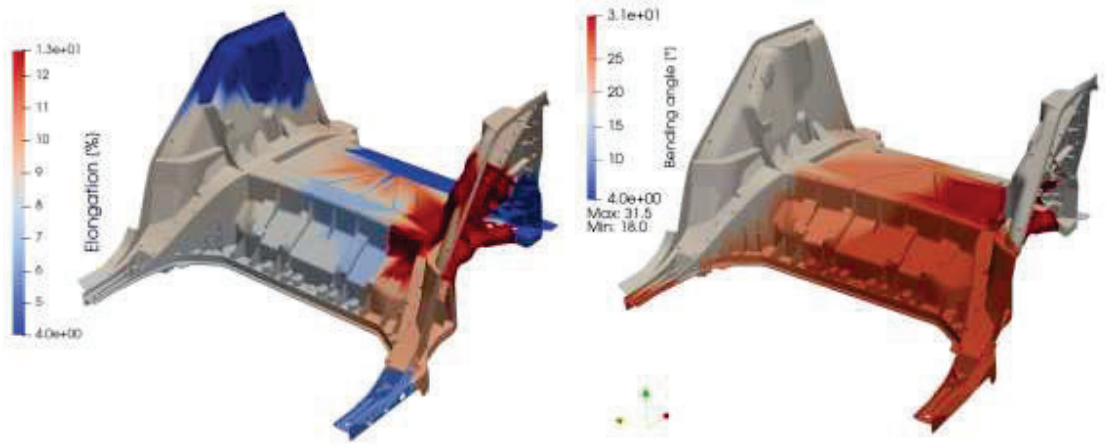

Figure 45 Geometrical interpolation of elongation and bending angles at break measurements of soft tool floor

Following the statistical analysis, the three most and three least severe SPR locations were selected for further analysis of the cast aluminium material in these locations, see Figure 46. The results of this analysis is described in Chapter 6.1.3.

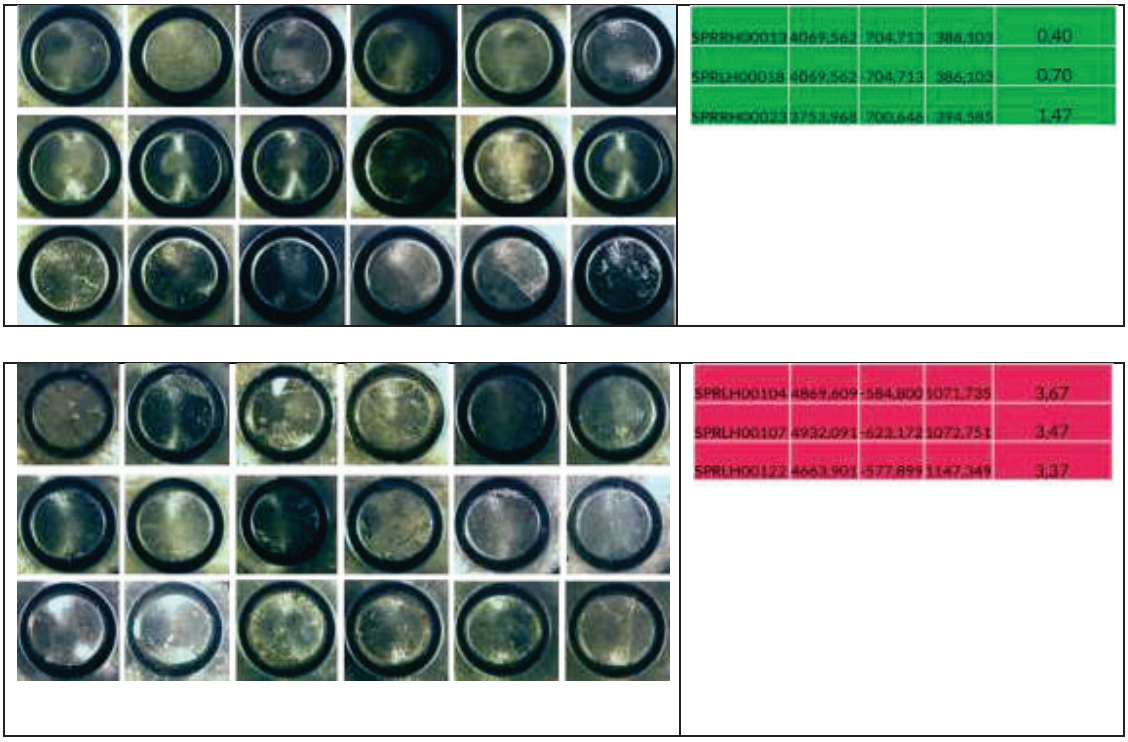

Figure 46 Cracking of dies from joints with lowest (top) and highest (bottom) crackiing severity

6.2.1.4 SPR Grouping strategy

Grouping strategies for rivet and die selection across varying material combinations require careful consideration of multiple competing factors. These factors include ensuring the joint quality is robust, minimizing production and investment costs, and considering production and equipment availability, whether in greenfield (new) or brownfield (existing) facilities or plants. Balancing these priorities effectively is important to achieve optimal outcomes in material joining processes. Moreover, it is a risk management and strategic decision that must be done.

To underpin these grouping strategies, several potential methods can be employed. Firstly, conducting extensive joinability testing is critical—both physical and virtual testing should be carried out with a diverse array of die-rivet combinations tailored to each specific material combination in the design. By systematically compiling and analysing these results, a robust database of joinability results can be developed. This database enables efficient grouping of material combinations based on compatibility and performance.

Secondly, refining and innovating rivet and die geometries can expand the range of materials that can be joined effectively, facilitating multi-range joining. These optimized geometries can improve versatility and adaptability in production scenarios, accommodating broader design and manufacturing needs. Again, simulations can be used to improve rivet and die designs.

Thirdly, narrowing down the available material combinations in the design stage can simplify the selection process and reduce complexity, ensuring that the chosen combinations align with production capabilities and performance goals. This can be implemented by more strict design guidelines available to design engineers.

Fourthly, establishing more flexible or optimized SPR joint requirements can allow for broader application scenarios and cost-effective solutions. Lowering specific joint performance thresholds may be suitable for non-critical applications while maintaining sufficient overall quality standards. Alternatively, specific SPR joints could be replaced with other joining methods, such as, clinch joints to reduce the total number of die rivet combinations.

Finally, exploring alternative or new or innovative joining methods, such as versatile-SPR techniques, can unlock new possibilities for efficient and reliable material joining. These methods might incorporate advancements in technology or novel approaches that address current limitations in traditional processes.

By integrating these strategies, manufacturers can find a balance or optimum between quality, cost, and production feasibility, enabling more effective material joining across a broad range of applications. The joinability reports from the RobuCAP project provided examples of successful grouping strategies for the selected material combinations through rivet and/or die optimization.

6.2.1.5 Guidelines for Improving SPR Joinability

1. Material Properties

To improve joinability, it is essential to focus on optimizing the material properties. The key for good joinability is sufficient ductility in the casting material. Measures for ductility include elongation to failure from tensile testing, bending angle and bending force in V-bend testing, Energi absorption from Charpy test. Major influence on the materials ductility has of course the alloys chemical composition and resulting microstructure. Given a given alloy the defect density in the material plays the most important role, as seen in this project shrinkage porosity is highly connected to the location in the casting and effects ductility and thus joinability on a very local level. Variations in castings can occur due to part geometry, melt flow and varying cooling conditions. Materials and locations with low defect density, as well as a beneficial microstructure, will exhibit improved joinability.

- **Ductility and Elongation to Failure**: Elongation to failure is a common measure for the ductility of materials. Elongation to failure values is usually obtained from standardized tensile tests. The specimen size is large in comparison to the area influenced by an SPR joint. Materials with elongation to failure greater than 10% are generally acceptable for joining processes. But most often tensile test specimen cannot be taken out from flange regions were joining is performed. This is a major disadvantage regarding the huge variability of ductility in the cast part. Thus, standard tensile tests are not recommended to evaluate joinability. Miniature tensile tests specimen could be taken from flange regions, but the sample preparation efforts would be very high.
- **Influence of defects on ductility**: Large defects like shrinkage pores are most detrimental to ductility, since they lead to stress concentrations and crack initiation during forming or generally under loading. Other defects like oxide films, intermetallic phases with sharp geometries could not be detected in the current castings but have to be considered detrimental to material ductility if present.
- **Testing Methods**: Traditional tensile and V-bend tests are not suitable for assessing joinability, as they do not provide accurate results in these contexts, due to the sample size and possible extraction locations. Instead, using smaller specimens from the relevant joining locations for testing can improve the accuracy. The **Pierce-Cupping Test (PCT)** is recommended for determining local ductility, particularly in the case of Self-Piercing Riveting (SPR), where it has shown good correlation with cracking and local material behaviour. Similar tests found in recent literature have shown aligning results for cast materials and heat-treated aluminium alloys.

2. Rivets and Dies

The rivet and die design play a crucial role in optimizing joinability. Several factors must be considered during the design phase:

- **Die Design**: Shallow dies, avoiding sharp corners, and using special dies with multiple forming steps (such as dual cavity dies) can enhance the joinability. Flaring the rivet above the die cavity has been shown previously to be beneficial for achieving the optimal joining force and material flow into a shallow die.
- **Rivet Dimensions**: Using smaller rivets reduces the deformed volume and allow for very shallow and small dies, this can decrease the risk of crack formation during the joining process. Rivet dimensions and materials need to optimized for both top sheet and bottom sheet in order to achieve good forming quality.
- **Rivet-Die-Grouping:** Grouping strategies for rivet and die selection across varying material combinations require careful consideration of multiple competing factors

3. Casting Geometry

Casting geometry significantly influences joinability, and certain design choices can help improve the quality of the joint:

- **Casting geometry** determines melt flow, cooling conditions and is crucial to other casting defects, like e.g. cold shuts. This influences the material properties, especially ductility and crack susceptibility (c.f. 1.)
- **Flange Geometry**: Tapered flanges are particularly problematic and should be limited to a maximum angle of 3 degrees to reduce the risk of joining issues. Additionally, ensuring that the flange is designed for optimal rivet placement is crucial for minimizing material deformation and cracking. Especially edge cracking can occur when riveting close to the edge.
- **Riveting Positioning**: Aligning the setter face of the rivet with the flange is the best practice for achieving high-quality joints in tapered flanges. Moreover, ensuring that the material flow into the die is properly "tilted" enhances the overall process and improves the flow of material during the riveting operation.

4. Riveting Process

The riveting process itself plays an important role in achieving high-quality joints:

- **Insertion Speed and Adhesive Use**: Riveting should be performed with an optimized insertion speed, as this influences both the joint's strength and the risk of cracking. Additionally, using adhesives in combination with riveting can act as a lubricant, influencing the flaring of the rivet and, consequently, joint quality. While adhesives may not significantly affect appearance quality (as shown for the cast material in this project), their role in the joining process should not be underestimated.

6.2.2 SPR Disassembly and re-assembly

Several disassembly methods such as drilling, grinding, and chisel peeling were considered. However, the chosen approach needed to minimize material wastage and offer easier accessibility. The initial plan involved using a spike tool with the rivet gun to disassemble the SPR joints. However, due to the unavailability of the spike tool, Atlas Copco recommended alternative disassembly methods, which were subsequently considered.

Atlas Copco proposed an alternative disassembly method that has already been developed and validated through prior testing: To conduct a preliminary test on rivet removal, the most effective approach is to machine a custom die and punch assembly compatible with a universal tensile testing machine. This setup can be used to drive a spike or punch through the rivet button, thereby pushing the rivet into the die for removal.

As illustrated in the reference images, one approach involves using a flat punch with an inward conical recess. However, it is often more common to use a spike-shaped punch that penetrates the centre of the rivet button and enters the rivet bore, effectively ejecting the rivet. Both punch designs are suitable for use with aluminium rivets, and either or both configurations can be evaluated depending on the specific application.

Figure 47 CAD models of proposed disassembly tools

The WH-16-FO4 soft tool batch, the 8ARH SPR position, was selected for the disassembly process conducted at RISE. At RISE, the SPR joints were disassembled using a drilling method. This approach proved to be efficient and allowing easy. After disassembly, the drilled holes were reused for reassembly using blind rivets. More specifications of he blind riveting procedure can be found in Chapter 6.2.5.3.

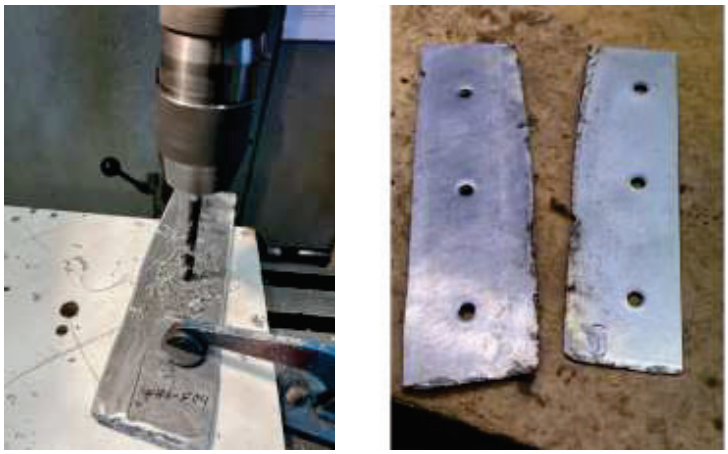

Figure 45 Drilling operation on SPR joints (left) and separated aluminium and steel material (right)

Figure 46 Reassembled the previously disassembled SPR joints using blind riveting.

6.2.3 Discussion and Conclusion WP 2.1

In conclusion, material properties significantly influence joinability, with macro-pores being the most detrimental factor. Their distribution is highly dependent on the position, flow length, and part geometry, making them a critical consideration during the casting process. Understanding the relationship between pore distribution and part design is essential for ensuring optimal joinability. Therefore, material analysis must be integrated with joinability analysis to achieve accurate results. Alternatively, material quality requirements for joining flanges should be clearly defined to mitigate potential issues. Since in this study the pore size and density was the most obvious difference distinguishing good and bad joinability, it cannot be with be ruled out that other defects can play a role on joinability in other alloys compositions or production circumstances even in absence of pores.

Regarding material characterization, traditional macroscopic mechanical testing methods, such as tensile testing or V-bending can be a tool to determine joinability on a larger testing area. Considering the small dimension of rivets or clinch joints, a more local material characterisation is sensible. Reducing specimen size and focusing on testing in relevant areas can enhance the accuracy of results. The Pierce-Cupping Test (PCT) presents a promising method for determining locally relevant material properties that directly affect joinability. However, the threshold values for this test must be customized based on the specific rivet-die combination to ensure reliability.

The work done at Stanley and Atlas Copco showed that joinability optimization can be effectively achieved through experimental and iterative rivet-die adjustments. This approach allows for the identification of the optimal process window and mitigates potential issues, such as cracking, by using multi-cavity dies or smaller rivets. Furthermore, careful selection of coupon sample extraction locations is crucial to ensure the validity of results. Recycled aluminium has shown promising results in terms of reduced cracking when processed under optimal conditions. However, special attention is needed for megacasting parts, which require thorough verification.

For a more reliable joinability analysis, a worst-case material state should always be considered, particularly when using snake tools or similar methods. In these cases, material from the end section should be utilized to account for potential variations in material properties. By addressing these key factors, it is possible to optimize material joinability, ensuring reliable and efficient joining processes.

Joinability optimization could be most likely accelerated by developing simulation methods, both for simulation of the casting process and resulting material defects, thus giving indications on critical areas and the possibility to prevent such areas in the design stage, but also for the simulation of the joining process where cracking criteria should be considered for optimizing rivet and die geometry.

6.2.4 FDF Joinability

The materials tested included CR240LA GI 50/50 with a thickness of 1.2 mm and snake tool aluminium, Alloy 4, "24+21" with a thickness of 3 mm. The tests were conducted at positions 1 and 24 of the snake tool. Three types of fasteners were used in the tests:

- M5x20, EP12, ZnNi + GC471
- M4.5x22, EP12, ZnNi + GC471
- M4x20, EP10, ZnFlake + Delta Seal

The joinability was assessed based on three main criteria:

1. Screw Penetration Time: The acceptable range was between 500 ms and 700 ms.
2. Thread Forming Torque: The torque should be within the screw limitation.
3. Head Overlap After Tightening: The overlap should be less than or equal to 0.5 mm.

Other parameters of interest included stripping torque and visual results. Three repetitions were conducted to assess stripping torque and final tightening. All results were taken from the equipment data log from the Atlas Copco KFlow equipment.

All tests were judged to be OK regarding penetration time. The lower times for M5x20 could be increased with a lower force. Slightly longer penetration times were observed for position 24 compared to position 1, which could indicate higher hardness or yield strength. Longer penetration times for M4.5x22 could be due to the longer screw tip.

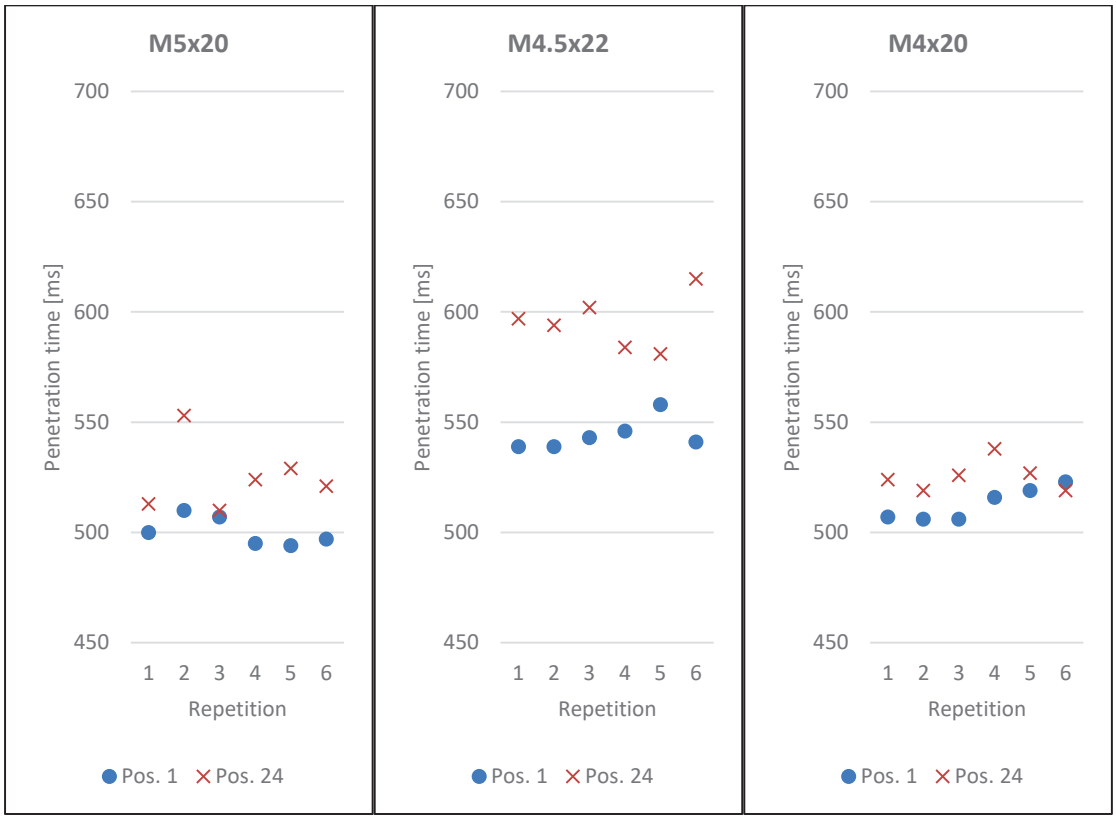

Figure 48 Penetration times of the FDF process for different fasteners and snake tool locations

Thread Forming Torque: All tests were judged to be OK with a significant safety margin to the absolute limit. There was no clear difference between positions 1 and 24. The trend indicated lower thread forming torque with smaller screw dimensions.

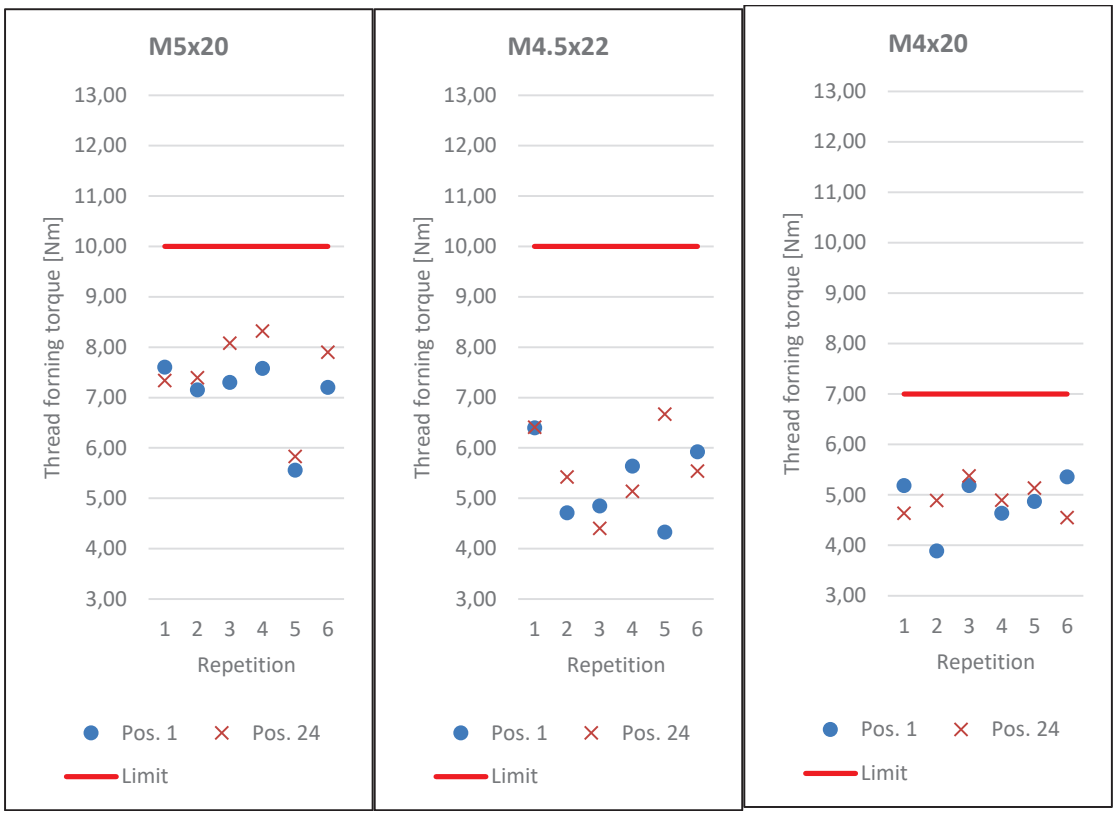

Figure 49 Thread forming torque of the FDF process for different fasteners and snake tool locations

Final Torque: M5x20 and M4.5x22 showed no stripping at 15 Nm. M4x20 showed stripping between 11 Nm and 14 Nm. Zero head overlap at final tightening was considered OK. There was no clear difference between positions 1 and 24.

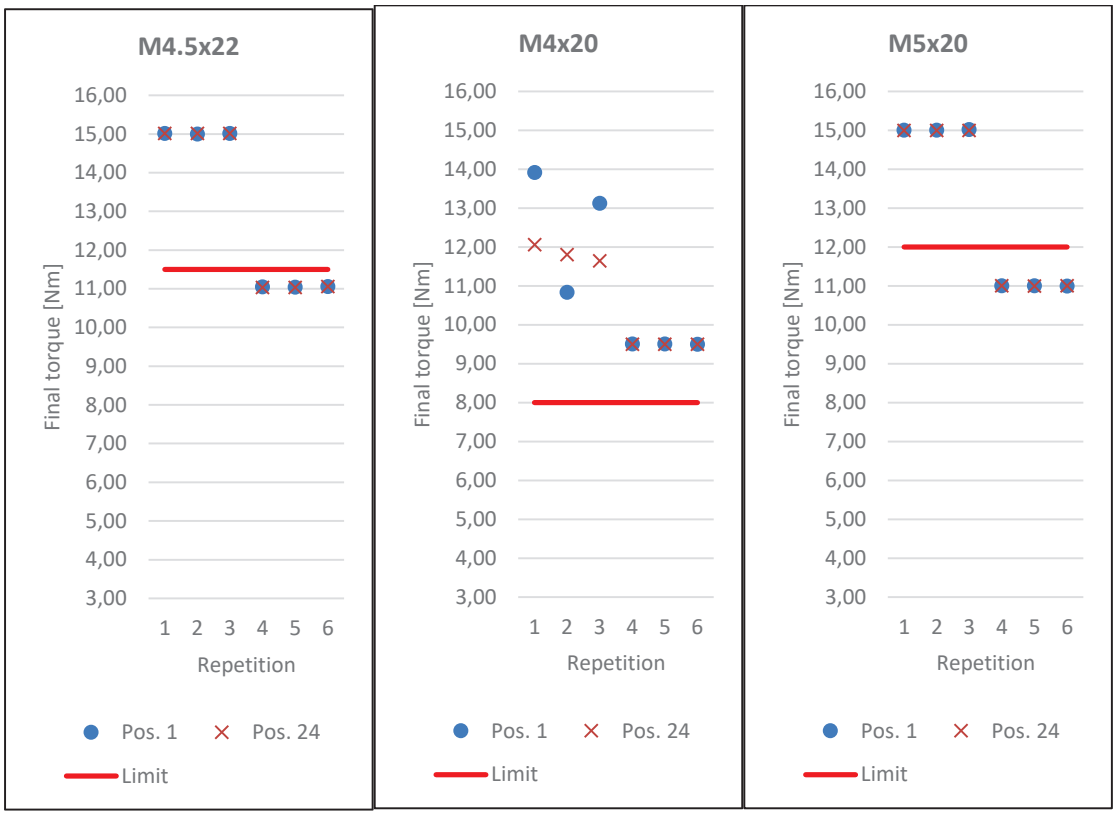

Figure 50 Stripping torque of the FDF process for different fasteners and snake tool locations. N.B. maximum torque of equipment is 15 Nm.

The joinability of all material combinations and fasteners was judged to be OK. Some trends were identified with respect to fastener type and snake tool position, but further investigation is needed to verify these trends. Possible next steps for FDF testing include:

- Testing thicker aluminium material (> 3 mm).
- Testing joinability with respect to geometry and fixturing.
- Extending testing with more repetitions to obtain better statistics.
- Confirming results with different coatings and tougher material combinations.
- Examining disassembly and re-assembly of joints.

6.2.5 Clinch Joinability

6.2.5.1 Snake tool results

The objective of this study was to evaluate the lap-shear strength of clinched joints at the Start (S), Middle (M), and End (E) positions of a snake tool batch. The general industrial testing practices were followed, as no fully defined requirement values for clinch joints currently exist under VCS 5531,521. The suggested acceptance criteria for joint quality included no visible cracks, a symmetrical and fully formed button, and a minimum interlock of 0.1 mm.

The material tested was 20A-2231-1015-(1.20 mm thick 240 LA micro alloy steel clinched to 3mm cast aluminium). Lap shear tests were conducted at a constant speed of 1 mm/min for all three joint positions.

Results and analysis:

The lap-shear test results for clinched joints made from 20A-2231-1015: 240 LA 1.20 mm micro alloy steel indicate a clear correlation between material position along the snake tool and clinching performance. Specimens from the Start section exhibited the highest peak force, reflecting superior shear strength and interlock quality. Middle-section specimens showed moderate strength and interlock characteristics, while End-section specimens failed at comparatively lower forces, suggesting reduced ductility. Overall, a progressive decrease in interlock strength was observed from the Start to the End of the batch, reinforcing the influence of position on joint performance.

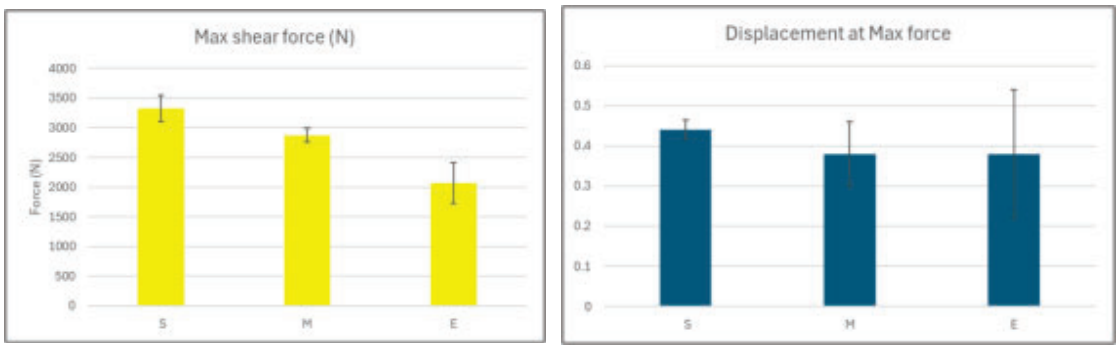

Figure 51 Max shear forces and displacement at max force for clinch joints at different snake tool locations

6.2.5.2 Soft tool results

Soft tool material was supplied to BTM for clinch trials, after which the resulting clinched joints were sent to RISE for crack inspection and cross-section analysis. BTM provided multiple material combinations of clinched soft floors, with one joint per combination selected for analysis. At present, not fully defined VCC requirement values exist for clinch joints under VCS 5531,521. Notably, the DP800 (1.3 mm) material combination could not be successfully joined using the clinching process.

The suggested acceptance criteria for evaluating clinched joints included:

- Absence of visible cracks
- A symmetrical and fully formed button
- A minimum interlock of 0.1 mm

Cross-section analysis was carried out on various material combinations used with the 3mm soft tool floor, noting that thicknesses may vary. The combinations analysed included:

- AL6-160-T851-F1 (2.00 mm)
- CR240LA GI50/50 (1.20 mm)
- CR240LA GI50/50 (1.00 mm)

- CR300LA GI50/50 (1.00 mm)
- CR4 GI50/50 (0.60 mm)

These evaluations aimed to assess the structural integrity and quality of the clinched joints across varying material combinations and thicknesses.

Results and Analysis:

AL6-160-T851-F1 (2.00 mm) + Cast Aluminum (3 mm):

In these material combinations, the interlocks were well-formed; however, cracks were observed around the inner circumference and along the cross-section. The position investigated here is (057-6RH) flange within the soft tool floor is illustrated in the figure below.

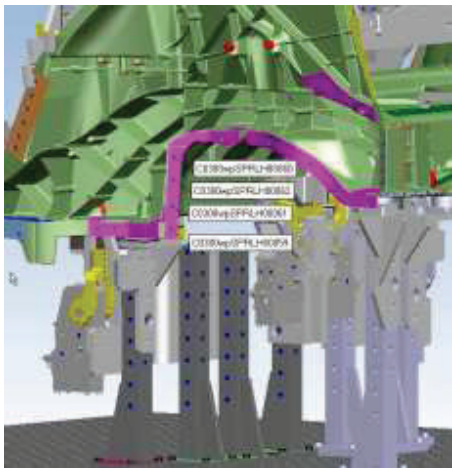

Figure 52 Cross-section of 057-6RH clinched joints, cracks observed in the inner circumference, cracks observed on the cross-section, Position of (057-6RH) within the soft tool floor

CR240LA GI50/50 (1.20 mm) + Cast Aluminum (3mm):

In these material combinations, the interlocks were not well-formed; however, no cracks were observed. The position investigated here is (85-7RH) flange within the soft tool floor is illustrated in the figure below.

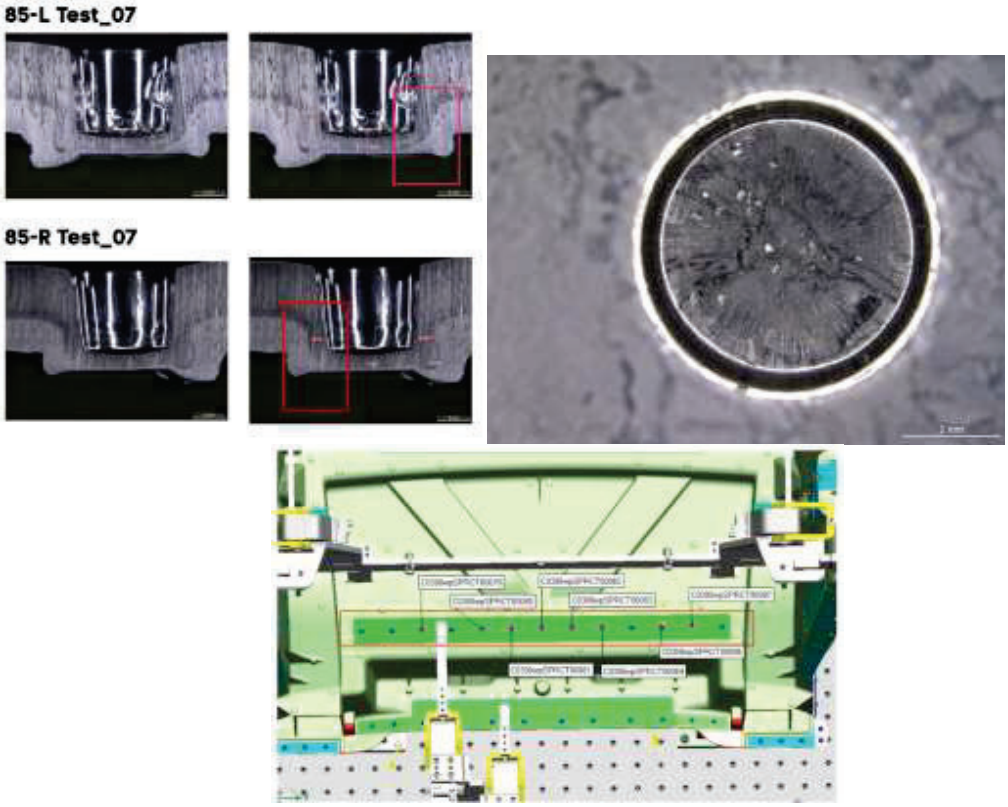

Figure 53 Cross-section of 085-7RH clinched joints no interlock was observed, cracks not observed on the cross-section, Position of (085-7RH) within the soft tool floor

CR240LA GI50/50 (1.00 mm) + Cast Aluminum (3mm):

In these material combinations, the interlocks were well-formed; however, no cracks were observed. The position investigated here is (90L-8BRH) flange within the soft tool floor is illustrated in the figure below.

Figure 54 Cross-section of 090L-8B RH clinched joints interlock was observed, cracks not observed on the cross-section, Position of (090L-8B RH) within the soft tool floor

CR300LA GI50/50 (1.00 mm) + Cast Aluminum (3mm):

In these material combinations, the interlocks were not well-formed; however, no cracks were observed. The position investigated here is (115R-09RH)flange within the soft tool floor is illustrated in the Figure below.

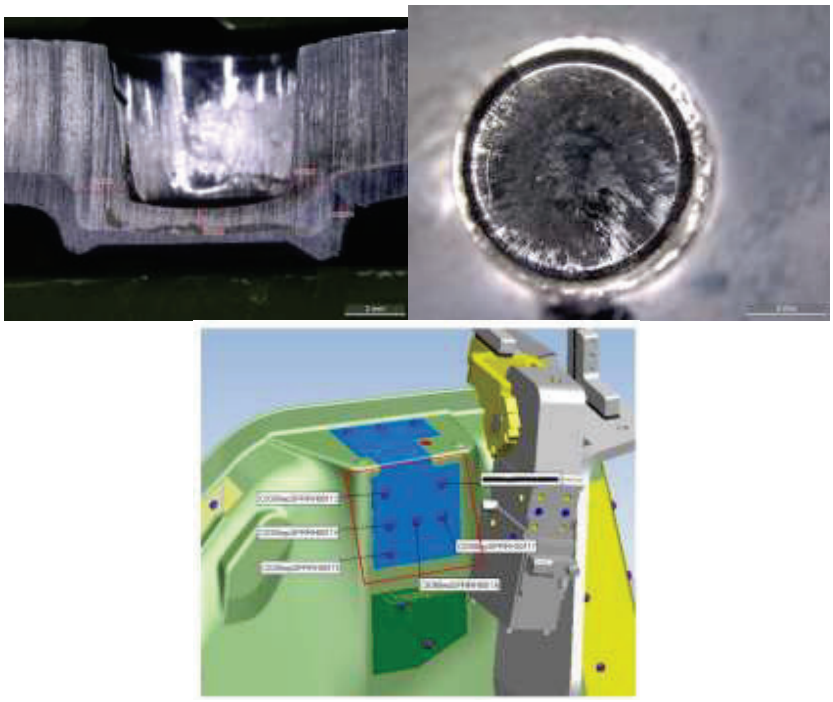

Figure 55 Cross-section of 115R-09RH clinched joints no interlock was observed, cracks not observed, Position of (115R-09RH) within the soft tool floor

CR4 GI50/50 (0.60 mm) + Cast Aluminum (3mm):

In these material combinations, the interlocks were well-formed; however, cracks were observed around the inner circumference. The position investigated here is (135-11RH) flange within the soft tool floor is illustrated in the figure below.

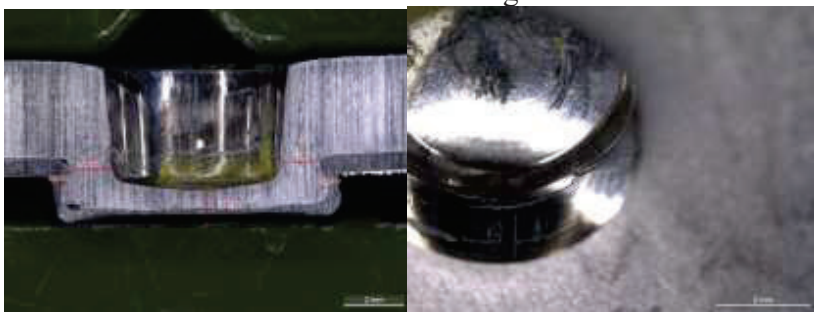

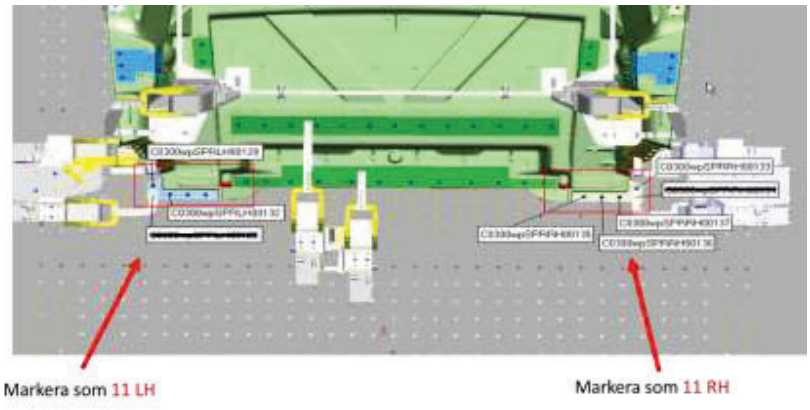

Figure 56Cross-section of 135-11RH clinched joints interlock was observed, cracks observed in the inner circumference, Position of (135-11RH) within the soft tool floor.

6.2.5.3 Clinch disassembly and re-assembly

Clinch soft tool floor components were selected from RISE's existing inventory. The plan was to utilize the same flange part from the soft tool batch at both RISE and BTM to ensure consistency in evaluation. For the disassembly and re-clinching trials, BTM used the 9LH flange, while RISE conducted disassembly and reassembly analysis using the 9RH flange. Several disassembly methods such as drilling, grinding, and chisel peeling were discussed. However, the chosen approach needed to minimize material wastage and offer easier accessibility. The clinched joints were disassembled by drilling.

Figure 57 Soft tool floor samples used for disassembly and re-assembly

Figure 58 Drilling of clinched parts

The reassembly strategy involves re-clinching operations to be conducted at BTM in order to restore the original joint structure of the soft floor assemblies. Additionally, blind riveting will be performed at RISE to support further testing and provide reinforcement where necessary. The objective of this reassembly phase is to evaluate the feasibility and performance of both re-clinching and blind riveting techniques with respect to structural integrity and joint strength. The lap shear results of blind riveted samples were performed.

Blind rivet specifications:

- Narrow section diameter: 4.6 mm
- Rivet body diameter: 6.39 mm
- Rivet length: 12.39 mm
- Hole fit: Suitable for 8 mm diameter

Figure 59 Blind rivet used in the reassembly process, Blind riveting process, Blind riveted parts

The shear testing was conducted using a Shimadzu Prov universal testing machine equipped with a 50 kN load cell. The material combination used for the trials consisted of DP600 steel (1.5 mm) joined with cast aluminum (3mm). Tests were performed at a constant crosshead speed of 3 mm/min to ensure controlled loading conditions. A total of four tests were conducted, including one preliminary trial followed by three valid measurements.

The primary objective of this experiment was to evaluate the shear strength and joint performance of the hybrid material assembly under controlled conditions.

Figure 60 Lap-shear strength of Blind riveted joints

Result and Analysis:

- Sample 1: Crack initiated at 4061.83 N, with a displacement of 9.30 mm
- Sample 2: Crack initiated at 4147.89 N, with a displacement of 9.32 mm
- Sample 3: Crack initiated at 4442.86 N, with a displacement of 10.19 mm

The observed failure mode across all valid samples was shear-out, where the rivet tore through the sheet material, resulting in the formation of an elongated hole. This failure mechanism is indicative of high stress concentration around the rivet under shear loading, particularly in dissimilar material combinations. The tested material combination demonstrated a high load-bearing capacity prior to failure, confirming its potential for structural applications. The observed failure mode in all samples was shear-out, where the rivet tore through the sheet, creating an elongated hole—indicative of the stress distribution under shear loading.

Figure 61 Shear out failure mode after lap-shear tests.

The testing also demonstrated the feasibility of disassembling and reassembling clinched joints without compromising the material quality. Furthermore, it reaffirmed the retention of joint strength, indicating the method's suitability for repair scenarios where structural integrity must be maintained.

6.2.6 WP2 Conclusions

The experimental studies in WP2 provided insights into the joinability of cast aluminium components using Self-Piercing Riveting (SPR), Clinching, and Flow Drill Fastening (FDF). Key conclusions are as follows:

Material properties, particularly pores, significantly influence SPR joinability. Pores cause local stress concentrations and initiate cracks. The Pierce-Cupping Test (PCT) emerged as a valuable method for local material characterization, showing good correlation with joinability. Iterative rivet-die adjustments proved effective for optimizing SPR processes, reducing cracking. Recycled aluminium showed promising results but requires thorough verification for megacasting parts.

Clinching revealed significant local property variations impacting joint quality. Lap-shear tests indicated a vague correlation between material position and clinching performance, with specimens from the start section exhibiting the highest shear strength. Cross-section analysis showed varying results across different material combinations, highlighting the need for optimized material properties and process parameters.

FDF joinability is influenced by material properties and fastener types. Tests showed acceptable penetration times and thread forming torque, with some trends identified concerning fastener type and snake tool position. Further investigation is needed for thicker aluminium materials.

Efficient disassembly methods, such as drilling, were evaluated for SPR and clinched joints. These methods allowed for easy reassembly using blind rivets or re-clinching, demonstrating procedures for repair and recycling or remanufacturing scenarios.

WP2 emphasized the importance of material properties, particularly ductility and defect density, in achieving high-quality joints. The PCT is a valuable tool for local material characterization, while iterative rivet-die adjustments optimize SPR joinability. Clinching and FDF processes showed promising results but require further refinement. The feasibility of disassembly and reassembly supports repairability and sustainable end-of-life strategies. WP2 has increased the understanding of mechanical joining processes for cast aluminium components, contributing to more robust automotive manufacturing practices.

6.3 WP3 Numerical studies

Numerical simulation with finite elements (FE) is a versatile tool for studies and analysis of various aspects related to continuum mechanics. In the project focus was aimed at modelling of selected joining processes.

This should enable studies on e.g. joinability and risk for cracks under conditions of varying material properties from the HPDC manufacturing of large aluminum components. Ultimately there are several motives for why this capability is sought, ranging from establishing efficient joining processes using the best rivet and die geometries and optimization opportunities to efficient performance analysis of the joined components and the joints themselves.

On the market there are many simulations software's serving various needs and with quite some overlap between different programs. In the early phase of the project some review of what was available within the consortium were made. It turned out that Deform, LS-Dyna and Simufact was in use among the partners. These are considered among the most suitable with only a few other options such as Abaqus.

Common between the different processes to study is the level of input data required. For all FE simulations one needs the geometries of the parts, process data and a suitable constitutive model together with relevant data from the actual materials.

In the project material data has been produced by tensile testing of test samples from castings in snake tool 1.0 and 1.2 as reported under 6.1.2.4. From these tests, average curves from start, middle and end have been created and extrapolated for use in FE simulation, see Figure 62. The average fracture strain from all samples of snake tool 1.2 is 9.0 % with a standard deviation of 3.0 percentage units which makes it necessary to extrapolate data to higher strain values for process simulations. Tensile testing gives some of the material characteristics but for accurate plasticity at higher strains this is insufficient. For full

characterization of metallic materials several more test methods are needed, especially when it relates to damage and fracture [1], [2].

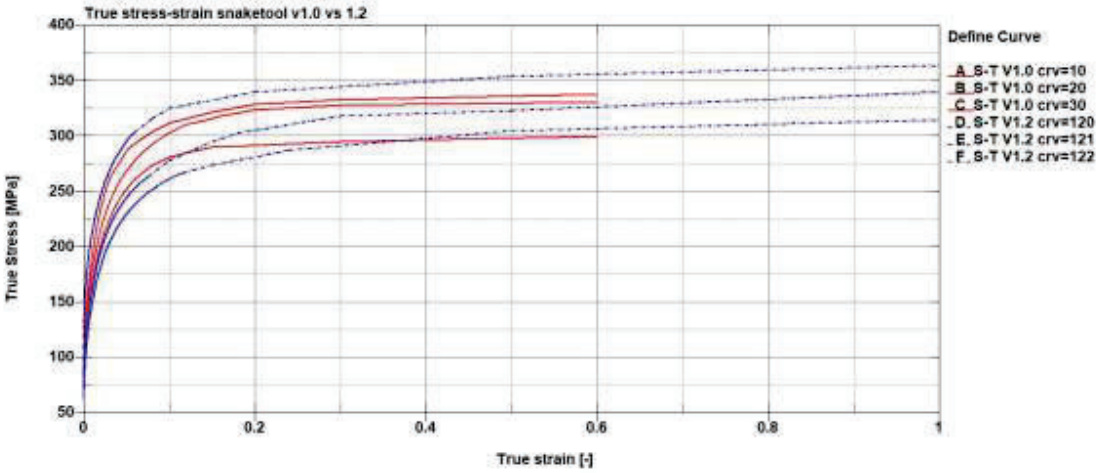

Figure 62 Manually extrapolated true stress true strain curves from snake tool 1.0 (red curves) and 1.2 (blue curves). Tensile test samples obtained from start (curve id's 10 and 120), middle (curve id's 20 and 121) and end (curve id's 30 and 123) along material flow in tool cavity.

VCC has provided material data from characterization procured from Crack Fem (VCC-CF) for exclusive use by RISE under a special agreement. This encompasses test data from various test set ups as well as from various locations on a soft tool rear floor together with user defined material and fracture model that requires a Crack Fem license to be run. Conversion of some of this data to input for LS-Dyna has been used for the simulations. As a first approach for the HPDC it was attempted to use the MAT224 (MAT_TABULATED_JOHNSON_COOK) in LS-Dyna, which is an elasto-viscoplastic material model with various options such as material softening, plastic failure strain as function of triaxiality etc. This however offered substantial difficulties to be used why the simpler MAT24 (MAT_PIECEWISE_LINEAR_PLASTICITY)

Corresponding data for the steel sheets have not been obtained by testing in the project to the same extent. Some already existing data have been approved for use within the project, see Figure 63.

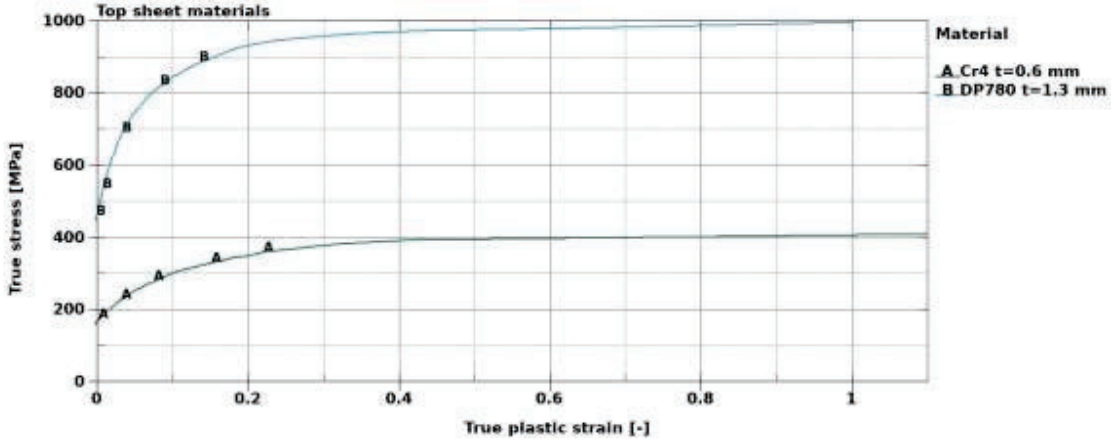

Figure 63 True stress vs True plastic strain for the top sheet material respectively. NB data from tensile tests have been manually extrapolated to higher plastic strains for simulation purposes.

Among the extensive information from VCC-CF is the fracture model and data from tests to generate data for this. Data corresponding to the instability and fracture curves as function of triaxiality for GISSMO (Generalized Incremental Stress State MOdel) in LS-Dyna was extracted from the VCC-CF. In Simufact there are a number of fracture models to choose from, given that data for the materials are available.

In the simplest, but still for many applications sufficient form a 2D-axisymmetric modelling concept is chosen for the studies of the SPR process. The model contains the tool set i.e. die, punch and blank holder geometries together with the rivet geometry and the blank specimens to be joined with their proper thicknesses. The tools are regularly modelled as undeformable, rigid bodies.

For the separation of the top sheet during joining with SPR there are alternatives for how the separation occurs. One way is to use thickness criteria that states that the top sheet is split by the rivet when the remaining thickness reach a certain level. This has the benefit of being more stable than the alternative to use some fracture model for the split which has the advantage of offering a more precise and physically based criteria for the separation. Instabilities from using fracture criteria can occur in as instantaneous progressive failure triggered by the initial failure.

To avoid distorted element shapes that affects the accuracy and even risks the fulfilment of the process simulation adaptivity is commonly used. This means that the elements shape is adjusted as the material deformations progress and cause shape deviations giving poor numerical accuracy.

Process conditions such as punch velocity and travelling distance, blank holder force and the friction coefficients has originally been set for the simulation based on given input. Experiments with different contact formulations and has been based on discussions and published data [3], [4], [5].

Two material configurations were chosen for the numerical studies, see Table 4, one that was expected to be simple and one that was expected to offer more challenges in terms of joinability aspects.

Table 4 Selected material configurations for numerical studies. In the following denoted #1 and #2 respectively.

#	Top part	Bottom part
1	CR4 GI50/50 0.6 mm	Aluminium
2	CR440Y780T-DP GI50/50 1.3 mm	Aluminium

General conclusion for numerical studies in WP3

- We have split the work into two material configurations for two partners individual SPR processes plus the clinching process and the PCT tests.
- We have material data from tensile tests start, middle and end for two snake tools in the project and from VCC-CF. The latter with several options. Additionally, we

have the material data for the top sheets which is based on some type data and not from measurements of the actual blanks.

- For the simulations there are many parameters influencing the outcome, both numerical such as related to mesh, contacts and simulation times and process related such as blank holder forces, friction coefficients.
- Some parameter settings for the process simulations needs to be based on experience and have some room for variations with influence on the results.
- We have no simple and clear definition of when a simulation result is satisfactory in comparison with a physical result that is often taken at face value.
- In cases were influence of material property variations should be accounted for it is extra valuable to take what deviation between simulation and experiment is acceptable into account.
- It is also somewhat uncertain whether numerical parameters should be the same for the two processes or whether they shall be optimised for each configuration.
- All these circumstances aside, a justified self-reflection is that the work would have benefitted from a more systematic approach for the numerical robustness.

6.3.1 SPR simulations

Work on Stanley SPR:

Both configurations according to Table 4 have been simulated. The basic settings and geometries were communicated by Stanley and many different settings based on bilateral discussions have been used in the process to improve the outcome. The results have been evaluated towards one experiment data set per case in terms of cross section images and force-displacement curves.

In Figure 64 comparisons between simulation using VCC-CF material data (stress-strain) and physical test results are shown. Here cross section images and force displacement curves from the two configurations show fairly good correlation. In the images the contour from the simulation is shown on top of the cross-section images. There are differences, for instance with respect to the geometry. For configuration #1 most significant differences occur beneath the rivet where the lug is less deformed along the leg of the rivet in simulation than in reality for #1 but not for #2. For #1 there's also a difference where the top sheet has been split. Both these differences might be caused by different material properties between the actual top sheet and that which is used for simulation. In general, the cross-section image for #2 shows better agreement apart from the void under the rivet which is smaller in the simulation due to locally larger thickness of the top sheet.

For the physical experiments there can also be some variations not entirely under control such as alignment, material properties variations and postprocessing that can cause cross sections after cutting and preparations to be slightly off centre.

Looking at the force displacement curves shown on top of Figure 64 where the simulation results are shown as a red curve placed over the graph from the physical tests shown in black. In the #1 simulation a sharp dip in the curve occurs when the rivet penetrates the top sheet and makes first contact with the underlying HPDC material. The corresponding dip in the experiments comes at a larger punch displacement which could indicate that the top sheet in the experiment is more ductile/has different fracture characteristics than what is used in the simulations and thus is cut through later. Perhaps this also is correlated to the geometry difference seen for #1 as described above.

As an increasingly larger area of the bottom surface of the HPDC comes into contact with the die the force is increasing until the final stage where the force is increasing rapidly as the final setting of the rivet is fulfilled. In this region a good correlation between simulation and experiment is found for #1.

For #2 the force displacement curves follow roughly the same development except for a slight dip for the simulation curve as the tip is starting to deform the top sheet locally. Then when the piercing of the top sheet occurs a drop in the force curve from simulation is found and that causes a reduced force for the rest of the process although the corresponding result from experiment is not visible.

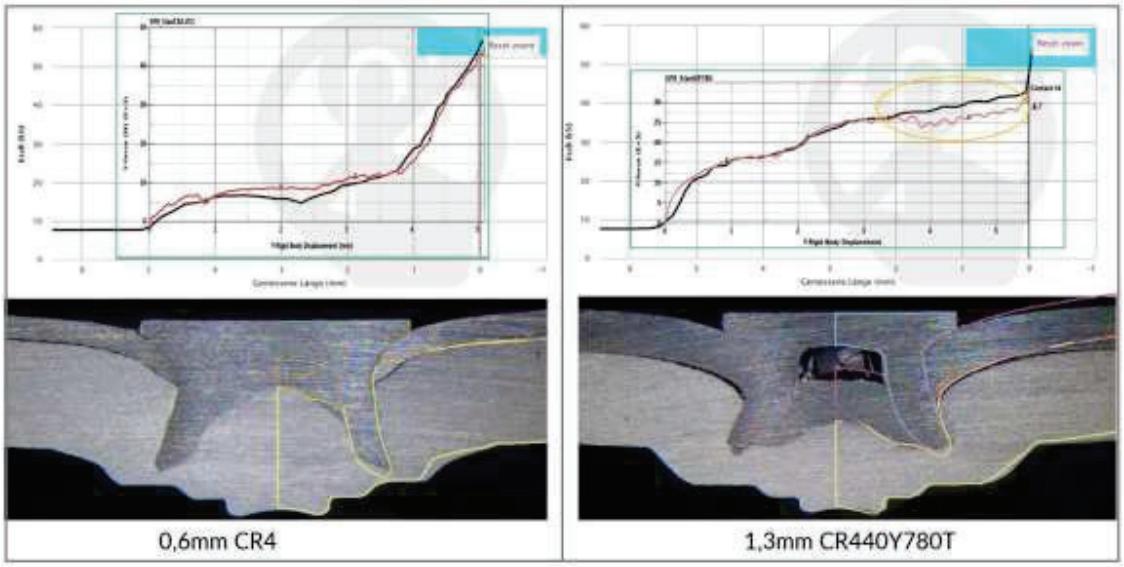

Figure 64 initial simulation results using LS-Dyna and material data from VCC-CF

As seen from these results there is room for improvement in various aspects. A large number of attempts have been made where different parameters have been adjusted without really clear-cut conclusions have been made. For instance, a review and update of the #1 model was done by Stanley which gave a significant improvement with respect to the cross section and the distance from the tip of the rivet to the bottom surface of the HPDC cast material in particular, see Figure 65. The updated model also gives slightly different punch forces as can be seen in Figure 66 where force curves from MAT24 using data from VCC-CF and snake tool 1.2 are displayed.

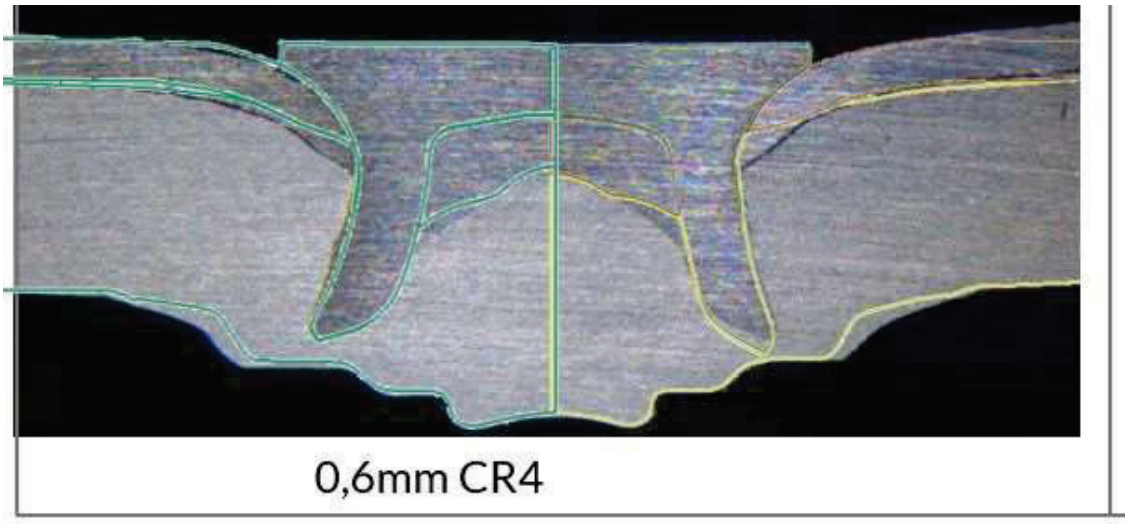

Figure 65 Cross section results from an updated model shown as a green outline on the left on top of the experimental result. On the right side the outline of the initial simulation is shown. A significant difference in the area of the rivet tip is found on comparing these two with each other and with the experimental results.

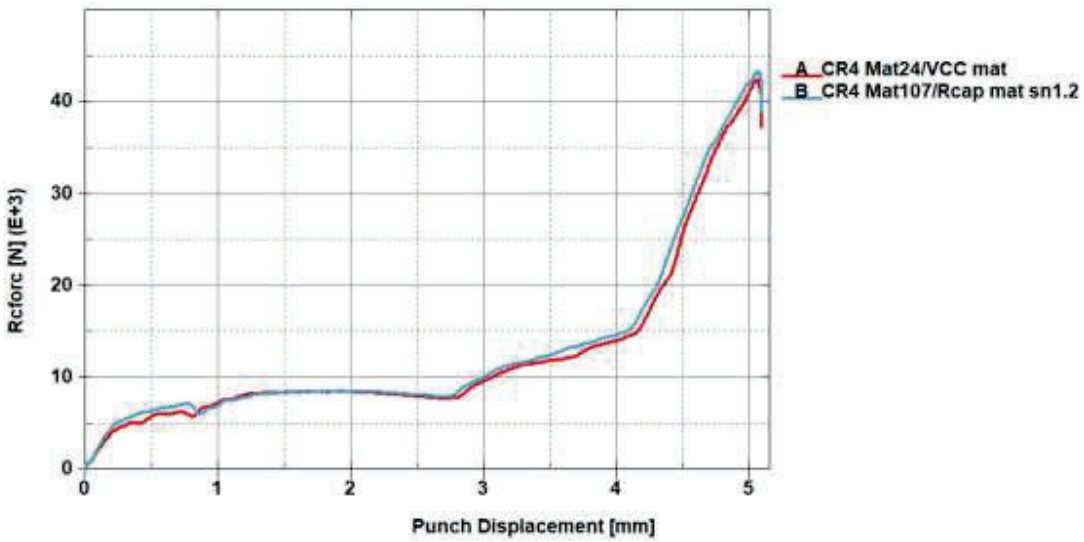

Figure 66 Punch forces as function of punch displacement for CR4 with MAT24 using the stress strain data according to curve A in Figure 67 together with the corresponding results for CR4 based on curve B in Figure 67.

Changes with respect to contact and friction, mesh size and mesh adaptivity frequence as well as with respect to the material model and data for the CR4 material was made. Instead of using the simple piecewise linear plasticity model in MAT_024 in LS-Dyna a material model named Modified Johnson-Cook, MAT_107 was used. Here also the stress strain curve for the CR4 material looks different see Figure 67.

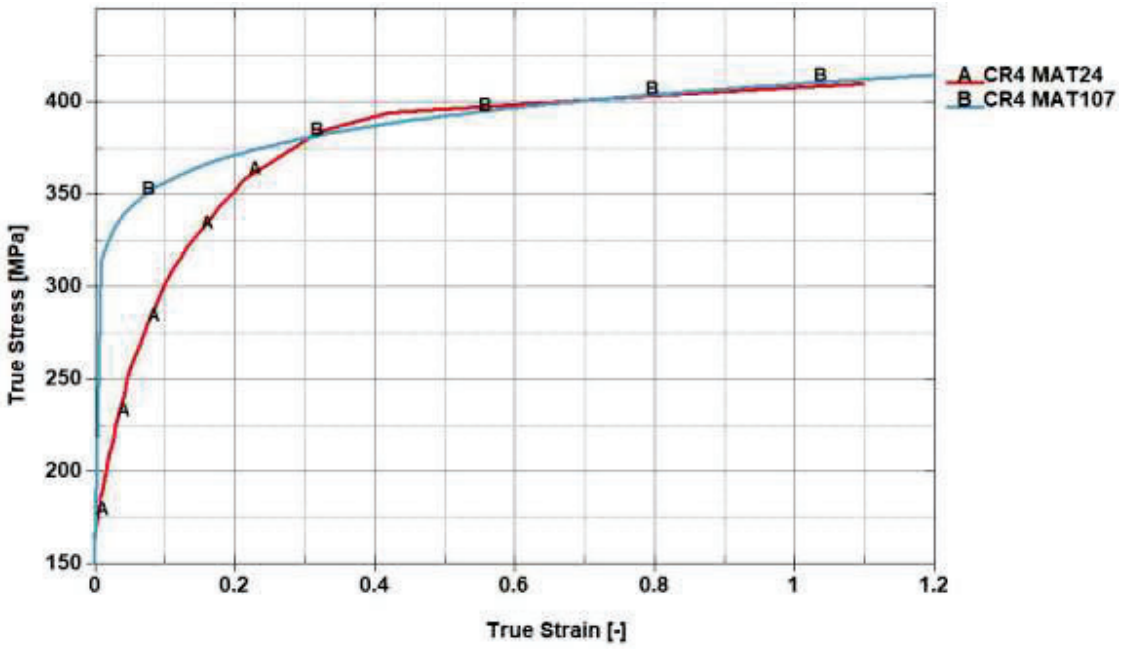

Figure 67 True stress true strain curves for CR4 where material curve A shows the data used with MAT24 and curve B shows the curve resulting from the parameters used in MAT_107.

By reviewing the differences between the models behind the simulated cross sections in Figure 65 it is not easy to point out a single parameter that lies behind the improvement. Isolating parameters one at the time and studying the differences it is concluded that the united action of the parameter settings that constitutes the difference. For example, if only the stress-strain curve for the top layer CR4 material is switched from graph A in Figure 67 to the one behind the MAT107 as shown as graph B in the same figure one gets the result as shown in Figure 68. Where on the left-hand side the result using graph A is shown and on the right-hand side the result from using graph B.

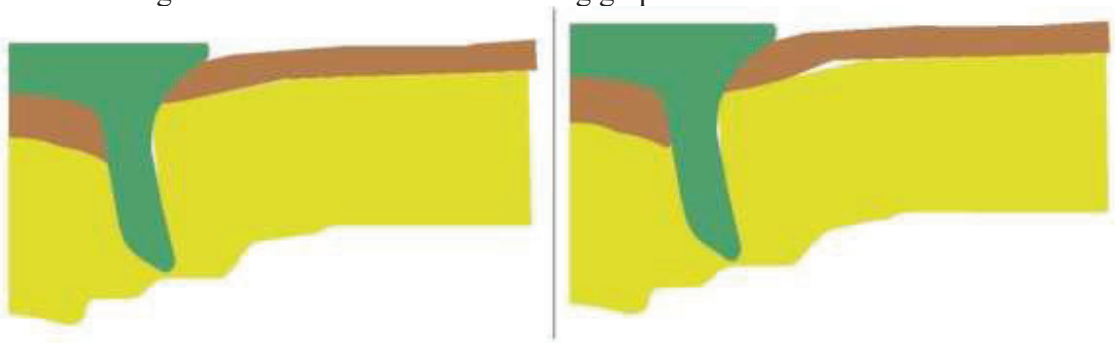

Figure 68 Resulting final state of simulations where the stress-strain curve for top layer is switched from curve A (left) to curve B (right) in Figure 67.

For some combinations of input variables certain aspects of the simulation works less well, in other words it is not entirely robust. For example, the mesh adaptivity sometimes cause elements to get stuck beneath the tip of the rivet causing sliver elements to either terminate the run with error or to give unphysical results. To remedy this a plastic failure strain can

be used to omit elements with a too high plastic strain from jeopardizing the entire simulation.

The SPR process set-up is sensitive to many parameters. The initial mesh size and the adaptivity frequence for updating the mesh needs to be chosen to fit the process time and amount of deformation between updates. For values outside a certain range the simulation might even end with error termination. Some settings work with another version (older or newer) of the software which might resolve some issues.

Contact friction is another important and notoriously difficult parameter to determine. Experiments to measure friction coefficient often does not correspond to exactly the same conditions. In the SPR process there are contacts between several parts and the number of possible combinations to evaluate becomes large if one would like to investigate this thoroughly. In [3] implications of different settings are evaluated and their impact on different outcomes are described.

An attempt to use GISSMO in LS-Dyna for the HPDC material with case #1 was done. In Figure 69 it can be seen the state of that simulation just before it terminates with error. The picture shows how elements have eroded prematurely both beneath the tip of the rivet and in the contact between the HPDC and the CR4 top sheet. Additionally, the elements on the symmetry plane have eroded thus the symmetry constraint is lost. Below the lower sheet to be joined a lose element is seen flying of in the negative vertical direction. Altogether this demonstrates that something fundamental is missing in the conversion from the VCC-CF model to GISSMO. An extension of the instability and failure curves beyond the measured points gives a slightly different behavior up to a point and ultimately the simulation gets struck in the rezoning phase where the mesh is to be updated. This adds to the suspicion that something is wrong in the GISSMO setup altogether.

Figure 69 GISSMO based on VCC-CF used with case #1, NB eroding elements on all contact surfaces and where boundary conditions are applied (dashed line).

Work on Atlas-Copco SPR:

Both configurations according to Table 4 have been simulated. The geometries and basic settings were communicated by Atlas-Copco and different settings based on bilateral discussions have been used in the process to improve the outcome. The results have been evaluated towards one experiment data set per case in terms of cross section images and maximum force.

In Figure 70 and Figure 71 comparisons between simulation using LS-Dyna for #1 and #2 using VCC-CF material data (stress-strain) and physical test results are shown. Here cross section images from the two configurations show varying amount of correlation. For #1 the top half of Figure 70 shows the cross section from one experiment together with the contour from a corresponding FE simulation. A fairly good correspondence is demonstrated but there are deviations, for instance at the tip of the top sheet outside the rivet where the sheet material in the experiment is more prolonged downwards along the rivet leg than the simulation. Inside the rivet the interface between the top sheet and the HPDC aluminium material lies higher. Both these observations can be interpreted as a difference in the behaviour of the top sheet. This can be caused by different material properties between simulation and experiment. Additionally, also by how the separation of the top sheet is handled in the modelling can influence this whenever the actual separation doesn't take place exactly when the remaining thickness is 10% of the original sheet thickness. The measures taken on the physical cross section is shown in red writing with

the matching figures from simulation in the lower half of Figure 70. The values are in the same order of magnitude but not sufficiently close.

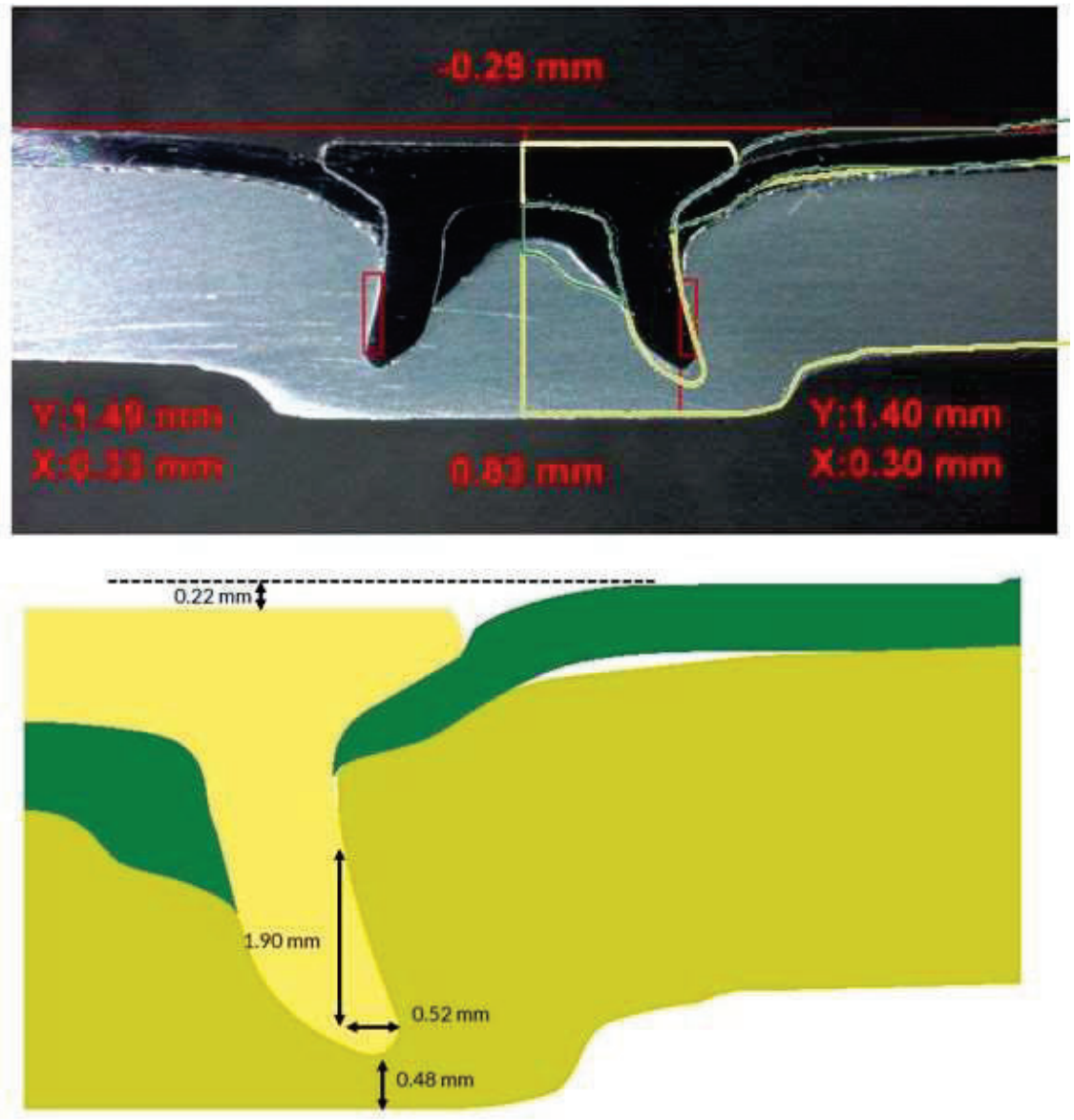

Figure 70 Cross section comparisons for #1, experimental cross section with outline from simulation on superimposed (top) and characteristic measures from simulation (bottom) for comparison with corresponding measures in the top image.

Figure 71 shows the same for #2. Here the cross-section comparison shows even more difference between simulation and experiment but here instead the top sheet in simulation is more prolonged along the rivet leg simulation. Moreover there´s significant differences in the deformation of the rivet leg itself. The simulation shows only minor deflection and thickening compared to the physical cross section. On the inside of the rivet the top sheet significantly thicker in the simulation than in the experiment which also has a void. Despite

this, some but not all of the measurements for comparison as shown in red on the cross-section image with corresponding measurements on the lower half of Figure 71 is surprisingly close which in this case might be pure coincidence.

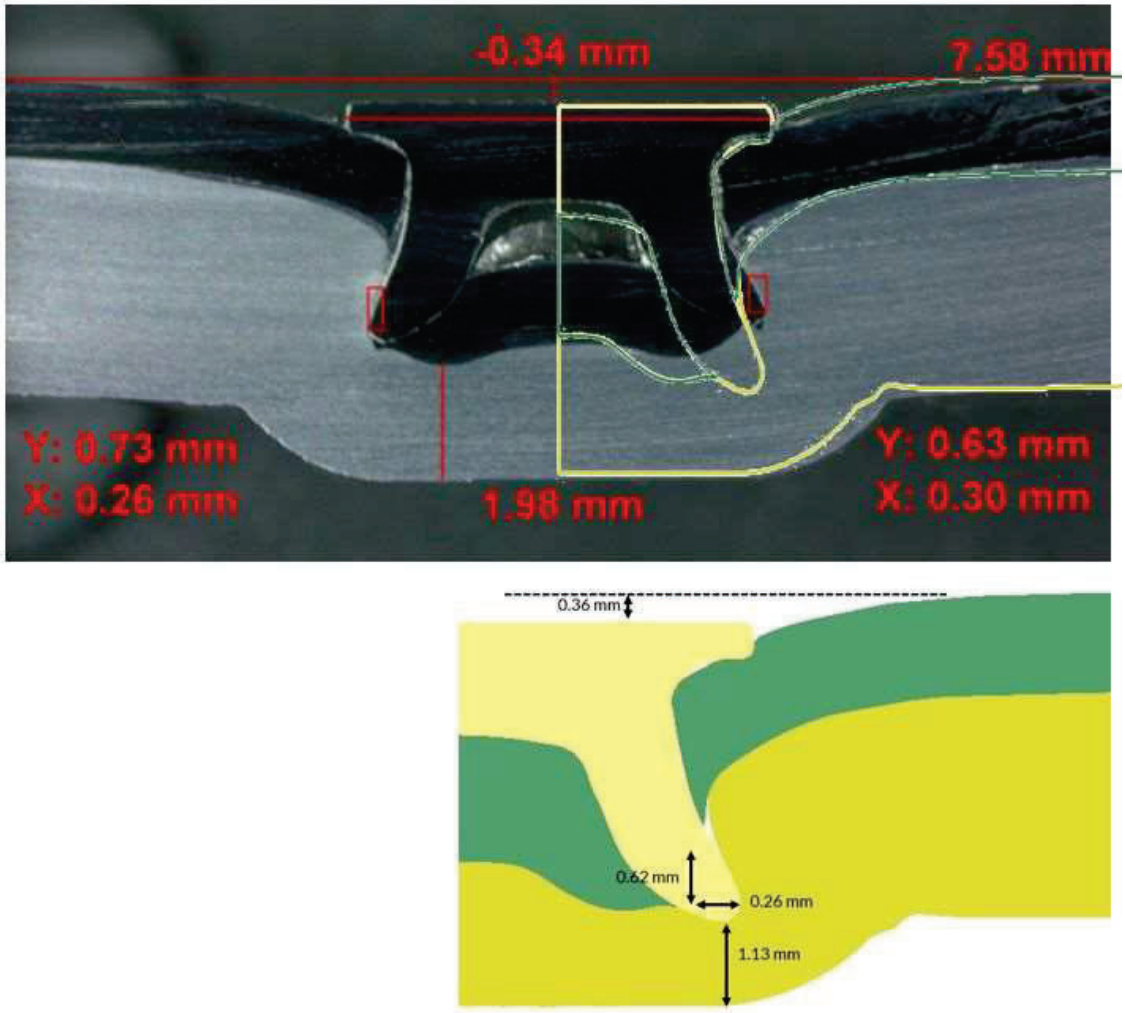

Figure 71 Cross section comparisons for #2, experimental cross section with outline from simulation on superimposed (top) and characteristic measures from simulation (bottom) for comparison with corresponding measures in the top image.

The simulated peak punch force for #1 is 56.2 kN which is the same as the experimentally measured value i.e. 56.2 kN. Corresponding values for #2 is 73.2 kN from simulation and 60.8 kN from experiment. The cross-section deviations for #2 gave rise to a suspicion that the thickness of the HPDC material in the experiment deviated from the nominal 3 mm. It was estimated that the thickness actually was closer to 4 mm than to 3mm. In the left half of Figure 72 the blue outline on top of the cross-section image a result from a simulation with 4 mm thick HPDC is shown. In this the correspondence between simulation and experiment is closer, especially in the tip region of the rivet but also with respect to the

contour of the top sheet outside the rivet. Largest remaining deviation is still in the rivet cavity were the top sheet shows differences compared to the physical experiment.

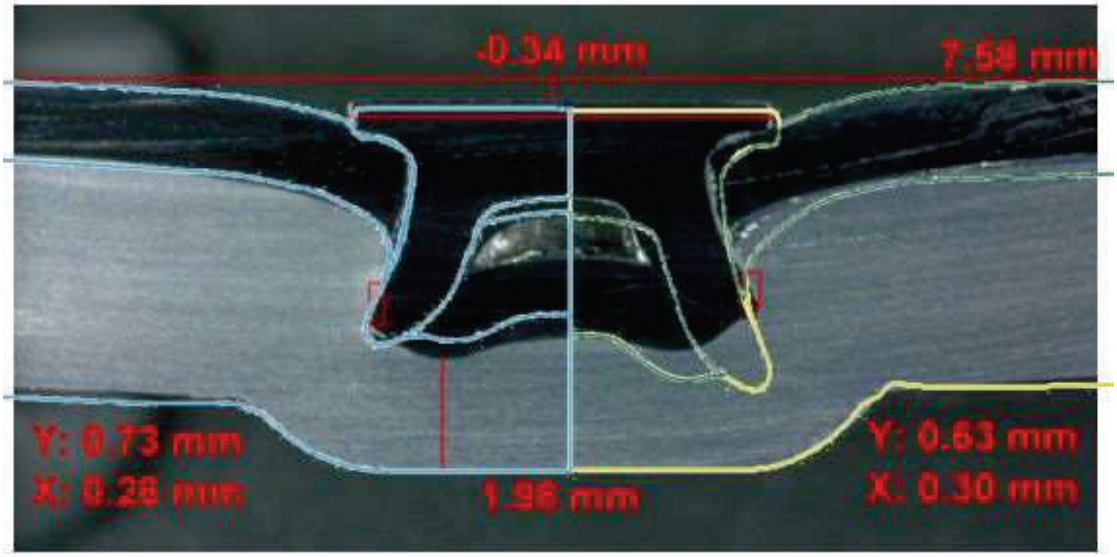

Figure 72 Cross-section from #2 with simulation using thicker HPDC material, 4 mm (left). Simulation using nominal thickness for the HPDC material (right).

Now with a thicker aluminium material the peak force from simulation amounts to 58.9 kN to be compared with the experimental value of 60.8 kN. Simulated force-displacement curves for both configurations can be seen in Figure 73. Here for #2 there´s also a slight difference during the first 1.5 mm of punch travel which can be attributed to an adjustment of friction coefficients.

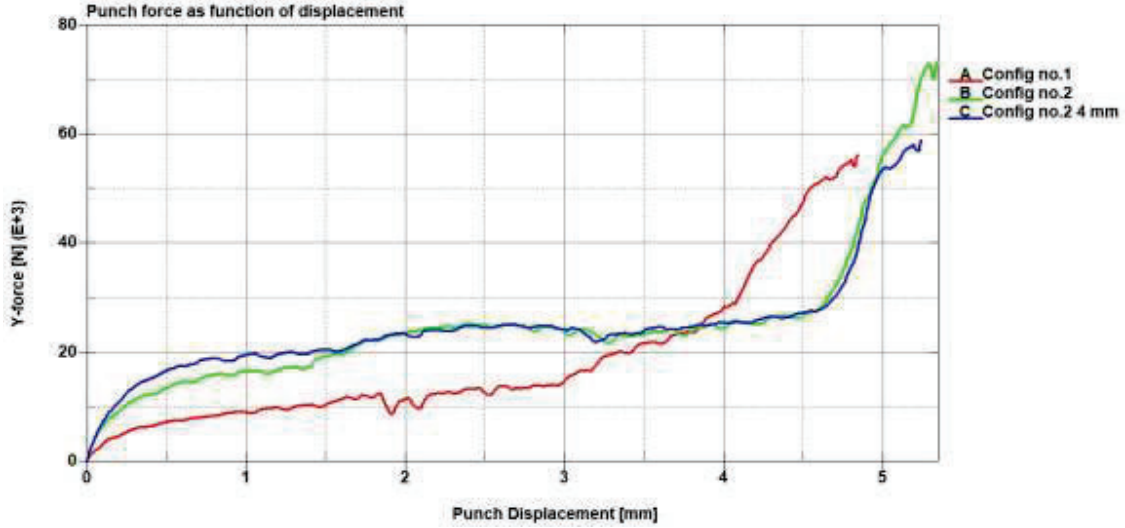

Figure 73 Force displacement curves for both configurations Curves B and C both refer to configuration #2 with curve C from the variant were the thickness of the HPDC material was increased from the nominal 3mm to 4mm.

There are parameters in the simulations partly unknown that can be tweaked for improved comparisons like the friction coefficient between the different parts in contact and some process and boundary parameters. Then there's the modelling aspects like meshing

discretization and adaptivity update frequency as well as the method for how the top sheet is separated in the simulation of the piercing process which here is based on split at a fixed remaining sheet thickness (10%). For a fixed parameter set that gives results reasonably close to reality it might still be possible to study trends of certain changes in the configurations.

For the physical experiments there can also be some variations not entirely under control such as alignment, material properties variations and postprocessing that can cause cross sections after cutting and preparations to be slightly off centre.

An attempt to use GISSMO in LS-Dyna for the HPDC material with case #1 was done. In Figure 74 it can be seen the state of that simulation just before the simulation gets stuck in some infinite loop. The picture shows how elements have eroded prematurely both beneath the tip of the rivet and in the contact between the HPDC and the CR4 top sheet. A large part of the HPDC material under the rivet is cut lose which is far from what to expect from a SPR process. Additionally, some elements on the symmetry plane have eroded thus the symmetry constraint is lost for these. Altogether this demonstrates that something fundamental is missing in the conversion from the VCC-CF model to GISSMO. An extension of the instability and failure curves beyond the measured points gives a slightly different behavior up to a point and ultimately the simulation gets struck in the rezoning phase where the mesh is to be updated. This adds to the suspicion that something is wrong in the GISSMO setup altogether.

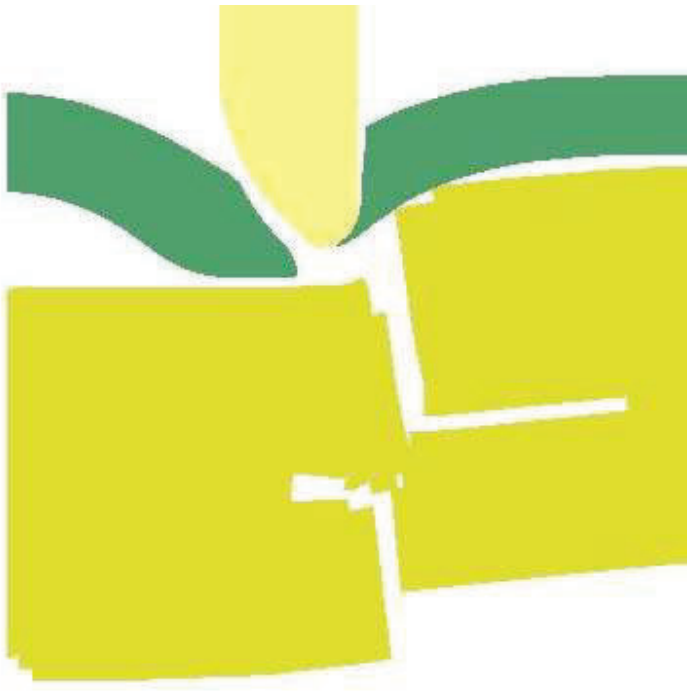

Figure 74 GISSMO based on VCC-CF used with case #1, NB eroding elements fully separates HPDC material early in the rivet setting process. Additionally, some elements in contact with the top sheet and on the symmetry boundary are eroded.

Simulations of both configurations have also been performed by Atlas Copco using Simufact software together with the material data obtained from the tensile testing of the snake tools as displayed in Figure 62. These results are in a global sense comparable to the results using LS-Dyna however Simufact is more developed to serve SPR simulations, much due to the long and involved collaboration with Atlas Copco.

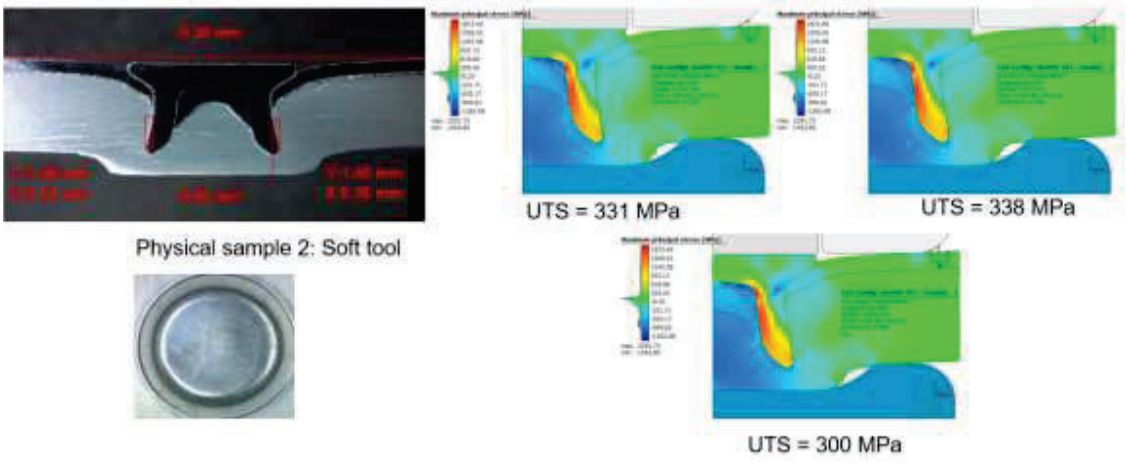

Figure 75 Cross-section of #1 using soft tool material together with Simufact simulation results in terms of max principal stress for the simulated axisymmetric cross-sections. The UTS value under each of the sub plots indicates which of the snake tool stress strain curves used.

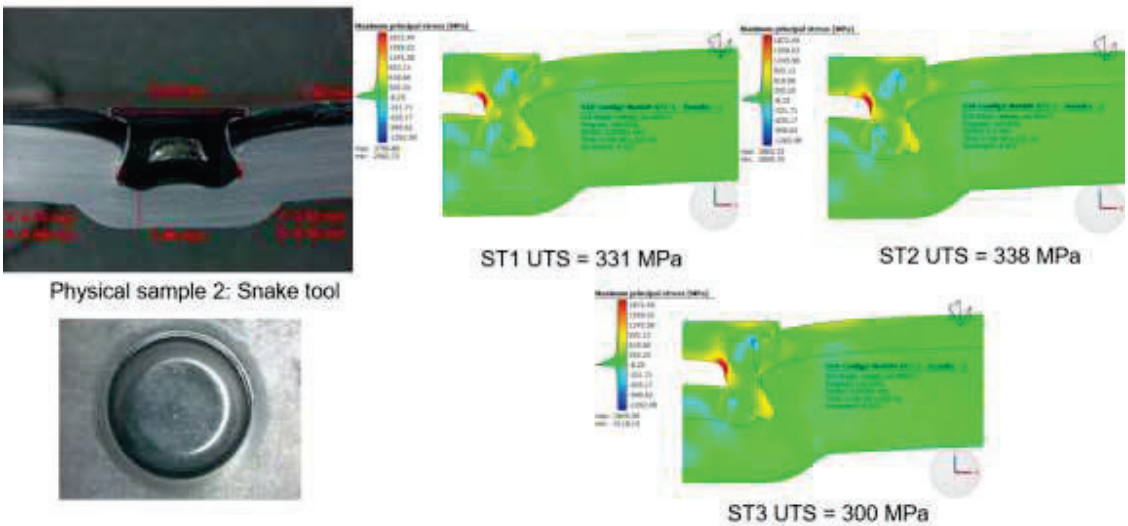

Figure 76 Cross-section of #2 using soft tool material, NB. The thickness relations in the top left image. Physical sample shown together with Simufact simulation results in terms of max principal stress for the simulated axisymmetric cross-sections. The UTS value under each of the sub plots indicates which of the snake tool stress strain curves used.

6.3.2 Pierce cupping test simulations

The pierce cupping test, see 6.1.2.8, was simulated both using the same principle as the SPR processes i.e. as 2D models both with and without adaptivity. For the sake of enabling

studies of results relevant for occurrence of fracture a 3D model in terms of a 15° sector of the full circle with appropriate boundary conditions was also used. A drawback was that the adaptivity did not work for the 3D model.

To make sure results were invariant for the choice of modelling comparison between these different modelling approaches were done, see Figure 77 which shows that the differences in maximum principal stresses values are small. A corresponding graph in Figure 78 is showing the punch forces for the three modelling approaches.

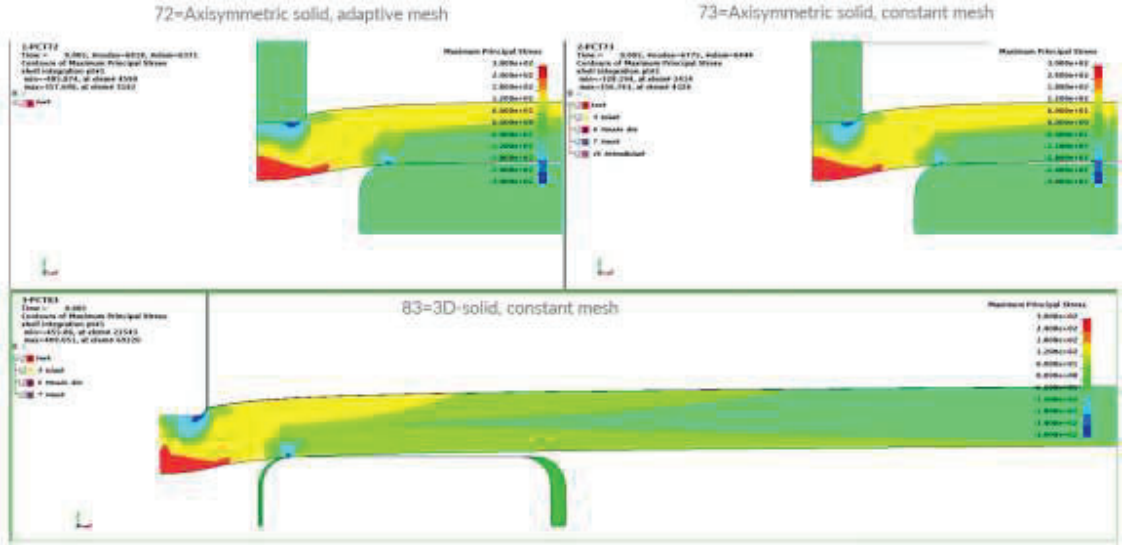

Figure 77 Comparison of maximum principal stress between modelling strategies, top left 2D axisymmetric with mesh adaptivity, top right 2D axisymmetric without mesh adaptivity and bottom 3D solid hexaeder mesh without adaptivity.

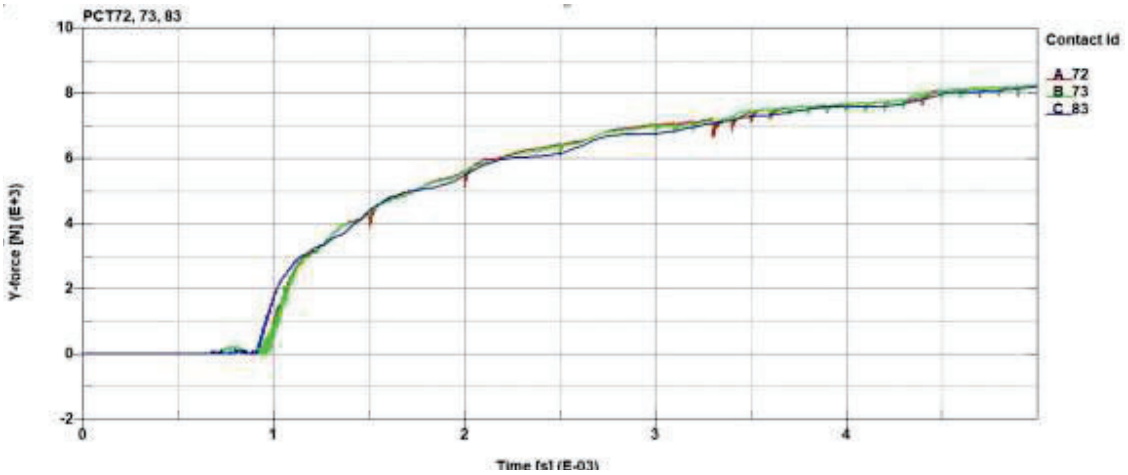

Figure 78 punch force for different modelling approaches, 72 denotes 2D axisymmetric with mesh adaptivity, 73 is the 2D axisymmetric without mesh adaptivity 83 the 3D solid hexaeder mesh without adaptivity.

For the contact between specimen an automatic surface to surface contact of mortar type was used with a friction coefficient of 0.07 [-].

For PCT the casted material was modelled using a piecewise linear model for the flow curve that uses von-Mises yield surface as implemented in LS-Dyna. The input data comes

from the true stress- true strain curves obtained from test specimens from start, middle and end of the flow length in the snake tool 1.2 HPCD component.

In Figure 79 the cross section from PCT tests done on material from start, middle and end along the flow length is shown tighter with corresponding simulation results as a light-yellow outline at depth 0.1 mm before the material at these test locations cracked. This way it can be seen that the largest difference in cross sections occur for the thickness which in the simulations was set to the nominal value 3.0 but in reality, there are thickness variations between the samples.

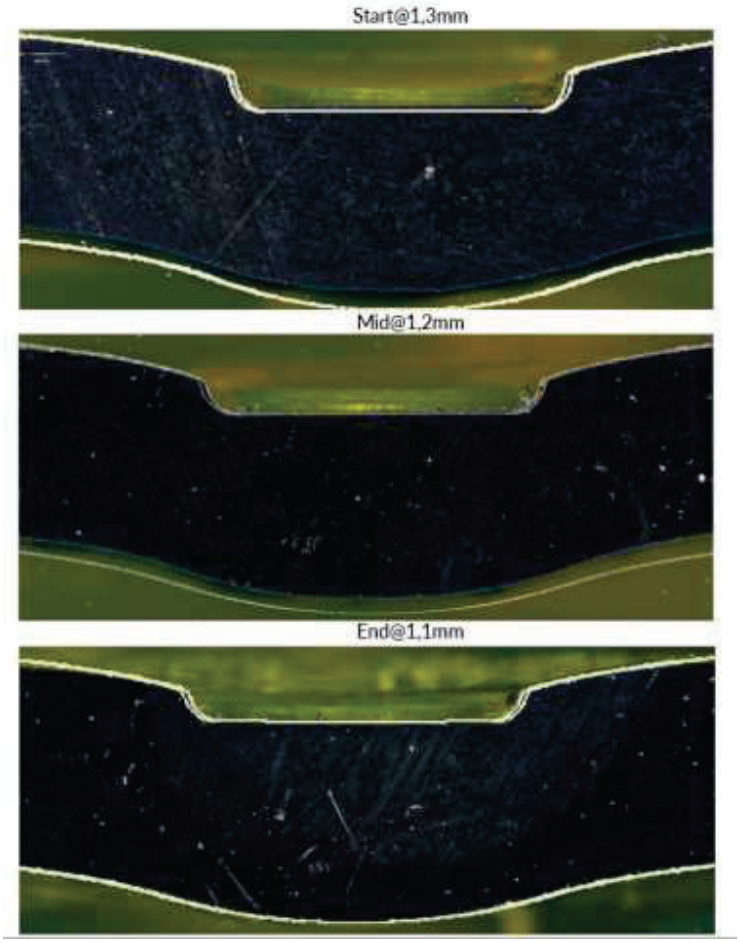

Figure 79 Cross section of PCT tested samples obtain from different positions along the flow length together with outline of corresponding simulated results.

Force displacement curves from the corresponding experiments and simulations are shown in Figure 80. Here it can be seen that the general shape of the curve from simulations resembles the experimental ones. The differences between simulation and experiments can mainly be attributed to the thickness difference in the physical samples whereas the simulation was set up with the nominal thickness. In hindsight it would have made sense to adjust the thickness according to average values for the physical specimens originating from the different positions.

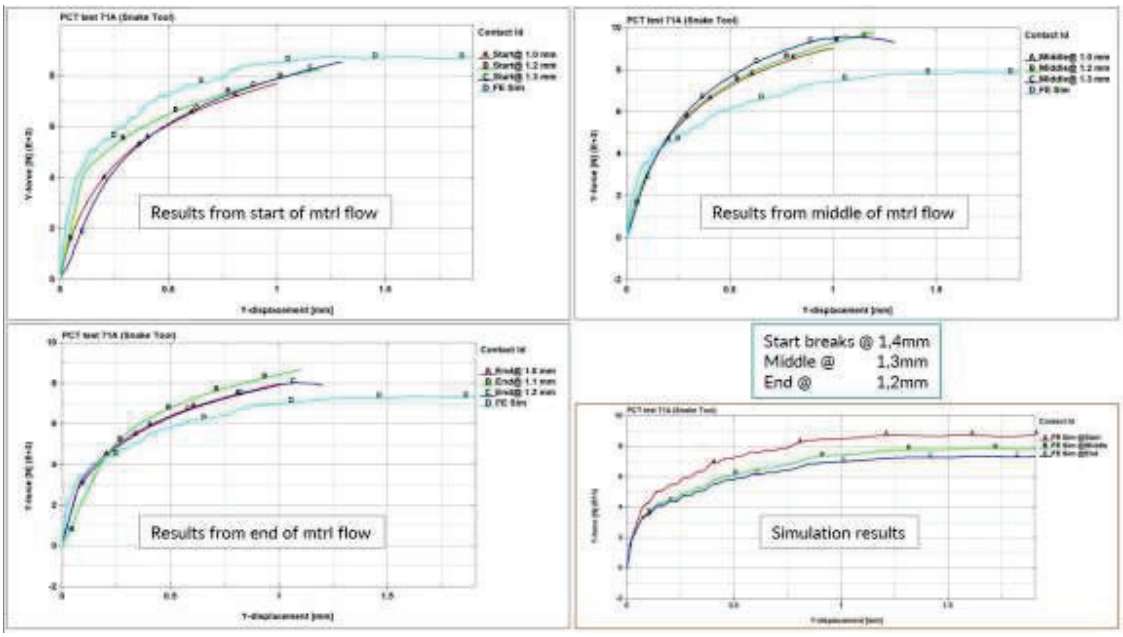

Figure 80 Force displacement curves from both experiments and simulations using data and material from the start, middle and end as indicated by labels in the figure.

To find measures to analyse the margin to fracture some alternative measures are displayed in Figure 81. In the left column different stress measures for one element have been selected, i.e. von-Mises, max principal deviatoric stress and max principal stress respectively. These diagrams in the left column show results from start, middle and end going from top-down. The right column in Figure 81 shows the triaxiality value for one specific element to see if the triaxiality value at the depth where fracture occurs can be used to tell if fracture occurs or not.

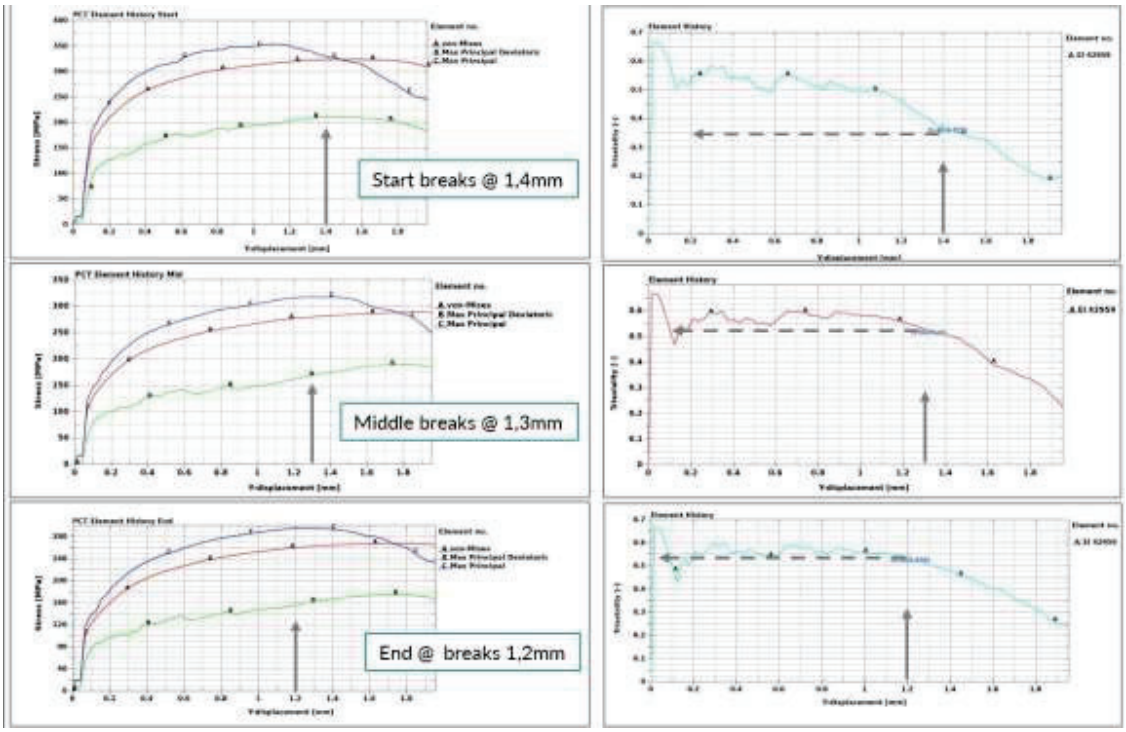

Figure 81 Stress measures from simulations. Graphs in left column shows von-Mises, max principal deviatoric stress and max principal stress for start middle and end respectively. Triaxiality values as function of punch displacements are shown in the right column.

An attempt to use GISSMO in LS-Dyna for the HPDC material with PCT was done. Here in contrast with what was described above for the SPR, the model is made of 3D elements instead of 2D axisymmetric ones. In Figure 82 it can be seen how elements have eroded prematurely beneath the punch. Additionally, the elements on the symmetry planes have eroded thus the symmetry constraint is lost. Further as the process progresses a hole through the HPDC part has been punched out. Altogether this demonstrates that something fundamental is missing in the conversion from the VCC-CF model to GISSMO. An extension of the instability and failure curves beyond the measured points gives a slightly different behavior but, still giving rise to the suspicion that something is wrong in the GISSMO setup altogether.

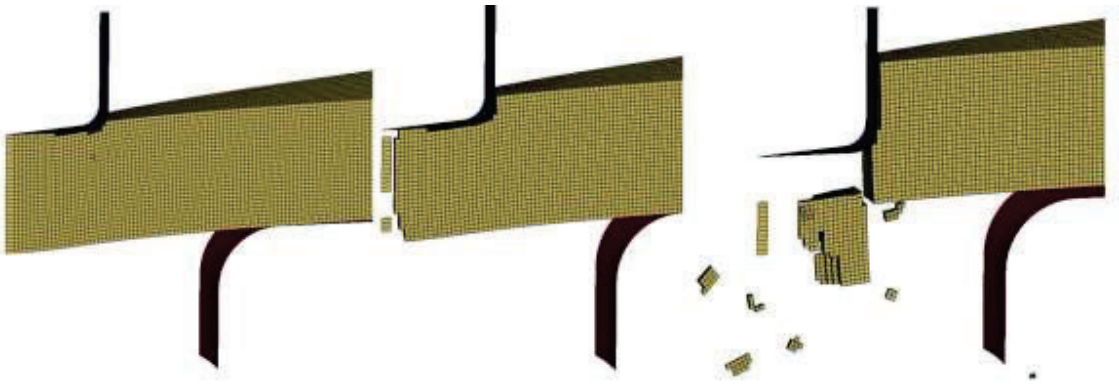

Figure 82 PCT test with GISSMO active is giving a unrealistic response indicating that the implementation of data from VCC-CF is wrong.

6.3.3 Clinching simulations

Among the chosen joining methods clinching is the one offering the largest challenges for simulation. This is partly because the large plastic deformations occurring without separating the materials as with SPR and to some extent also that the tools are deforming with the process in that wedges, supported by a circular rubber element are expanding giving room for the material transport during the process, see Figure 83. For clinching the focus has been on configuration #1 with the additional difference with respect to the SPR that the HPDC material here is on the top side of the stack to be joined.

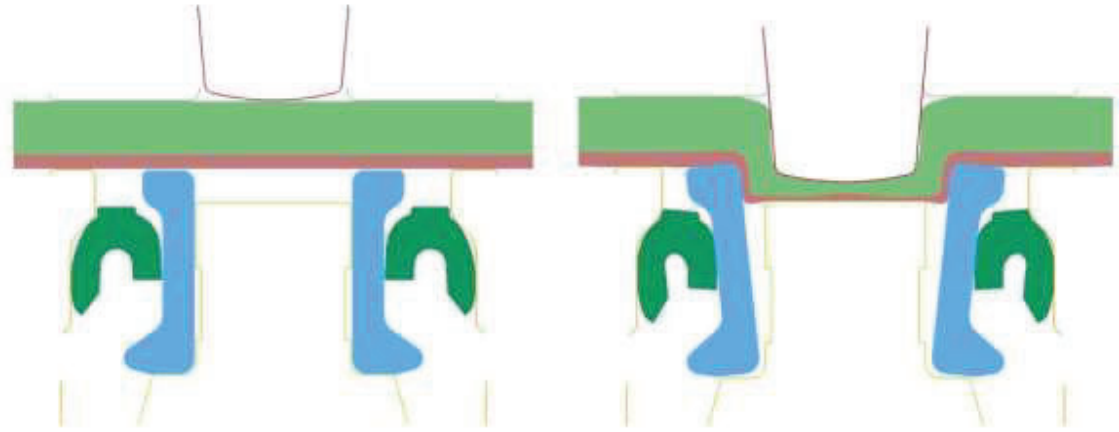

Figure 83 Cross section images displaying the wedges (blue) and rubber (dark green) beneath the two blanks. Status before (left) and after clinching process (right).

In modelling the rubber, data for the specific rubber was not available so various data sets and material models for this part was tested. It is difficult to access the deformation behaviour of the rubber support ring in physical tests since deformations inside the tool are unknown. In Figure 84 comparisons from using different settings for the rubber is shown in terms of how the area were the interlock should be is affected.

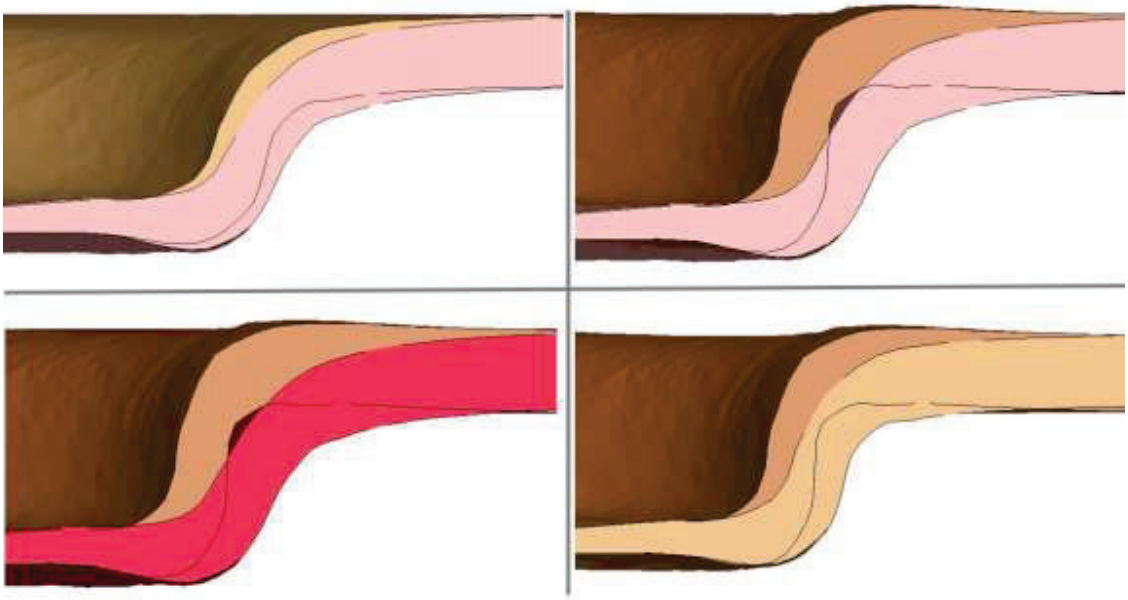

Figure 84 Varying influence on the interlock area from using different parameters for the rubber ring.

Due to the wedges in the tool the process is not quite axisymmetric so a 2D approach is not fully valid why a full 3D model has been developed, see Figure 85.

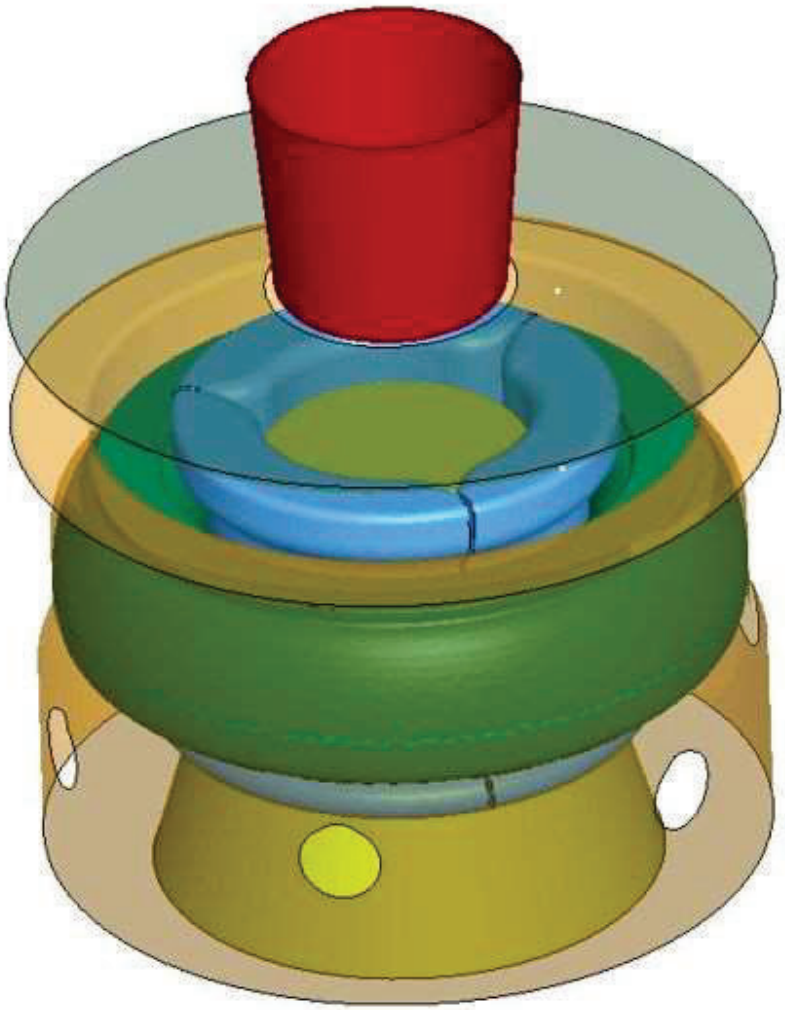

Figure 85 3D model of clinch set-up, die guard and blank holder in semi-transparent with the wedges covering 120° of the full circle in blue.

Quite some effort has been spent in trying to achieve clinching results with FE simulation that resembles the outcome from the corresponding process. The main challenge is to achieve an interlock that can lock the joining materials to each other. Here a number of parameters depending on both process and materials, some of which are difficult to obtain accurate values for, like friction, can influence the results. In Figure 86 the best result so far is displayed. Comparing the simulation from beneath the stack with the photo from experiment indicates that the elevation on the button in the simulation is not as pronounced as the experimental one. In Figure 87 the cross-section images from experiment and simulation are shown. It can be seen that an interlock between the sheets is missing entirely in the simulation. In the photo from experiment some key measures are noted. The only value from simulation that is meaningful to compare is the resulting thickness beneath the punch. The experiment measure is 0.82 mm compared to 0.80 achieved in the simulation.

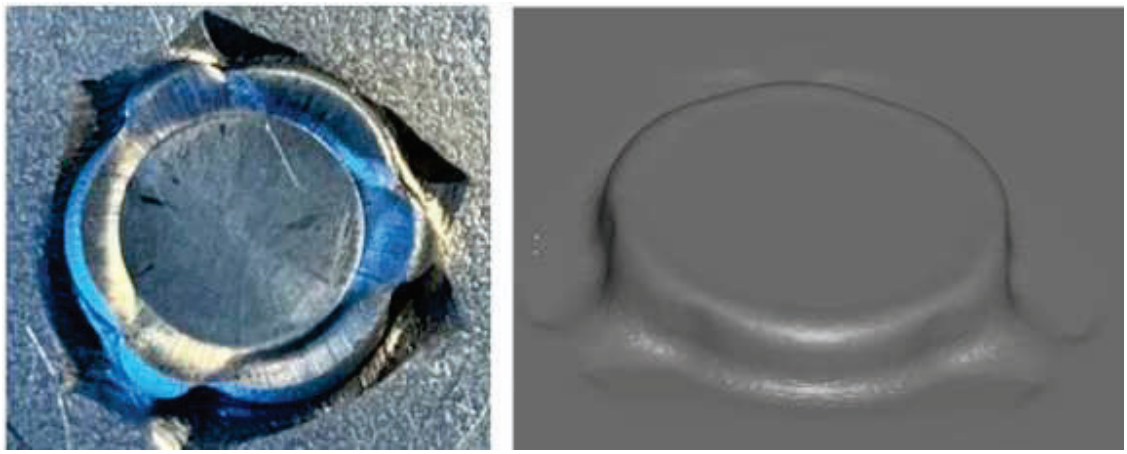

Figure 86 Experimental and simulated clinching results. Left image shows a physical result of #1 from the bottom side of the stack. The right side of the figure shows corresponding results from simulation.

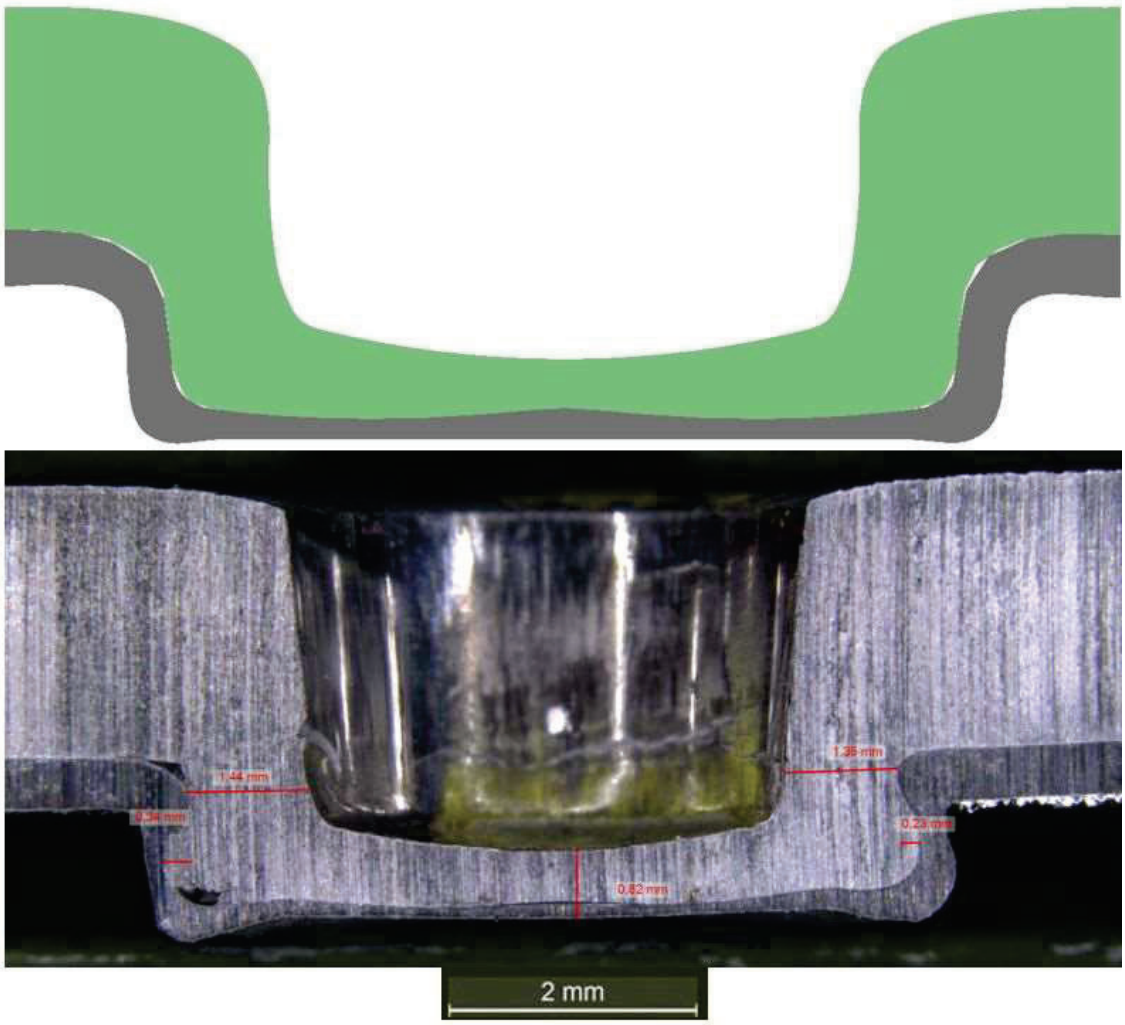

Figure 87 Cross sections of simulation (top) and experiment (bottom). Simulation gives no interlock at all whereas the interlock measure indicated in the image from experiment is 0.34 and 0.23 mm for the left and right side respectively.

Friction between all the surface from tools and blanks in contact are playing a significant role and have been adjusted to get a simulation result closer to reality and more adjustment is possible for further improvements. The joining process takes place quite fast which can be accompanied with close to adiabatic heating causing some material softening which also can contribute to difference since material data for elevated temperatures have not been used due to lack of data. Alternative material models exist that can accommodate these effects as well [6] however these require accurate material data to be used.

The main presumption is that the lack of correspondence between simulation and experiment comes from the large deformations causing severely distorted elements in the blanks to be joined which influence the behaviour. A common technique to resolve mesh quality deterioration accompanying large material deformation is to use mesh adaptivity [7]. This means that the element shape is updated as the deformation is progressing and by that maintaining the element qualities to guarantee accurate results also for large deformations. Here however the mesh adaptivity only works for 2D-axisymmetric but not for these 3D elements which seems to be an issue for the software developer.

Some other ways to circumvent the meshing issue could be to do intermediate manual remeshing just to verify the importance of the mesh quality. This means that an intermediary state is used to create a model of fresh elements either without the accumulated stresses and strains or with these mapped on to the new model.

Besides manual remeshing it should be possible to set the simulation up using meshless methods like Smooth Particle Galerkin method (SPG) [8]. With this technique spheres or discrete nodes instead of finite elements are used. These spheres which represents the state of the material in contrast to “regular” finite elements that uses Lagrangian mesh which means that we have a mesh deforming with the material points which then becomes a drawback for large deformations when mesh adaptivity does not work. Using recent developments for SPG large material deformations can be handled by displacement smoothing to stabilize the involved direct nodal integration. Another benefit of SPG is that failure can take place without removing material which then avoids the numerical instabilities associated with failure as in GISSMO with SPR. A first attempt was made to set up the model with SPG but there was not time enough to pursue this which would require more effort due to limited experience with meshless methods.

6.3.4 Flow drill fastening simulations

The sub-work package focusing on simulations of the FDF process targeted the known challenge of geometrical stability dependence on FDF joinability. It had been seen in previous industrial applications that in joining applications with a lower stiffness, and consequently higher deflections during the joining process, it was more difficult to achieve a successful joint. Thus, the project aimed to establish a working method to assess joinability w.r.t. geometrical stiffness, joining sequence, etc. It was proposed that numerical simulations were a key enabler to such a working method. Through numerical simulations, a given joining application could be transferred to a simplified and controlled set-up in a lab, i.e. a coupon test. A schematic illustration and decision strategy of the working method is shown in Figure 88.

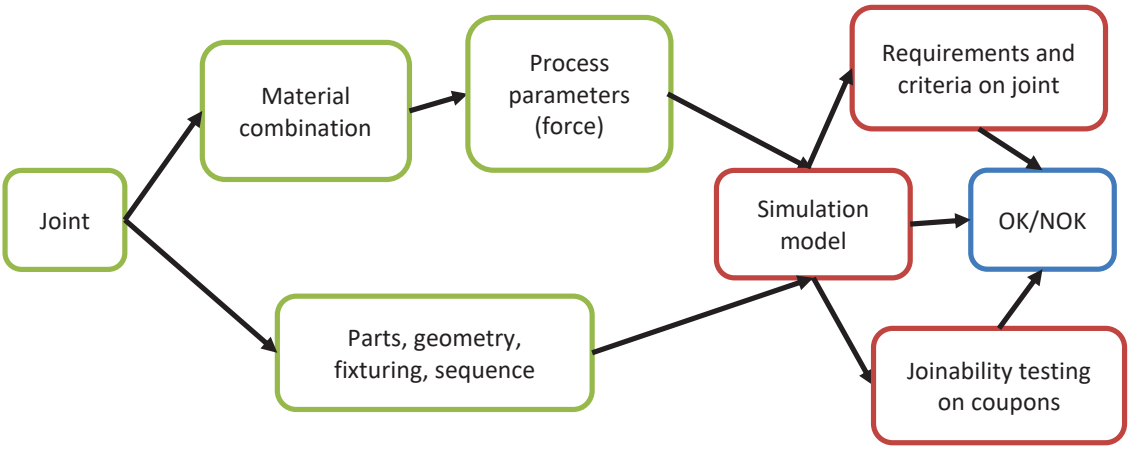

Figure 88 Schematic working method for joinability testing of FDF joints

The project focused on developing and evaluating simulations models to assess geometrical stiffness of a joint location on the soft tool floor. An experimental regime was carried out at Volvo Cars prototype plant to measure the geometrical deflections of a given force at given locations of the component. Multiple combinations of force locations and measurement locations were done.

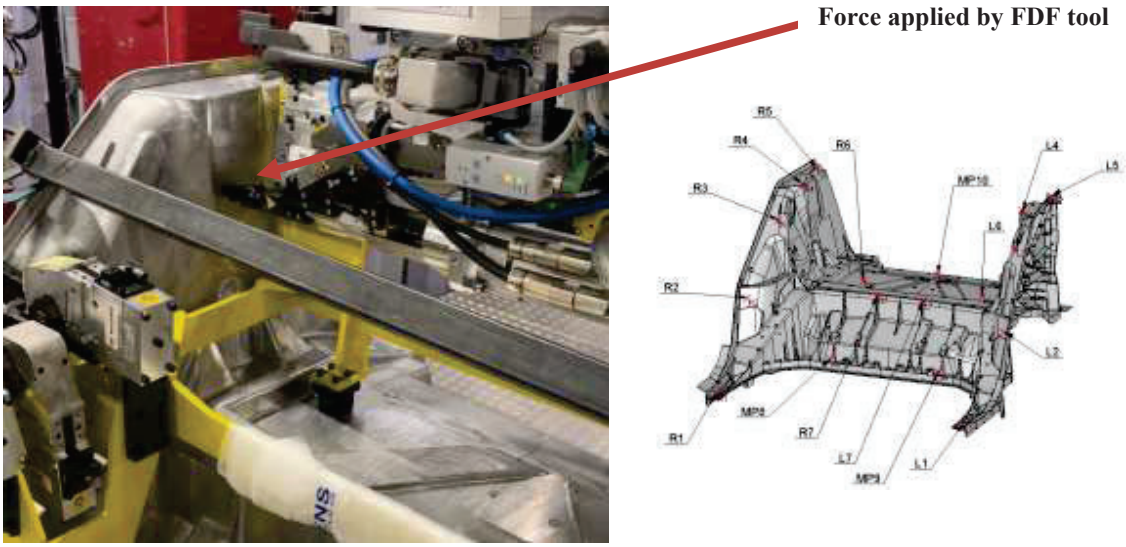

Figure 89 Geometrical measurements of FDF forces (left) and measurement locations (right)

The measurements of the experimental regime were used to assess the simulation models. Two methods were evaluated. Firstly, to build an elasto-plastic FE model was initiated. However, it was seen that to model and mesh all contact conditions and all materials including fixtures was judged a too extensive task and outside the scope of the RobuCAP project. Secondly, a more efficient elastic model was evaluated which has been seen to be efficient in previous applications. However, the model's assumption that the fixture is rigid was not accurate in the given prototype application where the fixture experienced

deflections. Thus, the experimental application used for evaluation was not considered relevant to an actual industrial case where the fixture should be nearly rigid.

Further research should be undertaken and focus on a more relevant and mature industrial application. It is recommended that the efficient elastic model is used to determine stiffness and subsequently transferred to a simplified coupon test. This approach should be used to determine joinability of a given material combination, fastener and arbitrary stiffness.

6.3.5 WP3 Conclusions

Conclusions from simulation of SPR

- The difference between simulated cross sections and force displacement values/curves are close enough to be useful for e.g. studying process parameter influences with some caution
- The reason for caution is the absence of a predefined criteria for determining when a simulation result is close enough to the corresponding physical result for SPR
- Parameter adjustments for simulations can be undertaken to close the gap between experiment and simulation.
- Comparisons have been made only towards a single physical experiment for each of the two configurations. Variations might occur that can affect the conclusions.
- This work has focussed on simple but robust material models an 2D simulations
- Attempted 3D simulations suffered from mesh adaptivity that did not work.
- A systematic approach is needed to delve deeper into the proper settings to reduce the difference between experiments and simulations.
- Conversion of VCC-CF data to GISSMO is missing some fundamental feature.

Conclusions from simulation of PCT

- The PCT can be simulated and gives a good correlation with experiments.
- Coupon thickness should be modelled based on thickness measurements in the specimen for proper comparison of e.g. force displacement curves.
- No conclusion has been made for the fracture from levels of studied stress measures and triaxiality in this study.
- A model for damage and fracture e.g. GISSMO in LS-Dyna or of other general type needs to be characterised and calibrated for detecting fracture according to tests.
- Conversion of VCC-CF data to GISSMO is missing some fundamental feature.

Conclusions from simulation of clinching

- A 3D set-up of the clinching process has been created to perform process simulations.
- The joining in terms of interlock between the parts to be joined could not be achieved.
- This is presumably due to the lack of a working remeshing algorithm.
- Other uncertainties that can contribute to the lack of interlock is the uncertainty of friction coefficients, material data for proper behaviour of the supporting rubber ring and the material model used for the constituents, improvement can be achieved by taking i.e. adiabatic effects into account.
- Intermediate manual remeshing and mapping of results onto a deformed state of the process with subsequent restart can be implemented to isolate the dependence of the mesh quality.
- An interesting modelling opportunity to evaluate for improvement is to switch to meshless methods, i.e. SPG.

Conclusions from simulation of FDF

- A way of working for FDF joinability testing with regard to geometrical stiffness was proposed.
- Geometrical measurements of the FDF process in the prototype production of the soft tool floor were done.
- The geometrical measurements showed excess deformations of the fixture due to the applied forces.
- The evaluated modelling approached were not suitable for the proposed working method or the excessive deformations of the fixture.
- Future research should focus on demonstrating the working method on a more relevant industrial application.

6.4 WP4 Alternative processes

The alternative methods WP focused on two main activities. Firstly, a master thesis was conducted which investigated cracking behaviour of cast aluminium components in various aspects. Specifically, it analyzed causes for cracking, its consequences on fatigue life and the use of adhesive in combination with SPRs to extend the fatigue life of such hybrid joints. Secondly, investigations of the capability of an innovative joining method, *plasma pin joining*, more known under its commercial name Tucker Plasma Joining.

6.4.1 Hybrid joining / thesis

Four-Point Bending Test: Fatigue Behavior of Hybrid Joints

The fatigue behavior of SPR joints under dynamic four-point bending loading was investigated as part of the master's thesis in the project, see the *Publications* Chapter.

6.4.1.1 Summary of the investigations:

Test Setup and Load Cases

The four-point bending tests were conducted to evaluate the fatigue behaviour of Self-Piercing Riveted (SPR) joints under varying conditions. The load case tested was defined with a radius (R) of 0.1, ensuring that tensile stress was consistently applied to the SPR buttons during the test. This configuration is critical for understanding the stress distribution and the potential for crack initiation at the rivet locations.

Test Conditions and Observations

Two different testing conditions were examined—non-adhesive and adhesive-bonded joints:

- **Non-Adhesive Joints**: For the non-adhesive configuration, the resonance frequency was measured to be approximately 41 Hz. This indicates the natural frequency at which the material exhibited oscillations during the fatigue loading.
- **Adhesive Joints**: In contrast, the adhesive-bonded joints were tested using a servo-hydraulic machine, with a frequency of 10 Hz. The use of adhesive in this configuration influences the overall joint behaviour, particularly in terms of damping and stress distribution, potentially leading to altered fatigue life characteristics.

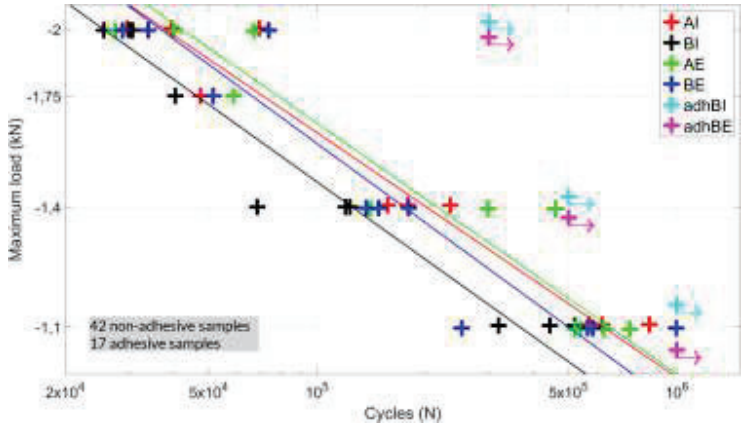

Figure 90 S-N diagram of the tested specimens

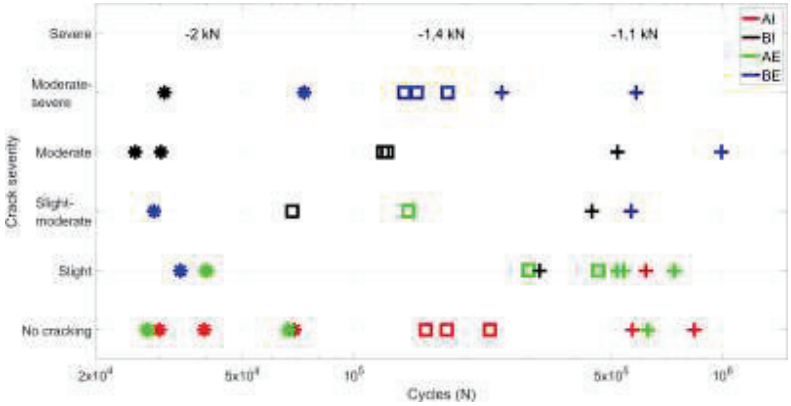

Figure 91 Analysis of crack severity and resulting specimen lifetime N.

The results of the four-point bending tests revealed the following key findings:

- **Cracking and Fatigue Life**: There was no significant correlation between cracking severity and fatigue life across both adhesive and non-adhesive joint types. Despite the presence of cracks in some specimens, these did not appear to directly correlate with the number of cycles to failure, suggesting that other factors, such as material properties or loading conditions, may have a greater influence on fatigue life than the observed cracking alone.
- **Variations in the End Part of Specimens**: Higher variations were observed in the end part of the specimens, which could be attributed to local stress concentrations or manufacturing inconsistencies. This variation is particularly important when considering the performance of joints under real-world conditions, where such localized effects can lead to premature failure.

- **Crack Initiation Points**: The initiation points of cracks were unclear, which complicates the identification of specific failure mechanisms. The absence of a clear pattern in crack initiation suggests that other factors, such as residual stresses or material heterogeneity, may be influencing the behaviour of the joints in a non-uniform manner.
- **Hybrid Joints Fatigue Behaviour**: Hybrid joints (adhesive-bonded and riveted) exhibited superior fatigue behaviour when compared to purely riveted joints. Despite the high cracking severity observed in some specimens, no fatigue limit was determined in this study, indicating that hybrid joints may offer a more robust solution in fatigue-sensitive applications. This finding highlights the potential of hybrid joining techniques to enhance joint durability, even under harsh fatigue loading conditions.

Conclusions

The four-point bending tests suggest that the presence of adhesive, in combination with riveting, enhances the overall fatigue performance of the joints. Although cracking was observed, it did not significantly correlate with the fatigue life, suggesting that hybrid joints have the potential to provide improved fatigue resistance, even in the presence of high cracking severity. Further research is needed to explore the exact mechanisms behind crack initiation and to establish a more definitive fatigue limit for hybrid joints under different loading conditions.

6.4.2 Tucker Plasma Joining trials

The Tucker Plasma Joining (TPJ) technology, developed by Tucker GmbH Stanley Engineered Fastening, was included as part of the RobuCAP project. The joining method offers a solution to challenges in automotive body design, particularly in joining ultra-high-strength steels (UHSS) to aluminium without the need for double-sided access and pre-drilled holes. Schematic drawings of the TPJ equipment are shown in Figure 92.

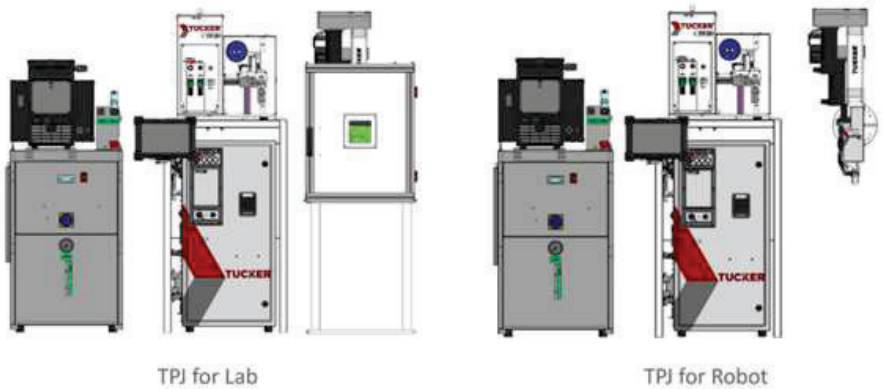

Figure 92 TPJ equipment drawings in static laboratory workstation (left) and for robot mounting (right)

TPJ offers several technological advantages that are relevant to the RobuCAP project:

- Single-sided access for joining between ultra-high-strength steel and aluminium.
- No need for pre-drilled holes.
- Reducing the need for complex tempering or customized heat treatments.
- Short process cycle time

The TPJ process comprises four sequential main steps:

1. **Clamping** Components are precisely aligned before joining.
2. **Preheating** Materials are preheated using plasma to ensure optimal joining conditions.
3. **Joining** Secure bonding is achieved using plasma-assisted techniques. The so-called Tucker Plasma pin penetrates both sheets.
4. **Backstroke** The system resets to complete the operation and prepare for the next cycle.

In the project, two assessments were performed with the TPJ equipment. Firstly, a joinability trial, assessing the methods capability to join challenging material combinations and secondly, a hardness testing assessing the effect of the plasma treatment on USIBOR material. These assessments are treated separately below.

6.4.2.1 Joinability trials

A total of six material combinations have been evaluated using the TPJ system installed at the RISE Hybrid Joining Testbed. These trials were conducted to assess the process robustness across a range of dissimilar material joints involving steels and aluminium alloys. The tested configurations are as follows:

1. CR240LA (0.7 mm) + AL6082-T6 (3.0 mm)
2. DP800 (1.3 mm) + AL6082-T6 (3.0 mm)
3. Usibor 1500 (1.5 mm) + AL6082-T6 (2.0 mm)
4. Usibor 1500 (1.5 mm) + AL6082-T6 (3.0 mm)
5. Usibor 1500 (1.5 mm) + Cast Aluminium (3.0 mm)
6. DP800 (1.3 mm) + Cast Aluminium (3.0 mm)

These trials contribute to validating the TPJ process for multi-material joining applications relevant to automotive structures. The trials were conducted using both a static laboratory workstation and the robot mounted tool, as seen in Figure 92. For the joinability assessment, the criteria listed below were used to define a successful joint.

- A clean and symmetrical crown formation in the bushing/draught.
- Complete penetration of pin and contact of the pin head with the surface of the top material.
- No melting on the top surface.

- Low penetration forces while minimizing end force requirements.

Figure 97 Acceptable crown formation (left), Approved head height position (more flush head position is possible), No Melt on the top of the material (right)

Based on the above-mentioned criteria, all trials were classified. A joint was classified as approved if all criteria were fulfilled in an acceptable manner. It should be mentioned that the results can potentially be improved through further optimization of process parameters. The Insufficient level denotes that joining was unsuccessful due to critical failure in achieving essential joint characteristics. As the criteria are not fully quantifiable and are subject to some interpretation, the collected engineering knowledge of the RISE and Tucker teams were used to classify the joinability results. Moreover, the requirement on process forces is highly dependent on geometrical stiffness, fixturing, etc which are dependent on the specific joining application. Thus, for final approval, the joinability must be assessed for a specific application and on a case-by-case basis.

The reported test results and parameters are based on multiple trials conducted for each material combination. The results below represent the best parameters identified through multiple trials, with evaluation based on meeting the joint criteria mentioned above. All material combinations fulfilled the joint criteria. In Tests 2 and 5, the plasma unit was mounted on a robotic arm. However, technical issues with the robot system made it difficult to continue with the testing on the robot system.

Table 5 Parameters, Results obtained from TPJ equipment for the joinability trials

Test no	Sheet (Thickness)		Parameters					Results		Position	Joint criteria
	Top sheet	Bottom sheet	Plasma paramter I [A]	t [ms]	V̇Gas [l/min]	Downholder force [N]	Head height position [mm]	Penetration force F [kN]	End Force F [kN]	Position of the equipment	Good crown, no surface melt, full pin penetration, low end force
1	240LA (0.7)	6082 T6(3)	230	1700	11	2500	0.7	2.4	2.6	Sytem on static box	Joint approved
2	240 LA (0.7)	6082 T6(3)	230	1700	11	2500	0.7	3.9	2.2	Sytem on robot	Joint approved

3	DP 800 (1.3)	6082 T6(3)	230	2700	11	200	0.5	3.5	3.5	Sytem on static box	Joint approved
4	Usibor 1500(1.5	6082 T6 (2)	200	1700	12	50	-1.2	2.5	2.9	Sytem on static box	Joint approved
5	Usibor 1500(1.5)	6082 T6 (2)	210	1900	11	300	-1.2	3	2.7	Sytem on robot	Joint approved
6	Usibor 1500(1.5)	6082 T6 (3)	220	2500	12	1000	-0.3	4.8	4.7	Sytem on static box	Joint approved
7	Usibor 1500(1.5)	Al cast (3)	230	2200	11	1300	-0.2	4	2.9	Sytem on static box	Joint approved
8	DP 800(1.3)	Al Cast (3)	200	2000	12	3000	-0.25	4.1	4.3	Sytem on static box	Joint approved

6.4.2.2 Hardness testing

Hardness trials were carried out on TPJ samples to evaluate the impact of plasma heating on the material hardness. Initially, the material combination of Usibor 1500 (1 mm) and Al cast (3 mm) was joined using the pin, with parameters detailed in Table 6. The same plasma parameters were then applied to the same material combination without pin penetration.

Table 6 Parameters, Results obtained from TPJ equipment for the hardness testing

Test no	Sheet (Thickness)		Parameters					Results		Position	Joint criteria
	Top sheet	Bottom sheet	Plasma paramter I [A]	t [ms]	V̇Gas [l/min]	Downholder force [N]	Head height position [mm]	Penetration force F [kN]	End Force F [kN]	Position of the equipment	Good crown, no surface melt, full pin penetration, low end force
1	Usibor 1500(1)	Al cast (3)	210	2100	11	700	-0.2	3.5	1.1	System on static box	Joint approved
Focal point control program (same plasma parameter without penetration of pin)											
2	Usibor 1500(1)	Al cast (3)	210	2100	11	700					

Hardness testing was conducted using the Mitsusawa MXT 50 equipment, applying the Vickers method. Measurements were taken on both the plasma-treated region of the USIBOR (1.0 mm) sheet and the untreated region, which served as a reference. Tests were conducted under two different loads: 1 kg and 0.5 kg. The cross-sections were prepared grinded and polished. The reference points were selected from areas on the cross-section were plasma treatment.

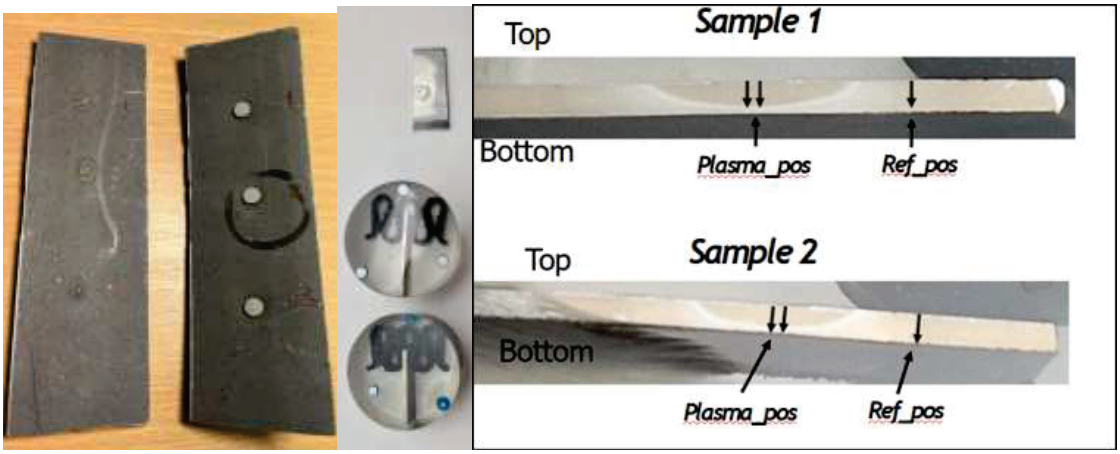

Figure 93 Usibor steel, Cross-section, Reference points from plasma treated cross-section.

The hardness measurement profiles are seen in Figure 94. The hardness remains relatively stable across all samples in the untreated region in the region of 450 HV. Plasma-affected areas maintains higher hardness values than their corresponding reference positions close to the top surface. However, a noticeable drop in hardness is observed for the plasma-processed samples when the plasma reaches the bottom. The plasma process leads to localized heating, which can cause tempering or softening effects especially toward the bottom side, where the thermal dissipation is less efficient. The top side retains higher hardness even after plasma exposure, suggesting that surface heating did not significantly degrade hardness near the surface but did affect the deeper layers. The heat transfer during the joining process is influenced by multiple factors including plasma exposure time, sheet thickness, and the degree of pin penetration. The plasma process influences the material hardness primarily on the bottom side, leading to a softening effect at greater depths. This reduction is more prominent in plasma-treated positions, indicating a potential trade-off between joint formation and thermal softening that must be considered during process optimization.

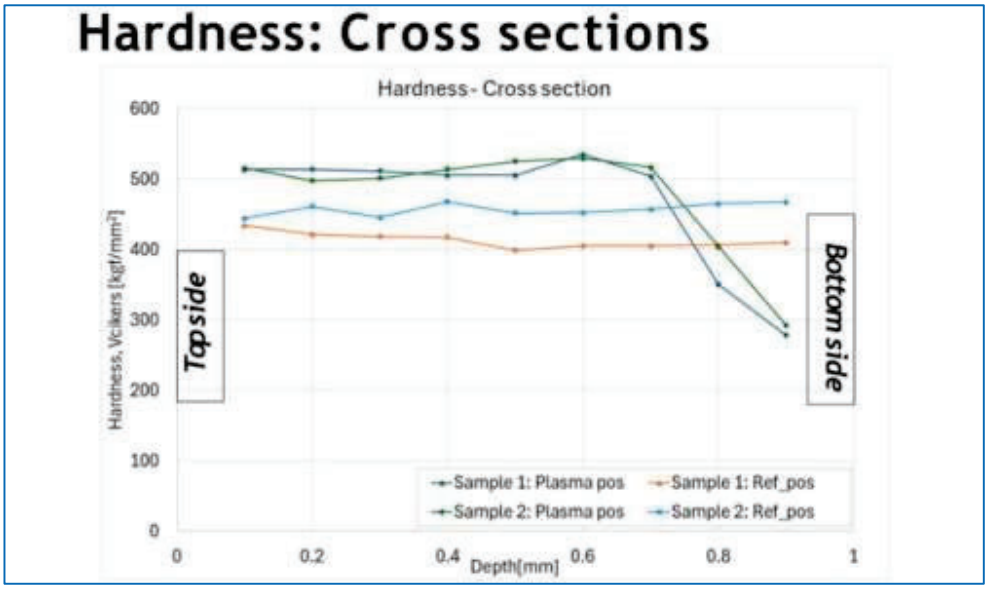

Figure 94 Hardness testing results

Plasma treatment has been observed to induce several notable changes in the material properties:

- Surface Hardening: The top surface undergoes a martensitic transformation due to rapid heating and cooling, resulting in an increase in surface hardness.
- Non-uniform Heating: As the plasma does not penetrate through the full thickness of the material, the bottom side remains relatively less affected by the heat. This leads to a softer microstructure at the bottom compared to the top surface.
- Coating Alteration: The AlSi coating on the surface is found to decrease in thickness within the plasma-affected zone.

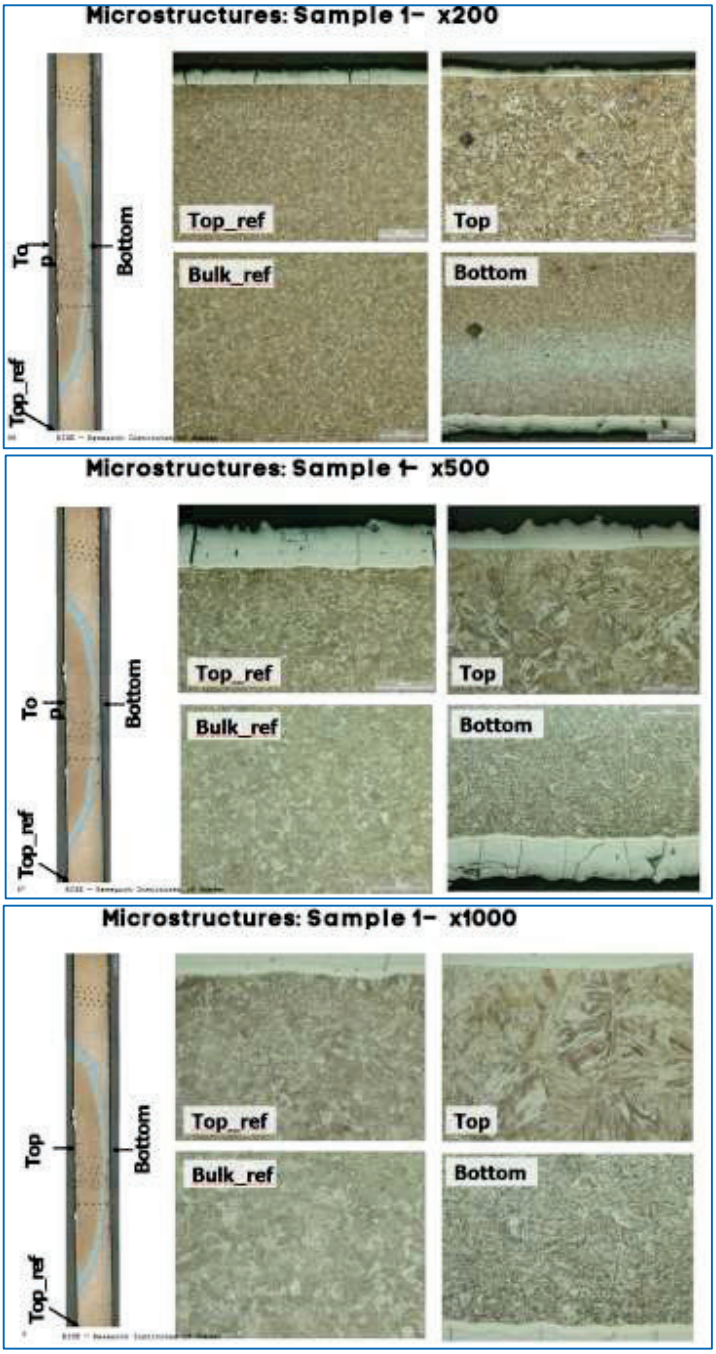

Figure 95 Microstructure analysis of Hardness tested samples

To fully understand the implications of these effects, additional investigations are necessary. Future studies should focus on microstructural analysis, phase transformation behaviour, and reduction in the coating thickness on joint performance and long-term durability.

6.4.2.3 Heat-Assisted SPR for Low-Ductility Cast Aluminium Alloys

Heat-assisted self-piercing riveting (SPR) is a relatively new method for joining low-ductility materials. It involves applying localized heat shortly before or during the joining process to exploit the increased formability of aluminium at elevated temperatures, or to permanently soften the material prior to joining [Lit reference]. Both strategies have been shown in the literature to reduce cracking in cast aluminium alloys.

Previous studies by RISE, Atlas Copco, and other partners [Vinnova Project: Skräddarsydda egenskaper i stål och aluminium genom lokal värmebehandling för optimerad fogning (TAMAPRO), Diarienummer: 2021-01928] explored induction and laser heating to apply targeted heat treatments directly on castings. These approaches effectively modified the microstructure and softened the material locally—provided the alloy composition responded well to thermal treatment. The heat treatment can be completed within seconds per joining position. With the possibility to parallelize heating, this enables a fast and energy-efficient pre-treatment, optimizing the microstructure precisely where needed.

In the investigated alloys, this approach reduced cracking to nearly zero—comparable to the results from full oven heat treatment described in Chapter 6.1.2.2.

7 Dissemination and publications

7.1 Dissemination

How are the project results planned to be used and disseminated?	Mark with X	Comment
Increase knowledge in the field	X	
Be passed on to other advanced technological development projects	X	
Be passed on to product development projects	X	
Introduced on the market	X	
Used in investigations / regulatory / licensing / political decisions		

7.2 Publications

The project generated several technical reports, which were communicated within the project. In addition, a public Master Thesis, examined by Chalmers Institute of Technology was published; *Impact of cracks on the fatigue behaviour of self-piercing rivet joints in die cast aluminium.*

8 Conclusions and future research

The RobuCAP project highlighted the role of material properties, particularly ductility and defect density, in determining the joinability of cast aluminium components. Variations in microstructure, such as pore density and distribution, significantly impact the mechanical performance and susceptibility to cracking during joining processes. The Pierce-Cupping Test (PCT) emerged as an effective method for local material characterization, providing reliable assessments of ductility and crack susceptibility.

Self-Piercing Riveting (SPR) was investigated through iterative adjustments of rivet-die combinations. The project demonstrated that reducing rivet size and using multi-cavity dies can minimize cracking and improve joinability. The importance of considering worst-case material states, particularly from the end sections of castings, was emphasized to ensure robust process optimization.

Clinching trials revealed significant local property variations that impacted joint quality. The lap-shear tests indicated a correlation between material position and clinching performance. Cross-section analysis showed varying results across different material combinations, highlighting the need for optimized material properties and process parameters to achieve high-quality clinched joints.

Flow Drill Fastening (FDF) joinability was influenced by material properties and fastener types. The tests showed acceptable penetration times and thread forming torque, with some trends identified concerning fastener type and snake tool position. Further investigation is needed for thicker aluminium materials and different coatings to fully understand the challenges and optimize the FDF process.

The project explored the use of recycled aluminium, demonstrating promising results in terms of reduced cracking when processed under optimal conditions. However, special attention is needed for megacasting parts, which require thorough verification to ensure consistent quality and performance.

Efficient disassembly methods, such as drilling, were evaluated for SPR and clinched joints. These methods allowed for easy reassembly using blind rivets or re-clinching, demonstrating the feasibility of maintaining material quality and joint strength in repair scenarios. This supports sustainable end-of-life strategies and enhances the circularity of automotive manufacturing.

Numerical simulations were conducted to predict joinability and optimize joining processes. The simulations showed good agreement with physical experiments but highlighted the need for further refinement in material models and process parameters. The use of GISSMO for fracture modelling in SPR and PCT simulations faced challenges in implementation, indicating the need for improved simulation techniques.

The fatigue behaviour of SPR joints with cracked joint buttons was investigated, revealing that cracking severity did not significantly correlate with fatigue life. Hybrid joints, combining adhesive bonding with riveting, exhibited superior fatigue performance compared to purely riveted joints. This suggests that hybrid joining techniques can enhance joint durability in fatigue-sensitive applications.

Tucker Plasma Joining (TPJ) was evaluated as an innovative method for joining dissimilar materials. The trials demonstrated high efficiency in joining ultra-high-strength steels to aluminium, producing strong joints. TPJ offers a promising alternative for improving joint robustness in multi-material applications.

Future research should focus on optimizing process windows and developing predictive models to enhance the robustness and efficiency of mechanical joining processes. This includes refining material models and process parameters to achieve consistent quality across different material combinations.

Further investigation into plasma or heat-assisted SPR techniques is needed to fully understand their potential in improving joinability for low-ductility cast aluminium alloys. These methods offer promising solutions for reducing cracking and enhancing joint quality.

Improving quality control measures is essential to ensure consistent performance and reliability of mechanical joining processes. This includes developing advanced testing methods and integrating real-time monitoring systems to detect and address variations in material properties and process conditions.

Research should focus on understanding recycling practices for secondary aluminium and developing strategies to reduce contaminations in a closed system. This includes investigating the impact of recycling on material properties and optimizing processes to achieve high-quality megacastings.

Enhancing process simulation techniques is crucial for predicting joinability and optimizing mechanical joining processes. This includes developing more accurate material models, refining simulation parameters, and integrating advanced fracture modeling techniques to achieve reliable and robust simulations. Moreover, AI or ML methods based on previous results or databases can be a promising alternative to make assessment of joinability even more efficient.

Overall, the RobuCAP project has advanced the understanding of mechanical joining processes for cast aluminium components, contributing to more robust and sustainable automotive manufacturing practices. Future research should build on these findings to further optimize processes, improve quality control, and enhance the circularity of automotive production.

9 Participating parties and contact persons

The RobuCAP project was carried out as a collaborative consortium consisting of Volvo Car Corporation, Atlas Copco, BTM Scandinavia and Tucker and lead by RISE – Research Institutes of Sweden.

Andreas Reeb	RISE
Peter Ottosson	
Oscar Andersson	
Priyanka Ravishankar	
Per Lindahl	Volvo Car Corporation
Martin Olsson	
Josefine Hansen	
Anna Widmark	Atlas Copco
Paul Briskham	
Zuzana Kotercova	
Tommy Pettersson	Stanley Tucker
Steffen Mathia	
Marie-Louise Lukk	BTM Scandinavia
Jan Nikamo	

References

[1] L. Pérez Caro, M. Schill, K. Haller, E.-L. Odenberger, and M. Oldenburg, "Damage and fracture during sheet-metal forming of alloy 718," *International Journal of Material Forming*, vol. 13, no. 1, pp. 15–28, Jan. 2020, doi: 10.1007/s12289-018-01461-4.

[2] S. Marth, "An Approach on Material Model Calibration for Modelling of Sheet Metal Deformation and Failure," Luleå University of Technology, Solid Mechanics, 2021.

[3] H. Zhao, L. Han, Y. Liu, and X. Liu, "Experimental and Numerical Investigations on the Impact of Surface Conditions on Self-Piercing Riveted Joint Quality," *Coatings*, vol. 13, no. 5, p. 858, Apr. 2023, doi: 10.3390/coatings13050858.

[4] Z. Kotercova, "Developing effective parameters for Self-pierce rivet insertion," University of Sheffield, 2020.

[5] D. Andersson and F. Saliba, “Virtual testing of self-piercing rivet connections,” 2020.
[6] J. Flodr, P. Kałduński, M. Krejsa, and P. Pařenica, “Numerical modelling of clinching process,” vol. 12, pp. 1670–1673, Apr. 2017.
[7] D. Qin, C. Chen, Y. Ouyang, J. Wu, and H. Zhang, “Finite element methods used in clinching process,” *The International Journal of Advanced Manufacturing Technology*, vol. 116, no. 9–10, pp. 2737–2776, Oct. 2021, doi: 10.1007/s00170-021-07602-5.
[8] L. Huang *et al.*, “Simulation of self-piercing rivet insertion using smoothed particle Galerkin method,” in *15th International LS-DYNA Users Conference*, 2018.